EXPERIMENTAL AND MODELING STUDIES OF TWO-POINT VELOCITY AND TEMPERATURE FIELDS IN TURBULENT PIPE FLOW

BY

JOAQUIM DE SYLOS CINTRA, JR.

B.S., University of Sao Paulo,Sao Paulo, Brazil, 1968
M.S., University of Sao Paulo,Sao Paulo, Brazil, 1971

Orientador: Barclay G. Jones

THESIS

Submitted in partial fulfillment of the requirements
for the degree of Doctor of Philosophy in Nuclear Engineering
in the Graduate College of the
University of Illinois at Urbana-Champaign

Urbana,Illinois

EXPERIMENTAL AND MODELING STUDIES OF TWO-POINT VELOCITY AND TEMPERATURE FIELDS IN TURBULENT PIPE FLOW

Joaquim de Sylos Cintra,Jr.,Ph.D.
Nuclear Engineering Program
University of Illinois at Urbana-Champaign, 1975

Experimental and modeling studies of the turbulent structure of both velocity and temperature fields were performed in a vertical pipe flow.

Several related objectives were emphasized in these studies; namely, to obtain additional two-point experimental information regarding the structure of both fields, to model two-point temperature and velocity correlation functions for this structure and, with the modeling results, to investigate the interaction between fluctuating velocity and temperature fields in turbulent pipe flow in terms of three-dimensional eddy diffusivity modeling.

Existing measurements of turbulent diffusivities in the literature in all three orthogonal directions for pipe flow suggest the desirability of developing "non-spherical" eddy models. Due to lack of adequate experimental data in the literature to verify these models for turbulent flow of water in circular pipes, a series of two-point experimental measurements was performed.

Two-point two component (axial and normal) fluctuating velocity signals were obtained with hot film (X-configuration sensors) anemometers separated in the radial direction as well as two-point axial component signals with axial separation. Two-point temperature measurements, including both axial and radial separations, were made in the thermally fully developed portion of the test section as well as in the thermal entrance region.

The fluctuating signals were analyzed digitally and both space and space-time correlations were calculated. The interpretation of the space-time curves from measurements with probe separations in the flow direction was done in terms of the usual convected frame structure. It was shown that

space time correlation curves with probe separations in the direction normal to the mean flow are extremely useful in estimating shapes of the turbulent eddies and in modeling two-point correlations in pipe flow.

Spatial scales for each velocity component and for temperature were determined and then used in the modeling of two-point space correlations in terms of axisymmetric forms. Isocorrelation curves were obtained from this modeling for both velocity and temperature fields. For the velocity field two axisymmetric models, one two-parameter and one four-parameter, were investigated. It was found that the two-parameter model was not adequate for a two-dimensional representation of the correlation functions for the two components of the fluctuating velocity (axial and normal) in pipe shear flow, but the four-parameter model provided a reasonably good description for this type of flow. In the temperature case axisymmetric forms similar to the ones used for the velocity field were examined in the light of the two-point experimental results. It was found that for the temperature field the appropriate angle of axisymmetry was larger than the one which yielded the best results for modeling the large scale velocity structure.

Finally the experimental and correlation modeling results were used to examine spherical and non-spherical eddy diffusivity theories and to test their prediction capabilities. A compartive study was performed in the spherical models by using the measured integral length scales and reported values for microscales. The agreement between the examined non-spherical eddy diffusivity theory and available experimental results was found to be reasonable within the limitations of this theory.

ACKNOWLEDGMENTS

The author would like to express his sincere and humble thanks to his thesis advisor, Prof. Barclay G. Jones, for his guidance, patience and friendship during all phases of this study. Prof. Jones' knowledge of experimental work and insight into the difficult problem of turbulence, coupled with timely and constructive criticism, have provided the author a valuable and rare, if not unique, educational experience.

Acknowledgements are also due to Prof. T.J.Hanratty, for his patience and time spent in stimulating discussion concerning several aspects of the problem of interpreting the experimental results.

A special note of appreciation should go to Profs. P.S. Toledo and R.R. Pieroni, the former for his guidance during the first stages of the author's graduate school career, and the latter for his personal interest and understanding during the author's stay at the University of Illinois.

Thanks for the data reduction assistance must go to Wu-Lieh Ho and Kian T. Huang.

The suggestions and support from the nuclear engineering machine shop and office staff are greatly appreciated. The patient efforts of the draftsman, Mr. Dave James, and the typist, Mrs. Diane Lecher, are also appreciated.

Partial support from the University Research Board and the Water Resources Center (B-067-ILL) in carrying out this work, is gratefully acknowledged.

Gratitude is also expressed to the Fundacao de Amparo a Pesquisa do E. de Sao Paulo (FAPESP) and the Instituto de Energia Atomica (IEA) for providing the author's financial support during his doctoral thesis research.

Only because of format requirements does the author leave until last his thanks to his children, Roberta and Marcelo, for the joy they brought to this time of his life, and his expression of love and appreciation to his wife, Wilma, whose companionship, encouragement and unselfishness have indeed made possible the realization of this lifetime ambition.

TABLE OF CONTENTS

CHAPTER Page

APPENDIX

LIST OF FIGURES

LIST OF TABLES

NOMENCLATURE

a, b	=	semi principal axis
A, B C, D	=	defining scalar functions in axisymmetric second order tensor representation
C_P	=	specific heat
D	=	pipe diameter
e	=	fluctuating voltage signal from hot film sensor
E	=	total voltage signal from hot film sensor
E_T	=	temperature power spectrum
ϵ_h	=	coefficient for thermal diffusion
ϵ_m	=	coefficient for momentum diffusion
f	=	Fanning friction factor
	=	frequency
G	=	system gain factor in converting hot film outputs
k	=	turbulent kinetic energy per unit mass
	=	wave number
k_t	=	thermal conductivity
K	=	correction factor-heat transfer balance in spheroids
K_s	=	correction factor-equivalent radius for drag on spheroids
ℓ	=	length scale
ℓ_L	=	Lagrangean length scale
ℓ_m	=	mixing length
ℓ_1, ℓ_2	=	free parameters-axisymmetric models
$L_{ii}^{(j)}$	=	integral length scale of i^{th} velocity component in j direction
$L_{tt}^{(j)}$	=	integral length scale of temperature fluctuations in j direction

m_1, m_2, n_1, n_2 = free parameters-axisymmetric models

$n = \varepsilon_M + \nu$ = total viscosity

n_c = characteristic frequency

N_R = initial entity Reynolds number

P = pressure

$\overline{P}$ = mean pressure

p = fluctuating pressure

Pr = molecular Prandtl number

Pr_t = turbulent Prandtl number

Pr_T = total Prandtl number

Q_{ij} = second order two-point covariance tensor

Q_1, Q_2 = defining scalar functions in axisymmetric second order tensor representation

r = radial coordinate

R = pipe radius

R^+ = dimensionless pipe radius

R_{ij} = second order two-point correlation tensor

Re = pipe Reynolds number

T = temperature

= averaging time

T_w = wall temperature

$\overline{T}$ = mean temperature

T_b = bulk temperature

T^* = friction temperature

T^+ = dimensionless mean temperature

t = time

$\mathcal{J}_{ii}^{(1)}$ = integral convected time scale of the $i^{\underline{th}}$ velocity component

$\mathcal{J}_{tt}^{(i)}$ = integral convected time scale of temperature fluctuations

$\mathcal{J}_{ii}^{E}$ = integral Eulerian time scale of the $i^{\underline{th}}$ velocity component

$\mathcal{J}_{tt}^{E}$ = integral Eulerian time scale of temperature fluctuations

U_i = $i^{\underline{th}}$ component of local fluid velocity

$\overline{U}_i$ = $i^{\underline{th}}$ component of local mean fluid velocity

u_i = $i^{\underline{th}}$ component of fluctuating fluid velocity

U_c = convection velocity (fixed separation-variable time delay)

u,v,w = components of fluctuating fluid velocity

U_b = bulk velocity

U_τ = shear velocity

U^+ = dimensionless mean velocity

$\overline{u_i u_j}$ = Reynolds stress

$\overline{u_i \Theta}$ = $i^{\underline{th}}$ component of turbulent heat flux vector

V_c = convection velocity (fixed time delay-variable separation)

V_L = Lagrangean fluid velocity

V_e = fluid entity velocity

X,Y,Z = components of position vector

x_1, x_2, x_3 = dimensionless wall distance

Greek Symbols

α = molecular thermal diffusivity

β, β_t = factors of anisotropy

δ = boundary layer thickness

ε_M = eddy diffusivity for momentum

ε_H = eddy diffusivity for heat transfer

Θ = fluctuating temperature

$\vec{\lambda}$ = vector defining axis of rotational invariance

λ_f = longitudinal velocity microscale

λ_t = temperature microscale

μ = molecular dynamic viscosity

μ_t = turbulent viscosity

ν = molecular kinematic viscosity

ξ_1, ξ_2, ξ_3 = components of separation vector-asixymmetric system

ρ = density

τ = time delay

τ_m = optimum time delay for cross-correlation with axial separation

τ_m^* = optimum time delay for cross-correlation with transverse separation

τ_{ij} = shear stress tensor

τ_o = shear stress at the wall

$\emptyset$ = angle of axisymmetry

$\emptyset_e$ = aspect ratio

ψ_x, ψ_y, ψ_z = distortion factors for momentum interaction

ψ^1 = distortion factor for heat transfer

Superscripts

$\overline{\quad}$ = denotes long time average

+ (except for U, T, Y and R) = refers to large entity system

' = denotes root mean square of a fluctuating quantity

$\sim$ = denotes quantity evaluated in the axisymmetric coordinate system

(i) = denotes $i^{\underline{th}}$ separation direction

$< >$	=	denotes ensemble average
$\hat{}$	=	denotes estimated quantity
$\vec{}$	=	denotes vector quantity

Subscripts

ij	=	denotes velocity components
MP	=	denotes distance referred to the mid-point between probes
W	=	denotes distance referred to the wall probe
WD	=	denotes distance referred to the downstream probe

1. INTRODUCTION

Heat and momentum transfer in confined steady-state turbulent shear flows are of prime interest in engineering applications. Practically all flows in closed ducts and channels encountered in current technology, e.g. heat exchangers, nuclear reactors, etc., are of the turbulent type.

Due to the random nature of the physical quantities which describe these transfer processes, e.g. velocity, pressure, temperature, etc., they can commonly be analyzed in terms of their statistical properties. It is currently impractical to obtain explicit analytical descriptions of velocity, temperature or pressure fluctuating fields. All theories of turbulence, both analytical and semi-empirical, are constructed on statistical properties of these random quantities. The present experimental research is concerned with semi-empirical theories based on "eddy diffusivity" concepts. In many of these theories, e.g. Prandtl's (1925) mixing length hypothesis, Von Karman's (1930) similarity hypothesis [see Schlichting (1968)], Taylor's (1932) vorticity transport theory, and more recently, Jenkins (1951), Azer and Chao (1960) and Kudva et.al. (1968), simplifications are made on the governing equations by introducing eddy diffusivities determined from length scales and characteristic velocities. These characterizing quantities are expected to be related to the geometry of the problem and the type of flow and are usually obtained experimentally.

In these previous models only "spherical eddies" are considered and, therefore, they require the specification of only one length scale. The model for eddy diffusivities proposed initially by Tyldesley and Silver (1968) and with more details by Tyldesley (1969, 1970) can allow the eddies to deviate from a spherical shape. Therefore, it requires, at least, a two-parameter representation of the eddies which can be obtained directly from iso-correlation plots, i.e. by cross-correlating two-point fluctuating signals. Although always

possible, this approach may require an excessive number of data points to become useful. If some symplifying assumptions are made with respect to the properties of the two-point correlation tensor, it is then possible to reduce the amount of experimentation needed and to take two-point measurements only along some appropriate directions in the flow field. Isotropy and axisymmetry are two possible simplifying assumptions.

In the present work the structure of both velocity and temperature fluctuating fields in a pipe flow and the prediction capabilities of these eddy diffusivity models are examined in connection with two-point measurements along two orthogonal axes in the flow field. The need to make these measurements is due to the unsatisfactory status of the reported two-point experimental results for turbulent flow of water in circular pipes, as shown in section 2.3.

Therefore, the first objective of this study is simply to obtain additional two-point experimental information regarding the structure of temperature and velocity fields in a turbulent pipe flow. To the best of our knowledge this thesis contains the first published results from two-point, transverse separation, two-component velocity measurements in a water pipe flow. Also new are the results from the two-point, both axial and radial separation, temperature correlation measurements in the thermal entry region, as well as the ones with axial separation in the thermally fully developed portion of the test section.

The second objective is the two-point temperature and velocity correlation modeling, by using axisymmetric forms. The purpose of this modeling is to provide a basis to pursue the last objective of this thesis, namely, an investigation into the Kudva et.al. (1968) and the Tyldesley and Silver (1968) eddy diffusivity models. The experimental input for this correlation and eddy diffusivity modeling is provided by space-time correlation curves and length scales along two orthogonal directions, namely, parallel and normal to the mean flow. These correlation curves and scales are obtained for both axial

and normal components of the fluctuating velocity and for the fluctuating temperatures. The interpretation of space-time curves from measurements with separations in the flow direction has become common in terms of a convected frame structure. However, little attention has been paid so far to similar measurements with separations in a direction normal to the mean flow. It is shown in this study that such measurements are extremely useful in estimating shapes of the turbulent eddies and modeling two-point correlations.

Brief descriptions of both analytical and semi-empirical theories as well as of the previous experimental investigations are provided in Chapter 2. The basic turbulence concepts involved in this study are also included in this chapter.

The heat transfer and fluid flow facility and the experimental anemometry techniques used in this investigation are presented in Chapter 3. Systems for both data collection and data processing are explained in this chapter.

In Chapters 4 and 5 are presented, respectively, the velocity and the temperature results.

The results of Chapters 4 and 5 are applied in Chapter 6, firstly, to model two-point correlations and, secondly, to test the eddy diffusivity theories mentioned previously. The conclusions are summarized in Chapter 7.

Finally an error analysis for the correlation measurements is presented in Appendix A,and Appendix B contains a complete listing of the equations used in the axisymmetric models examined in Chapter 6.

2. BACKGROUND AND FUNDAMENTAL CONSIDERATIONS

2.1 Governing Equations for Turbulent Velocity and Temperature Fields

The velocity field for the laminar flow of a viscous incompressible fluid can be described by the Navier-Stokes equations and the Continuity equation respectively

$$\frac{\partial U}{\partial t} + U_j \frac{\partial U_i}{\partial x_j} = -\frac{1}{\rho}\frac{\partial P}{\partial x_i} + \nu \frac{\partial^2 U_i}{\partial x_j \partial x_j} \qquad (2.1\text{-}1)$$

$$\frac{\partial U_i}{\partial x_i} = 0 \qquad (2.1\text{-}2)$$

For the temperature field one additional equation, namely the energy equation for a moving medium, is required

$$\frac{\partial T}{\partial t} + U_i \frac{\partial T}{\partial x_i} = \alpha \frac{\partial^2 T}{\partial x_j \partial x_j} \qquad (2.1\text{-}3)$$

In order to apply (2.1-1) and (2.1-2) to a turbulent flow Reynolds (1894) postulated that the instantaneous velocity and pressure could each be represented as a sum of a mean quantity and a random fluctuating quantity.

$$U_i = \overline{U}_i + u_i \qquad (2.1\text{-}4a)$$

$$P = \overline{P} + p \qquad (2.1\text{-}4b)$$

With the following additional assumptions:

a) Equations (2.1-1) and (2.1-2) can represent the instantaneous velocity field

b) Ergodic hypothesis is valid (long time average = statistical average)

Reynolds obtained, after substituting (2.1-4) into (2.1-1) and (2.1-2) and

taking a long time average, relations which represent the mean motion in a turbulent flow

$$\frac{\partial \overline{U}_i}{\partial t} + \overline{U}_j \frac{\partial \overline{U}_i}{\partial x_j} = -\frac{\partial \overline{P}}{\partial x_i} + \frac{\partial}{\partial x_j}\left[\tau_{ij} - \rho\overline{u_i u_j}\right] \quad (2.1\text{-}5)$$

$$\frac{\partial \overline{U}_i}{\partial x_i} = 0 \quad (2.1\text{-}6)$$

The quantity $-\rho\overline{u_i u_j}$ on the RHS of (2.1-5) represents the contribution to the total stress tensor due to the turbulence and it is commonly known as Reynolds stress tensor.

Following a similar procedure for the temperature one can arrive at relations describing the mean temperature field on a turbulent flow

$$\frac{\partial \overline{T}}{\partial t} + \overline{U}_j \frac{\partial \overline{T}}{\partial x_j} = \frac{\partial}{\partial x_j}\left[\alpha \frac{\partial \overline{T}}{\partial x_j} - \overline{u_j \theta}\right] \quad (2.1\text{-}7)$$

where $$T = \overline{T} + \theta \quad (2.1\text{-}8)$$

Again, the quantity $-\overline{u_j\theta}$, on the RHS of (2.1-7) represents the effect of the turbulence in the transport of heat and it is commonly known as turbulent heat flux vector.

By subtracting (2.1-5) from (2.1-1), (2.1-6) from (2.1-2) and (2.1-7) from (2.1-3), and by using again (2.1-4) and (2.1-8) one can arrive at the following equations, describing the behavior of the fluctuating parts of the velocity and temperature fields.

$$\frac{\partial u_i}{\partial t} + u_j \frac{\partial \overline{U}_i}{\partial x_j} + \overline{U}_j \frac{\partial u_i}{\partial x_j} = -\frac{1}{\rho}\frac{\partial p}{\partial x_i} + \frac{\partial}{\partial x_j}\left(\overline{u_i u_j} - u_i u_j\right) + \nu \frac{\partial^2 u_i}{\partial x_j \partial x_j} \quad (2.1\text{-}9)$$

$$\frac{\partial u_i}{\partial x_i} = 0 \quad (2.1\text{-}10)$$

$$\frac{\partial \theta}{\partial t} + u_j \frac{\partial \overline{T}}{\partial x_j} + \overline{U}_j \frac{\partial \theta}{\partial x_j} = \frac{\partial}{\partial x_j}\left(\overline{u_j \theta} - u_j \theta\right) + \alpha \frac{\partial^2 \theta}{\partial x_j \partial x_j} \quad (2.1\text{-}11)$$

Starting with (2.1-9) and (2.1-10) one can derive the dynamic equations for the Reynolds stresses and the turbulent heat fluxes.

$$\frac{\partial \overline{u_i u_j}}{\partial t} + \overline{U}_k \frac{\partial \overline{u_i u_j}}{\partial x_k} = - \overline{u_j u_k} \frac{\partial \overline{U}_i}{\partial x_k} - \overline{u_i u_k} \frac{\partial \overline{U}_j}{\partial x_k} - \frac{\partial \overline{u_i u_j u_k}}{\partial x_k}$$

$$- \frac{1}{\rho}\left(\frac{\partial \overline{p u_j}}{\partial x_i} + \frac{\partial \overline{p u_i}}{\partial x_j}\right) + \frac{1}{\rho} \overline{p\left(\frac{\partial u_i}{\partial x_j} + \frac{\partial u_j}{\partial x_i}\right)} + \nu \frac{\partial^2 \overline{u_i u_j}}{\partial x_k \partial x_k} -$$

$$2\nu \overline{\left(\frac{\partial u_i}{\partial x_k}\right)\left(\frac{\partial u_j}{\partial x_k}\right)} \quad (2.1\text{-}12)$$

$$\frac{\partial \overline{u_i \theta}}{\partial t} + \overline{U}_j \frac{\partial \overline{u_i \theta}}{\partial x_j} = - \overline{u_j \theta} \frac{\partial \overline{U}_i}{\partial x_j} - \overline{u_i u_j} \frac{\partial \overline{T}}{\partial x_j} - \frac{\partial \overline{u_j u_i \theta}}{\partial x_j} - \overline{\frac{\theta}{\rho} \frac{\partial p}{\partial x_i}}$$

$$+ \nu \overline{\theta \frac{\partial^2 u_i}{\partial x_j \partial x_j}} + \alpha \overline{u_i \frac{\partial^2 \theta}{\partial x_j \partial x_j}} \quad (2.1\text{-}13)$$

Since the solution of (2.1-12) and (2.1-13), representing second order moments between velocity components or temperature-velocity component, depends on the knowledge of the third order moments it is clear that we still have more unknowns than equations. This is the well known closure problem in turbulence. Therefore, some sort of closure has to be made at one level or another in order to solve the system of equations describing the turbulent velocity and temperature fields.

2.2 Turbulence Models

2.2.1 General Approaches to Analytical and Semi-Empirical Modeling

One of the earliest closures was proposed by Boussinesg (1877, 1899) in terms of an eddy viscosity concept defined, for example, for a two dimensional flow by

$$-\overline{u_1 u_2} = \epsilon_M \frac{d\overline{U}_1}{dx_2} = \frac{\mu_t}{\rho} \frac{d\overline{U}_1}{dx_2} \qquad (2.2\text{-}1)$$

Similarly for the turbulent heat flux we may have

$$-\overline{u_2 \theta} = \epsilon_H \frac{d\overline{T}}{dx_2} \qquad (2.2\text{-}2)$$

Since then several proposals have been made for an equation to calculate the eddy viscosity, e.g. Prandtl's (1925) mixing length hypothesis, Von Karman's (1930) similarity hypothesis (see Schlichting (1968)) and Taylor's (1932) vorticity transport theory. In all of them the eddy viscosity is defined as the product of a length scale times a characteristic velocity, the latter being related to the normal gradient of the mean velocity.

In 1945 Prandtl proposed his turbulent kinetic energy model initiating the so called "transport models" in which at least one of the elements in the eddy viscosity model (length scale, characteristic velocity or the eddy diffusivity itself) is given,not by an algebraic equation,but by the solution of a transport differential equation. For example, Prandtl (1945) proposed that the eddy viscosity should be the product of a length scale times the square root of the turbulent kinetic energy of the fluid, the latter being given by the solution of a transport differential equation. Following this

line of thought other models have been proposed, e.g. Nee-Kovasnay (1969) (transport equation for $n = \varepsilon + \nu$), Rodi-Spalding (1970) (equations for kinetic energy k and $k\ell$). An extensive listing of all these models with a brief description of each one can be found in Launder and Spalding (1972).

Another approach to the turbulence problem is by solving the equations for the Reynolds stresses and the turbulent heat fluxes instead of making them related to the gradients of the mean quantities through the use of eddy diffusivity concepts. Of course all those models will depend on the simultaneous solution of several partial differential equations, the number being set by the level of the closure used. One point, 2nd order closure models have been proposed, for boundary layer flows, among others by Daly-Harlow (1970) (differential equations for $\overline{uv}$, $\overline{u^2}$, $\overline{v^2}$, $\overline{w^2}$ and ε), Hanjalic-Launder (1972) (differential equations for $\overline{uv}$, k and ε) and Donaldson (1972a, 1972b) (differential equations for $\overline{u^2}$, $\overline{v^2}$, $\overline{w^2}$, $\overline{uv}$, $\overline{u\theta}$, $\overline{v\theta}$ and $\overline{\theta^2}$). Examples of one point higher order (typically 4th) closures can be found in the works of Loitsiansky (1939), Chou (1945), Davydov (1959a, 1959b) and Deissler (1958, 1960). A good and concise discussion of high order closures can be found in Brodkey (1967).

Two-point, 2nd order closure models have been proposed under various simplifying assumptions. The most common have been isotropy and homogeneity. In both cases additional guesses about the behavior of the triple correlations (coordinate space) or the corresponding transfer term (wave number or frequency space) are required to close the equations.

Deissler (1963, 1965), by neglecting triple correlations, has shown that there is no steady-state solution for the homogeneous case with uniform velocity and temperature transverse gradients. The solutions for the spectrum functions of velocity and temperature fluctuations apply only to decaying turbulence. Deissler (1961) also has studied the effect of inhomogeneity

in the transverse direction in a constant shear flow by expanding the covariances in power series for small separations. However, his results are good only for small Reynolds numbers (up to 5500) caused, mainly, by neglecting the triple correlations.

Finally, since all the moments of any random variable can be obtained if one knows its probability density function, Lundgren (1967, 1969) has proposed a different approach to the turbulence problem by solving the integro-differential equation for the joint probability density function of the velocity fluctuations instead of an infinite set of partial differential equations for the moments.

2.2.2 "Eddy Models" for Turbulent Heat Transfer

Although the treatment given to turbulence phenomena in the models based on eddy concepts may appear oversimplified they are still extremely useful in real practical applications, e.g. the case of heat transfer to a confined steady state turbulent shear flow. The reason this occurs is that the other models either require the simultaneous numerical solution of several partial differential equations which is time consuming and expensive or can be applied only to very particular situations which are soldom found in the real world.

In order to evaluate the Reynolds shear stress and the turbulent heat flux with an eddy diffusivity model one has to know either both eddy diffusivities separately or just one and then the ratio between them.

In Prandtl's (1925) mixing length theory the transfer of momentum can be visualized as the result of the interaction between lumps of fluid which travel certain distance (in his theory the mixing length) with some characteristic velocity and the surrounding fluid. Starting with this basic and simple concept several authors have worked out models for the transfer of heat

in a turbulent medium. Their results have been presented in terms of an expression for the eddy diffusivity for heat transfer or, more commonly, the ratio εH/εM.

Jenkins (1951) by assuming that:

- the eddies are spherical with a diameter equal to twice the mixing length ℓ_m,
- the eddies travel a distance equal to the mixing length with a constant velocity v', and
- the surface temperature of the eddies varies linearly with time,

has arrived at the following relation for εH/εM

$$\frac{\epsilon_H}{\epsilon_M} = Pr \frac{\frac{2}{15} - \frac{12}{\pi^6}\left(\frac{\ell_m v'}{\alpha}\right)\sum_1^\infty \frac{1}{n^6}\left[1 - \exp\left(-n^2\pi^2\alpha/\ell_m v'\right)\right]}{\frac{2}{15} - \frac{12}{\pi^6}\left(\frac{\ell_m v'}{\nu}\right)\sum_1^\infty \frac{1}{n^6}\left[1 - \exp\left(-n^2\pi^2\nu/\ell_m v'\right)\right]} \qquad (2.2\text{-}3)$$

where

$$\epsilon_M = \left(\frac{\ell_m v'}{\nu}\right)^2\left[\frac{2}{15} - \frac{12}{\pi^6}\left(\frac{\ell_m v'}{\nu}\right)\sum_1^\infty \frac{1}{n^6}\left[1 - \exp\left(-n^2\pi^2\nu/\ell_m v'\right)\right]\right] \qquad (2.2\text{-}4)$$

Azer and Chao (1960) by assuming that:

- the eddies are spherical with a diameter equal to the mixing length,
- the velocity of the eddy varies linearly during the flight, and
- the heat loss from the eddy is characterized by some film heat transfer coefficient h ,

have suggested the following equations.

$$Pr < 0.6 \qquad \frac{\epsilon_H}{\epsilon_M} = \frac{1 + 135\,Re^{-0.45}\exp\left[-\left(\frac{r}{R}\right)^{0.25}\right]}{1 + 380\left(Re.\,Pr\right)^{-0.58}\exp\left[-\left(\frac{r}{R}\right)^{0.25}\right]} \qquad (2.2\text{-}5)$$

$$Pr > 0.6 \qquad \frac{\epsilon_H}{\epsilon_M} = \frac{1 + 135\, Re^{-0.45} \exp\left[-\left(\frac{r}{R}\right)^{0.25}\right]}{1 + 57\, Re^{-0.46} Pr^{-0.58} \exp\left[-\left(\frac{r}{R}\right)^{0.25}\right]} \tag{2.2-6}$$

In 1968 Kudva et al. modified somewhat Jenkins' model in order to introduce some statistical properties of the random temperature and velocity fields. Their assumptions:

- the eddies are spherical with a diameter equal to the microscale (λ_f for momentum transfer and λ_t for heat transfer),
- the eddies travel a distance ℓ_L (Lagrangian length scale) with a constant average velocity V_L, and
- the surface temperature of the eddies is equal to the temperature of the surrounding fluid.

With these assumptions they arrived at

$$\frac{\epsilon_H}{\epsilon_M} = \frac{D_1}{D_2} \frac{1 - \frac{90}{\pi^4} \sum_1^\infty \frac{1}{n^4} \exp\left(-2n^2\pi^2/D_1\right)}{1 - \frac{90}{\pi^4} \sum_1^\infty \frac{1}{n^4} \exp\left(-2n^2\pi^2/D_2\right)} \tag{2.2-7}$$

with

$$D_1 = Re.Pr \left(\frac{\lambda_t}{D}\right)^2 \left(\frac{D}{2\ell_L}\right)\left(\frac{V_L}{U_b}\right) \tag{2.2-8a}$$

$$D_2 = Re \left(\frac{\lambda_f}{D}\right)\left(\frac{D}{2\ell_L}\right)\left(\frac{V_L}{U_b}\right) \tag{2.2-8b}$$

So far we have described models in which eddies are supposed to be or behave like spheres.

Tyldesley and Silver (1968) have presented a different approach to eddy diffusivity modeling by introducing their concept of a "fluid entity" with an arbitrary shape. In order to work out this idea analitically they have assumed the "eddies" as being spheroids with uniform temperature T_e and moving throughout the flow field as a solid with velocity V_e. By starting

with simple relations like the equation of the slow motion of an spheroid, written as

$$R^2 \psi \left(\frac{d\vec{V}_e}{dt}\right) = - \frac{9\mathfrak{D}}{2} \left(\vec{V}_e - \vec{U}\right) \qquad (2.2\text{-}9)$$

and the equation for the heat transfer across its surface as,

$$\rho c_p R^2 \psi^1 \left(\frac{dT_e}{dt}\right) = - 3 k_t \left(T_e - T\right) \qquad (2.2\text{-}10)$$

they have derived expressions for the transport coefficients for momentum (ε_μ) and heat (ε_h), in terms of distortion factors ψ and ψ^1. These factors take the value one whenever spherical "entities" can be assumed. They also have extended the same approach to energy and mass transfers. Following the notation used by Tyldesley (1969), we have

$$\varepsilon_\mu = \frac{2\mu}{27} \langle \psi_y N_R^2 \rangle \left(\frac{1}{4 - \langle \psi_y / \psi_x \rangle}\right) \qquad (2.2\text{-}11)$$

and

$$\varepsilon_h = \frac{\mu}{9} \langle \psi^1 N_R^2 \rangle \left(\frac{Pr}{1 + 3Pr \langle \psi^1 / \psi_y \rangle}\right) \qquad (2.2\text{-}12)$$

Equations (2.2-11) and (2.2-12) express only molecular transport between the eddies. In order to apply this model to predicting the bulk behavior of a turbulent fluid and to include the effects of turbulence they repeated the previous analysis, considering now the transport of momentum and heat between large eddies. Their final transport coefficients for the large "entity"

system, respectively , for momentum and heat transfers, are given by (Tyldesley (1969))

$$\varepsilon_\mu^+ = \frac{2(\varepsilon_\mu+\mu)}{27}\left(\frac{\langle \psi_y^+ N_R^{+2}\rangle}{4-\langle \psi_y^+/\psi_x^+\rangle}\right) \qquad (2.2\text{-}13)$$

$$\varepsilon_h^+ = \frac{(\varepsilon_\mu+\mu)}{9}\left(\frac{\langle \psi^{1+} N_R^{+2}\rangle Pr_T}{1+3Pr_T\langle \psi^{1+}/\psi_y^+\rangle}\right) \qquad (2.2\text{-}14)$$

Therefore with this approach, the ratio between eddy diffusivities, given by (2.2-15) takes into account, for the first time, the anisotropy of the large scale structure of the turbulent temperature and velocity fields.

$$\frac{\epsilon_H}{\epsilon_M} = \frac{Pr(1+3Pr)\langle \psi^{1+} N_R^{+2}\rangle\left(81+2\langle \psi_y N_R^2\rangle\right)}{\Delta_e}$$

$$\Delta_e = 27(1+3Pr) + 3Pr^2\langle \psi_y N_R^2\rangle + Pr(1+3Pr)\langle \psi^{1+}/\psi_y^+\rangle \left(81+2\langle \psi_y N_R^2\rangle\right) \qquad (2.2\text{-}15)$$

The previous review of models for eddy diffusivities and turbulent Prandtl number is not exhaustive but it is believed to be complete within the scope of the present work.

2.3 Previous Experimental Investigations

We shall now proceed to examine the experimental results for properties of the turbulent temperature and velocity fields in pipe flow and boundary layer studies which we feel are pertinent to this investigation.

Measurements of the fluctuating component of the temperature in pipe flow have been reported by Kudva and Sesonske (1972), for ethylene-glycol; by Burchill (1970), for water; by Hochreiter and Sesonske (1969,1974), for liquid metals, and by Bremhorst and Bullock (1970,1973), for air. Most of

these authors have obtained also, from an analysis of the turbulent time signals, autocorrelation functions, micro- and macroscales, and spectra. However, in all cases these temperature results have been obtained for fully developed conditions for both the temperature and velocity fields.

Some measurements of the fluctuating component of the temperature in the thermal entrance region in pipes have been reported by Brown and Gauvin (1966) and Tanimoto and Hanratty (1963), both in air flows. In both papers results for RMS values only have been presented without any further analysis like the calculation of correlations and scales of turbulence. Mean temperature profiles in the thermal entry region of pipes with air flow have been reported by Johnk and Hanratty (1962b), for constant wall heat flux, and by Hishida (1967) and Abbrecht and Churchill (1960), for constant wall temperature.

Non-isothermal measurements, in terms of the components of the heat flux vector (either axial $\rho c_p \overline{u_1 \theta}$, radial $\rho c_p \overline{u_2 \theta}$ or both), have been reported in some of these and other studies, e.g., Bourke and Pulling (1970) and Ibragimov et.al (1969), in pipe flows, and Johnson (1959), Verollet and Fulachier (1969), Trinite and Valentin (1972) and Pessoni (1974), in thermal boundary layers.

These heat flux results have been used for calculating eddy diffusivities. Hochreiter (1971) has shown that the use of mean temperature gradients or temperature-velocity cross-correlations may lead to quite different results for the diffusivities. Uncertainties in the values of the turbulent heat fluxes and difficulties in estimating gradients seem to be the cause for this discrepancy. Reviews of experimental data for the ratio between the diffusivities for momentum and heat (turbulent Prandtl number) by Hughmark (1971) and Blom (1970), among others, have shown a fair amount of scatter.

Radial and tangential eddy diffusivities for heat and mass transfer have been reported by Quarmby and Quirk (1972, 1974). Their results have shown the need for "eddy models" capable of predicting eddy diffusivities in more than one direction. Concerning this problem Buleev (1964) has proposed

a generalization of the semi-empirical approach of Prandtl and von Karman for the case of an arbitrary fluid flow.

So far we have dealt with single point studies, i.e., measurements with single or multi-sensor probes, but all sensors located at the same point in the flow field. However, two-point measurements, as a means of examining the structure of the turbulent temperature and velocity fields in pipe flows, are relatively scarce. Such measurements, as are available, are commonly presented as cross-correlation or cross-spectral functions or as integral length scales.

For the axial velocity component some correlation functions and/or scales have been reported by Morton and Clark (1971) (both in the flow direction and normal to it), Meek (1972) (transverse scales only) and Howard (1974) (longitudinal scales only), in water flows and by Sabot and Comte Bellot (1972b), (for both parallel and normal directions), in air flows.

In air, isocorrelation plots for the normal component of the velocity have been presented by Sabot et.al. (1973), but only at one radial location in pipe flow of air.

Concerning the two-point turbulent temperature field, experimental results have been presented by Bobkov et.al. (1966, 1968) and Subbotin et.al. (1964), for flows in circular tubes, and by Ibragimov et.al. (1968a, 1968b), for flows in square channels. However, in all cases, only two-point transverse separation measurements have been reported.

Finally, for studying large scale structure in a boundary layer, Fulachier et.al. (1974) have gone one step further by suggesting the use of three point measurements. They have reported a few results for double and triple space-time correlation functions for temperature fluctuations in a boundary layer over a heated flat plate. By comparing the three with the two point correlation results, obtained in a plane parallel to the plate ($y/\delta=0.034$), they have interpreted qualitatively the effects from the adjacent fluid fields, above and below this plane, on the temperature fluctuations.

3. EXPERIMENT DESCRIPTION

3.1 Heat Transfer Loop Facility

All measurements reported here were carried out in the heat transfer loop pictured schematically in Fig. 3.1-1 and described in detail by Burchill (1970).

The 1750 rpm centrifugal pump driven by a 7 1/2 HP electric motor can produce flow rates with pipe Reynolds numbers up to approximately 100,000.

The test section is vertical, has a circular cross section with an O.D. of 4 1/4 in., a 0.120 in. thick wall and is 28 feet long.

The heated section begins after hydrodynamic development length of 56 diameters thus providing fully developed profiles at that location. Three heaters with separate controls and located in sequential axial segments make up the heated section and can dissipate a maximum total power of 21.3 KVA which corresponds to a wall heat flux of 7700 BTU/hr ft^2. This arrangement allowed measurements at three different axial locations with respect to the thermal entrance point without moving the measurement devices.

The mass flow rate and the bulk fluid velocity were determined by measuring the pressure drop across a sharp edged orifice of 1.62 in. diameter. Two 50 in. U-tube manometers located near the pump, one filled with Hg and the other one with 1.75 s.g. indicating fluid, were used for that purpose. Another set of two 36 in. U-tube manometers located near the heater controls was used to double check the readings.

Bulk water temperatures were monitored at the inlet and outlet of the test section and in the retention tank with Fe-Co thermocouples. The reference temperature used was the ice-point and the voltage from the thermo couples was measured with a Honeywell Model 2745 portable precision potentiometer which allowed readings to ± 0.001 mV.

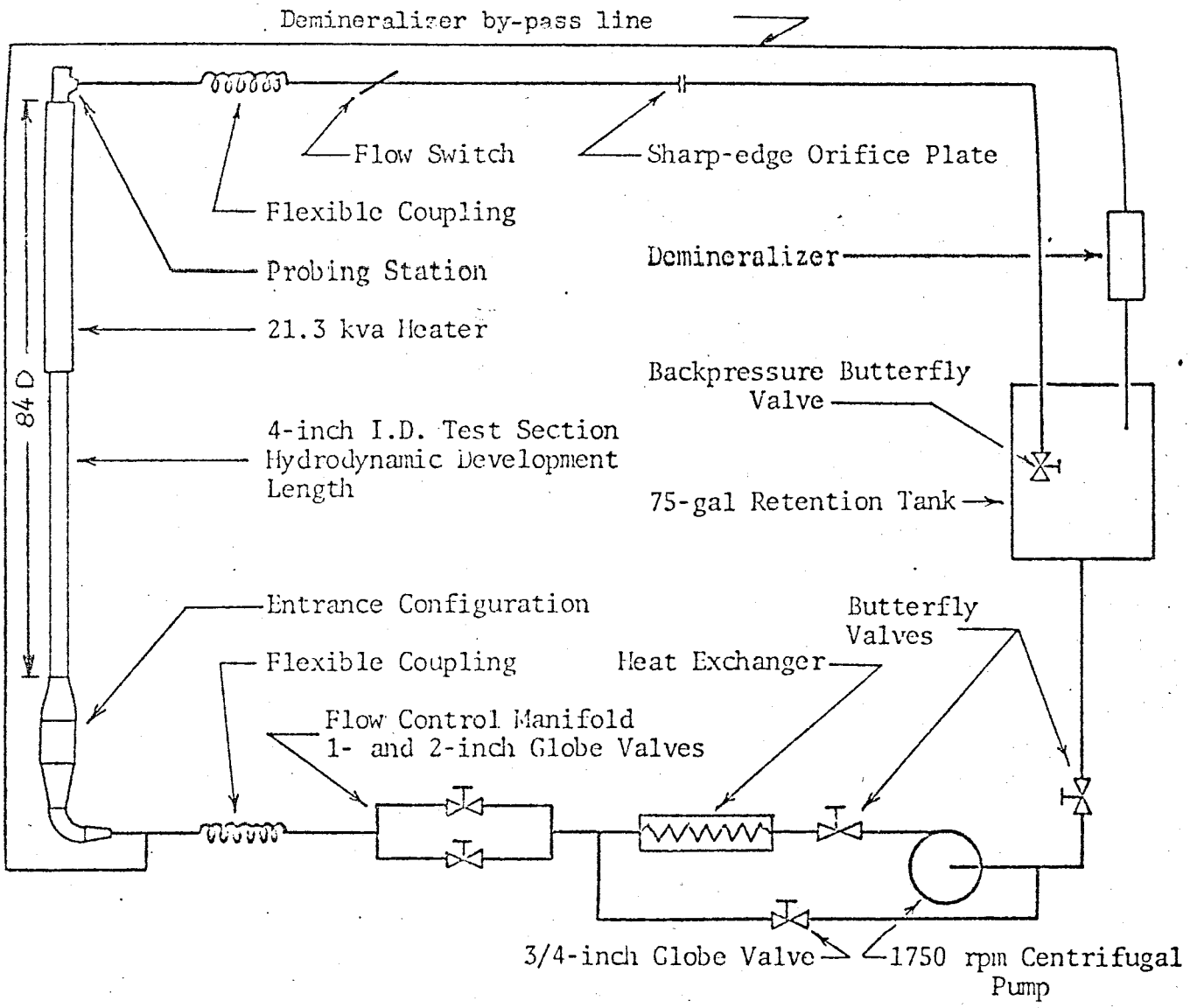

Figure 3.1-1: Turbulent Heat Transfer Loop Schematic

The fluid used in the experiments reported here was demineralized water to allow the use of uncoated hot film sensors. During all the runs part of the flow was continuously circulated through the demineralizer by-pass line in order to keep the water conductivity below 1 micromho/cm. Also all metal parts in contact with water were made of stainless steel.

A traversing mechanism was designed and built by Burchill (1970) to enter the test section from the top. This mechanism allowed radial traverse as well as axial positioning. (from the top down to a position 67.5 diameters from the test section entrance)

In the course of the present experimental research a special block to hold two probes (radial separation measurements) and an extra rod to hold another probe (axial separation measurements) were added to that mechanism. The block was designed and built to hold two probes separated by an adjustable distance. The distance between probes was set by using spacers of various sizes and was measured with an optical micrometer. The radial separation was then known within ± 0.005 in. The entire block with the two probes was then attached to the traversing mechanism.

For the axial separation measurements one probe was attached to the central moving rod in the traversing mechanism and the other one to the radially fixed rod. The axial separation was obtained by moving the radially fixed rod downstream. The separation between probes was determined by measuring the distance between a pointer and a fixed reference block with a ruler and was known within ± 0.01 in.

In Fig. 3.1-2 is shown schematically the upper portion of the test section illustrating relative probe positions for both radial and axial separation measurements.

The probe's separation and wall zero position were set before insertion into the test section in a calibration tube with the same inside diameter as

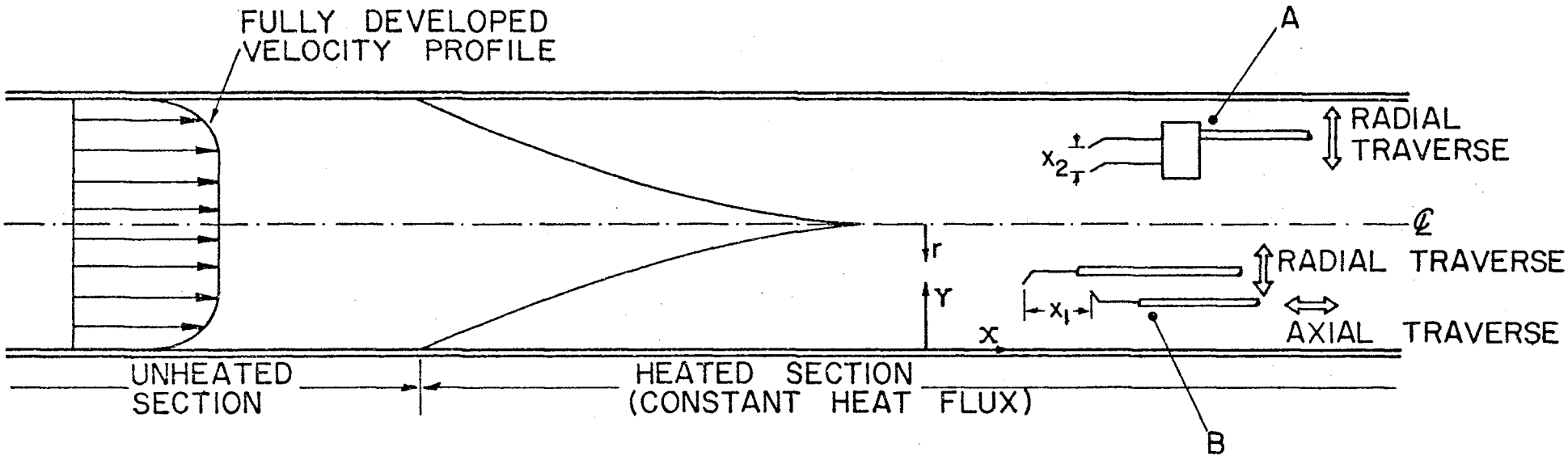

Figure 3.1-2: Test Section Illustrating Relative Probe Positions
A- Radial Separation Measurements
B- Axial Separation Measurements

the test section. The radial positioning inside the test section was obtained through a pair of high precision bevel gears which allowed radial location to be known to ± 0.001 in.

All velocity measurements reported in the present work were made under isothermal conditions with the flow rate and the water temperature set, respectively, at 56,590 pipe Reynolds number and 80° F.

All temperature measurements were taken with the same flow rate as the velocity ones and with a constant wall heat flux of 3820 BTU/hr ft^2. The exit bulk water temperature was kept at 80°F.

3.2 Measurement Instrumentation and Data Acquisition Techniques

Both velocity and temperature fluctuating signals were measured with uncoated hot film sensors made by Thermo-Systems, Inc. (TSI).

For the two-point two component velocity measurements two end flow 'x' probes (TSI 1241 AR-20 and/or TSI 1241-20) were used, thus requiring four channels of anemometry. The data acquisition system for that set of measurements is pictured schematically in Fig. 3.2-1. Each channel of anemometry was made up of:

- DISA Type 55D01 Anemometer
- DISA Type 55D10 Linearizer
- BAY LAB Model 5123 DC amplifier used as a low pass filter with a -3 db setting (-18 dB per octave decay) at 1 KHZ
- TSI model 1015C correlator used for AC coupling with cutoff frequency set at 0.1 HZ.

The four filtered signals were then recorded on magnetic tape on a SANGAMO 3564 FM Tape Recorder. The input signals were monitored with a 4-channel TEKTRONIX Model 5103N Oscilloscope. Another oscilloscope, TEKTRONIX Type 531A, was used for observing the recorded signals.

At each different separation and/or radial location a 10 minute recording

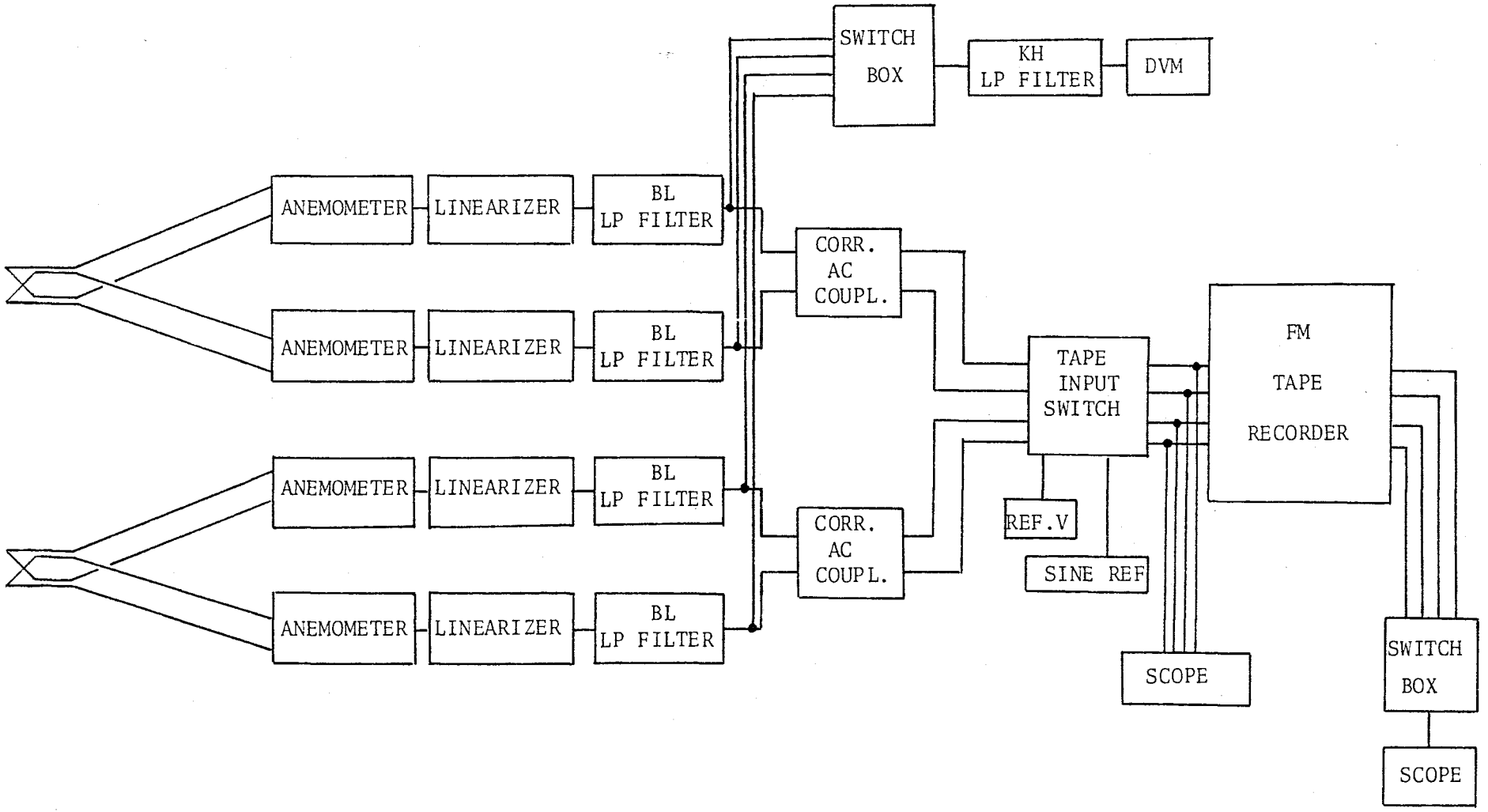

Figure 3.2-1: Two-Point 'X' Sensor Probes Instrumentation
(CTA Mode)

was made consisting of a 2 minute 100 Hz reference sine-wave, provided by a WAVETEK Model 110 function generator, and an 8 minute turbulence signal. The recording speed used was 3 3/4 ips, enough for a flat response from DC to 1.25 KHZ.

The velocity sensitivities of the sensors were determined, on line, by measuring the DC level of the linearized signals with a KROHN-HITE Model 3750 filter operating in the low pass mode (cutoff frequency .02-.1 HZ and -24 dB/ octave decay), and a DARCY Model 330 digital multimeter. These velocity sensitivites were determined by a least squares linear fit to the data consisting of DC output levels and the corresponding mass flow velocities as measured by the orifice plate. This calibration was performed several times (typically 5 times for an 8 point run) during the same experiment. This procedure was followed due to the need for a very accurate knowledge of the ratio between the sensitivities (S_A/S_B) of the two sensors in the same probe as shown in Section 3.3. The ratio S_A/S_B changed with time due to differences in the drift experienced by each sensor caused probably by deposition of microorganisms on the films. The average deviation in those ratios between two consecutive calibrations, for all runs, was ± 3.52% (with peaks of approx. ± 10.5%). In Fig. 3.2-2 are presented typical velocity calibration curves for one of the sensors in an 'X' probe, showing the effect of drift.

For the two-point temperature measurements, with both radial and axial separations, two single-sensor probes (TSI 1210-20 and/or TSI 1210BV-20) were used. The data acquisition system for those sets of measurements is pictured schematically in Fig. 3.2-3. Each channel of anemometry was made up of:

- DISA Type 5501 Anemometer operating in the Constant Current Mode (CCA) in which the hot film sensors act as resistance thermometers and respond only to temperature changes.
- BAY LAB Model 5123 DC Amplifier used to DC offset the temperature signal and as a low pass filter with a -3 db setting (-18 dB/octave decay) at 1 KHZ.

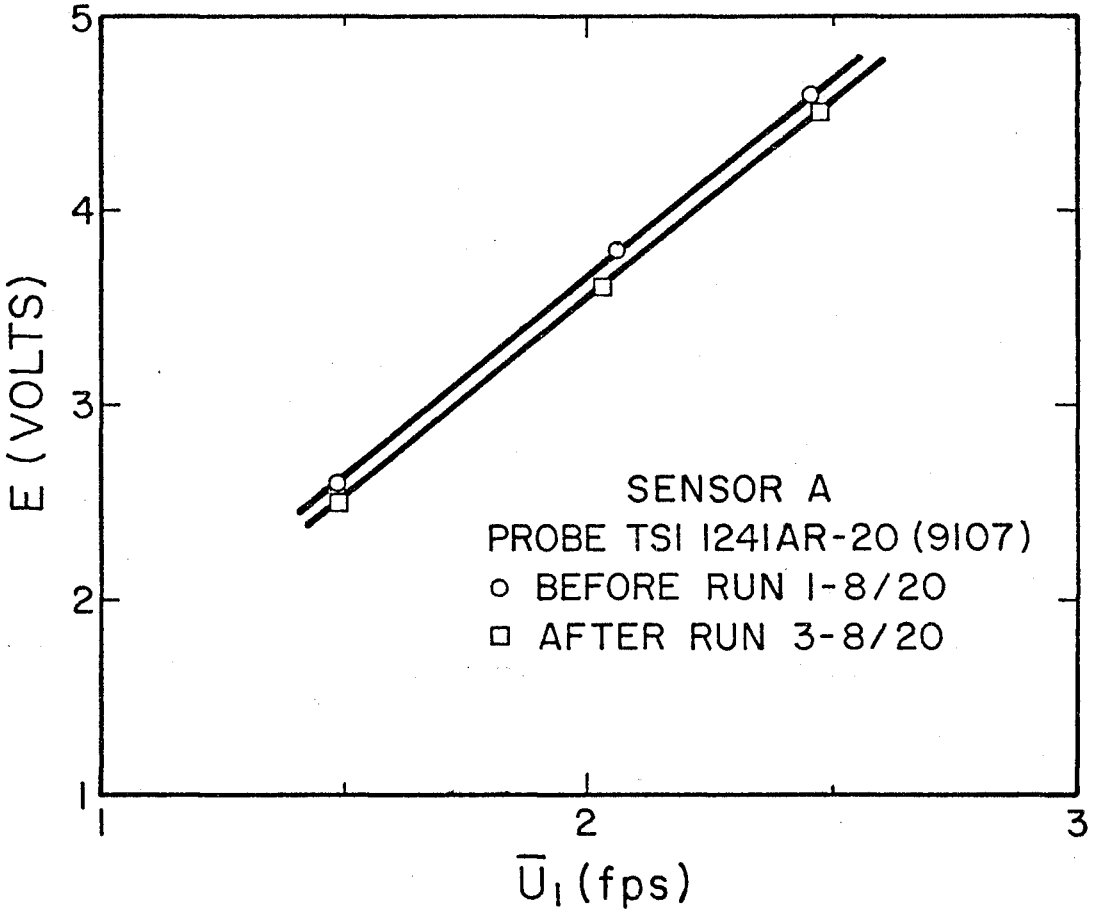

Figure 3.2-2: Typical Velocity Calibration Curves

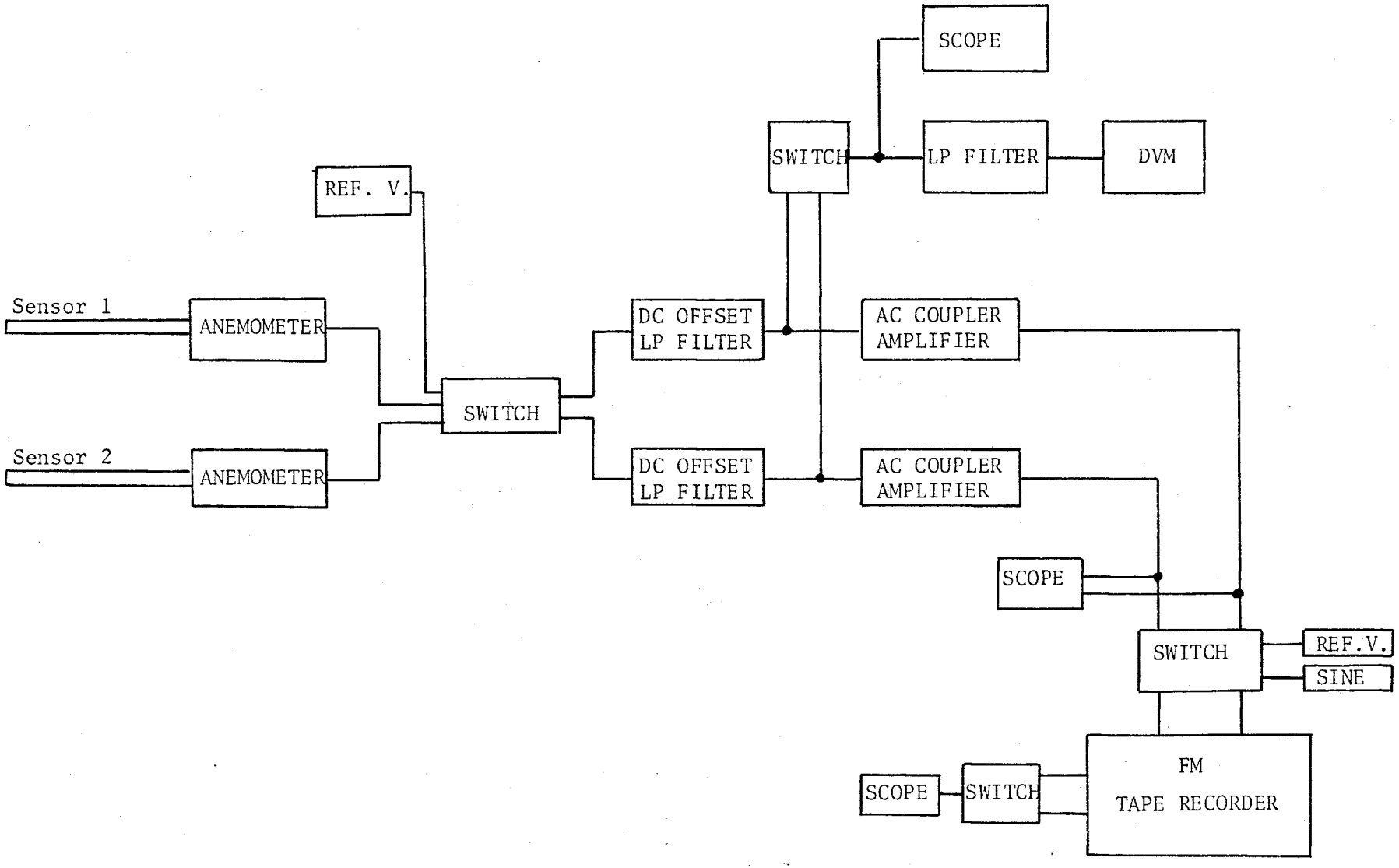

Figure 3.2-3: Two-Point Single Sensor Probes Instrumentation
(CCA Mode)

- TSI Model 1015C correlator used for AC coupling with cutoff frequency set at 0.1 HZ (-18 dB/octave decay) and signal amplifier with a calibrated gain of x10.

The mean temperature variation with location was observed as tenths of a volt change in the DC level of the output signal. In order to get the best accuracy in these measurements a 10-10.5 volts signal output size was chosen, the DC offset in the BAY LAB amplifier was set to -9.50 volts (maximum available -10 volts) and the most sensitive scale of the DVM (DARCY Model 330 digital multimeter) was used. The 10-10.5 volts signal size was chosen due to the anemometer output amplifier characteristics. Below 10 volts the gain decreases. Above that the amplification would be very flat but the remaining BV-DC (Bridge Voltage minus DC offset) level would be too large for the DVM scale used. Two 5.4 volts mercury cells in series were used to check the stability of the DC offset in the BAY LAB amplifier. As before the two filtered signals were then recorded on a magnetic tape.

The temperature sensitivity for each sensor was obtained by a least squares linear fit to the data consisting of DC output levels and the corresponding exit bulk temperature as measured by the exit thermocouple under isothermal conditions. This calibration was done for each run and observed to be very stable. In Fig. 3.2-4 is shown a typical CCA calibration curve.

The data acquisition system used for the two-point axial separation, axial velocity measurements is pictured in Fig. 3.2-5. The modes of operation for the various instruments were identical to the ones used for the transverse separation velocity measurements.

For the axial separation measurements, of both axial component of the velocity and temperature, a compensation procedure was used to account for interference effects on the signal from the downstream probe. That was accomplished by the usual offsetting technique suggested by Corsin-Comte Bellot

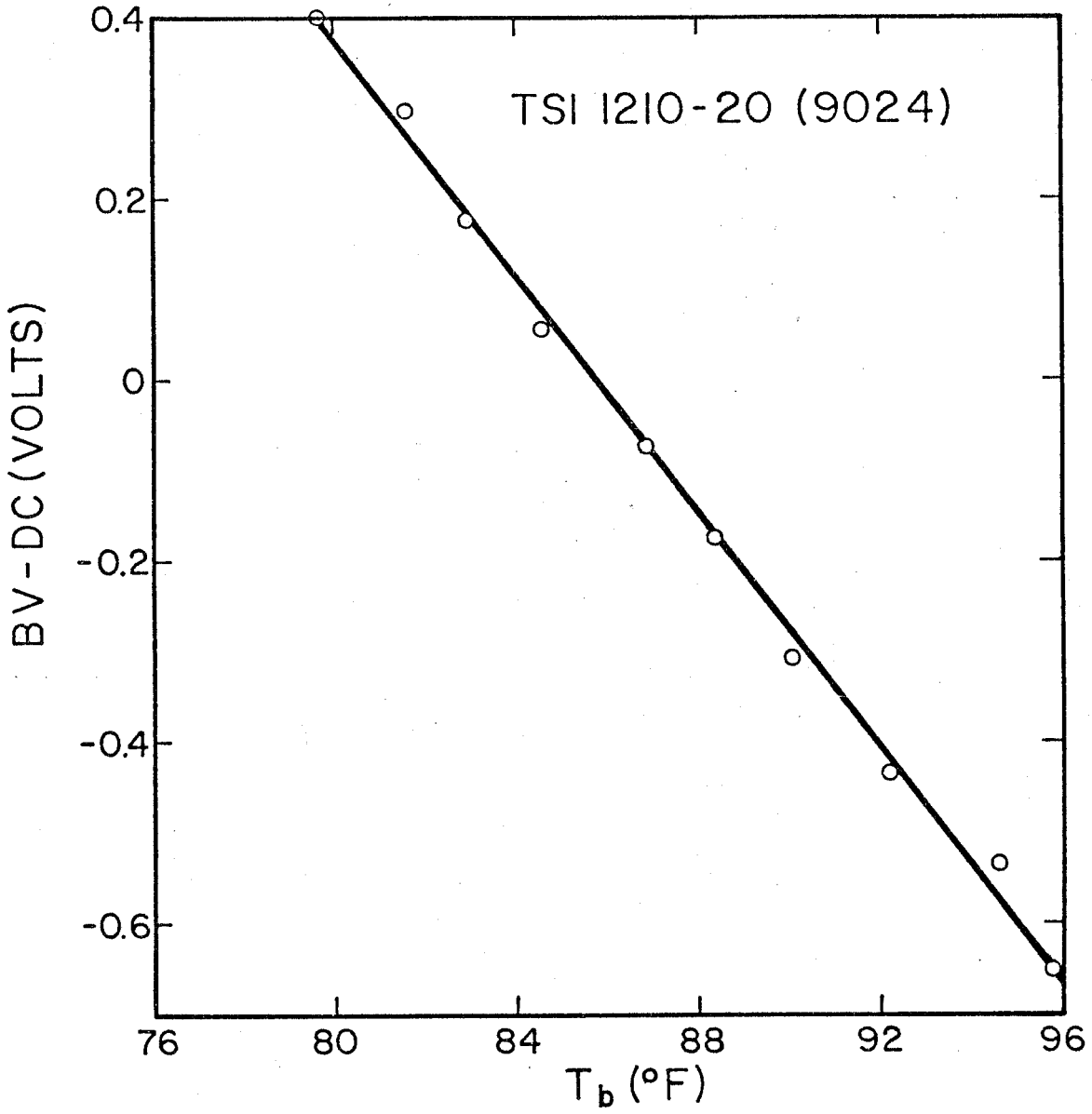

Figure 3.2-4: Typical CCA Calibration Curve

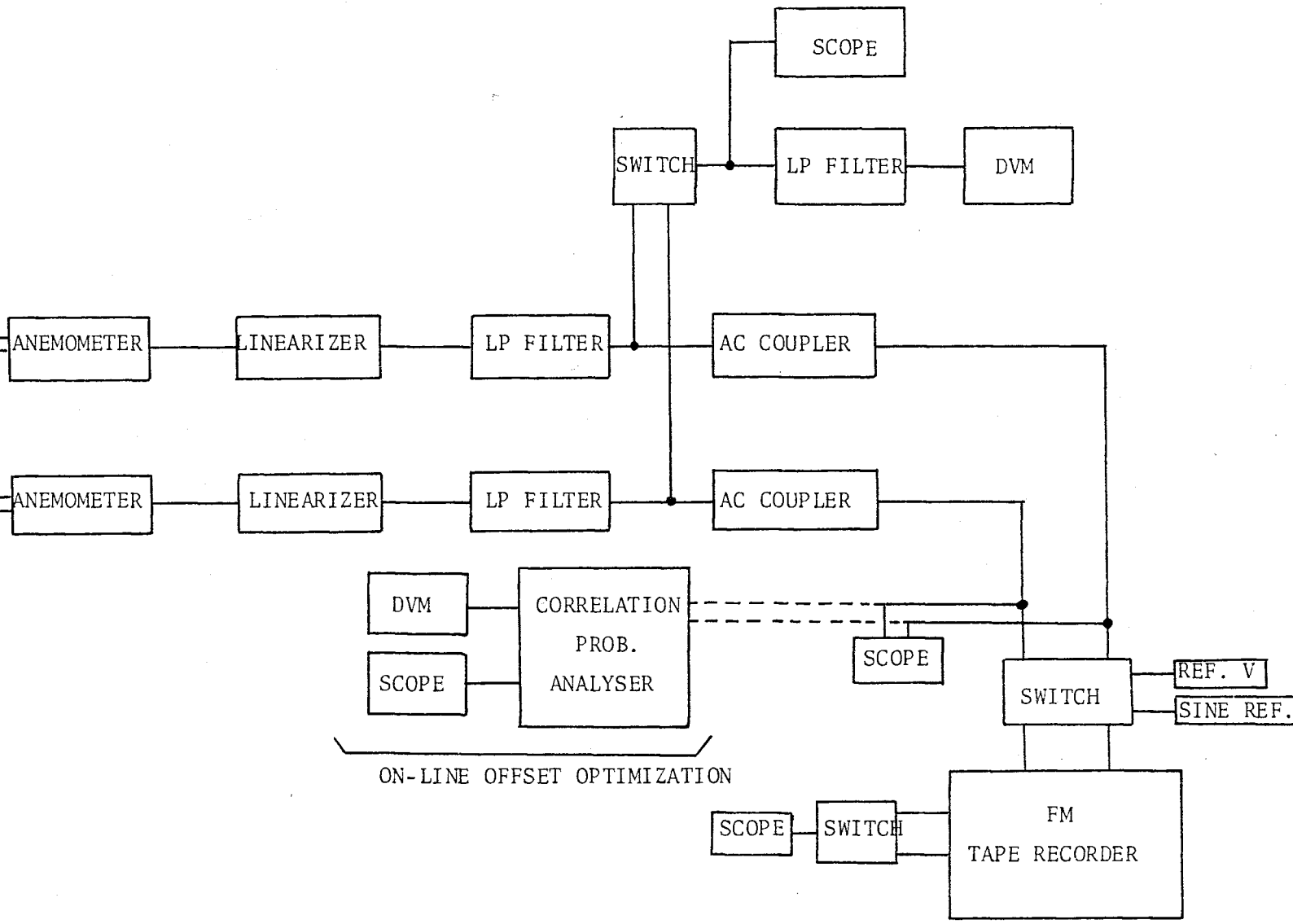

Figure 3.2-5: Two-Point Single Sensor Probes Instrumentation (CTA Mode)

(1971) and used by Planchon (1974), Howard (1974) and others.

Before recording each data point an optimization with respect to radial offset was made by running the signals, on line, through the Correlation and Probability Analyser and cross-correlating them (Fig. 3.2-5). The correlation coefficients when plotted against the radial offsets, for each axial separation, produced curves as shown in Fig. 3.2-6. The recording of the fluctuating signals for later off-line processing was then made with an offset corresponding to the point where the magnitude of the cross-correlation began to show no significant effect of the wake of the upstream sensor. Similar curves were obtained in the two-point axial separation velocity measurements and the same optimization procedure was followed.

Another "interference" was also observed in the temperature measurements. In Fig. 3.2-7, again correlation coefficients are plotted versus radial offsets but for two different probe arrangements (A and B). In case A besides the expected wake interference effect, evident by the existence of an offset peak, we can also see some sort of "shielding" effect due to the position of the upstream probe body between the downstream sensor and the wall. No attempt was made to explain in detail that effect and throughout all the measurements configuration B was always used.

3.3 Data Analysis Systems and Techniques

The fluctuating signals, recorded for both the two single sensor (temperature and axial velocity) and the two point 'X' probe measurements, were processed with a TSI 1065A Digital Correlation and Probability Analyser.

Figure 3.3-1 shows pictured schematically the data processing instrumentation for the two-point, two-component, velocity measurements. The four tape recorder output signals were monitored with a 4-channel Tektronix Model 5103N Oscilloscope. In order to extract from those signals the axial and the normal components of the fluctuating velocity two TSI Model 1015C

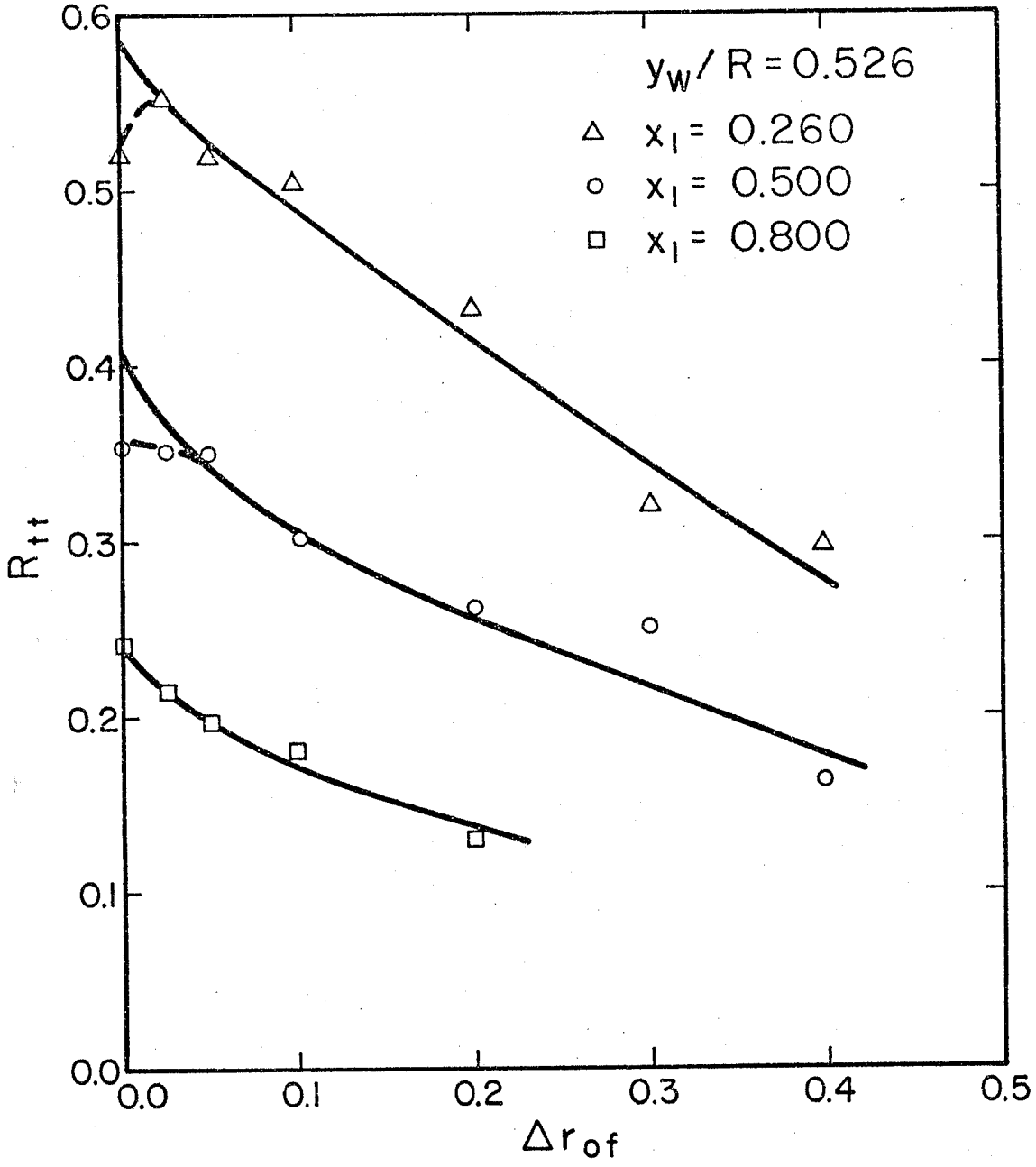

Figure 3.2-6: Radial Offset Optimization-Two-Point Axial Separation Temperature Measurements

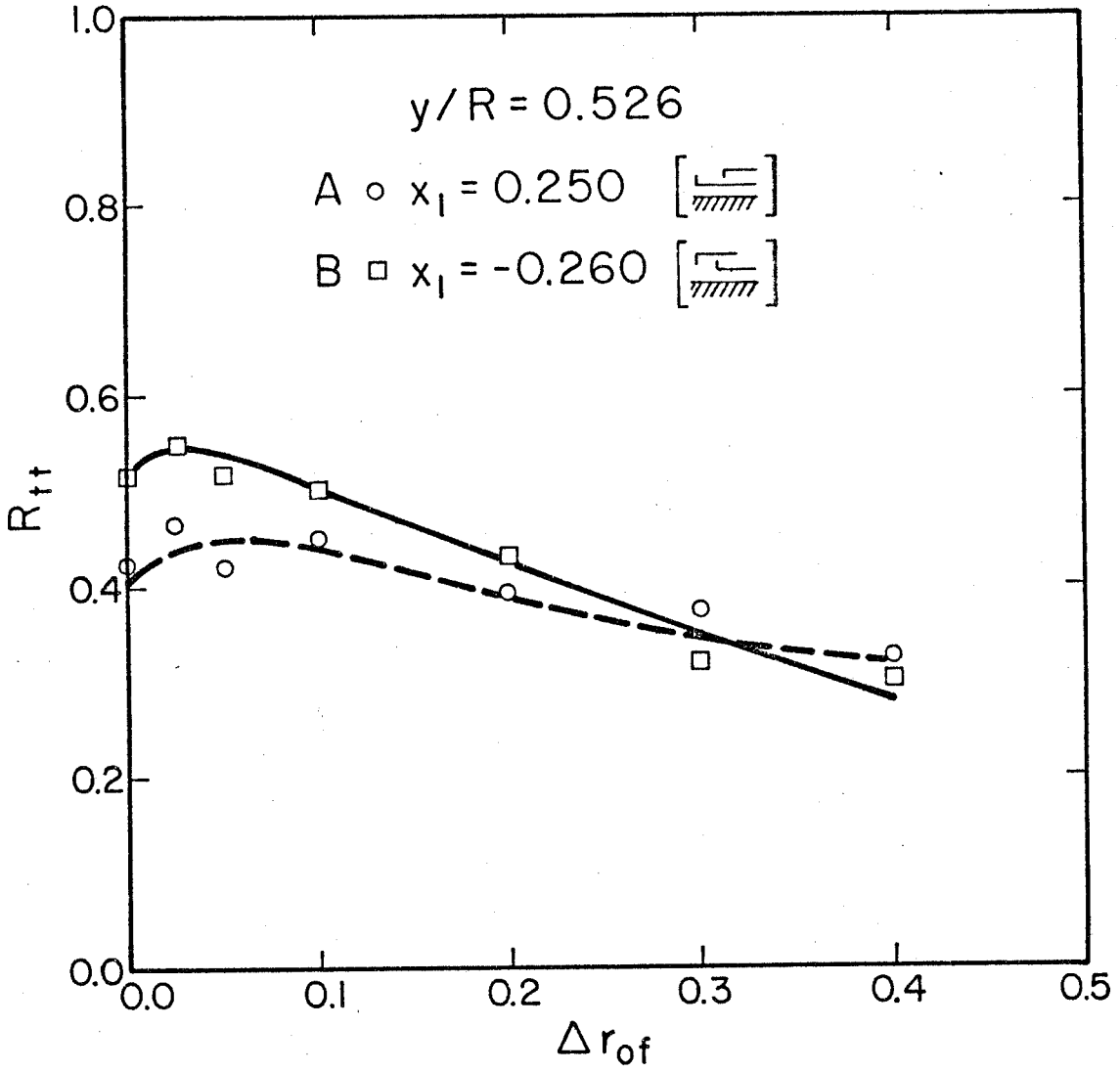

Figure 3.2-7: Probe Body Interference-Two-Point Axial Separation Temperature Measurements

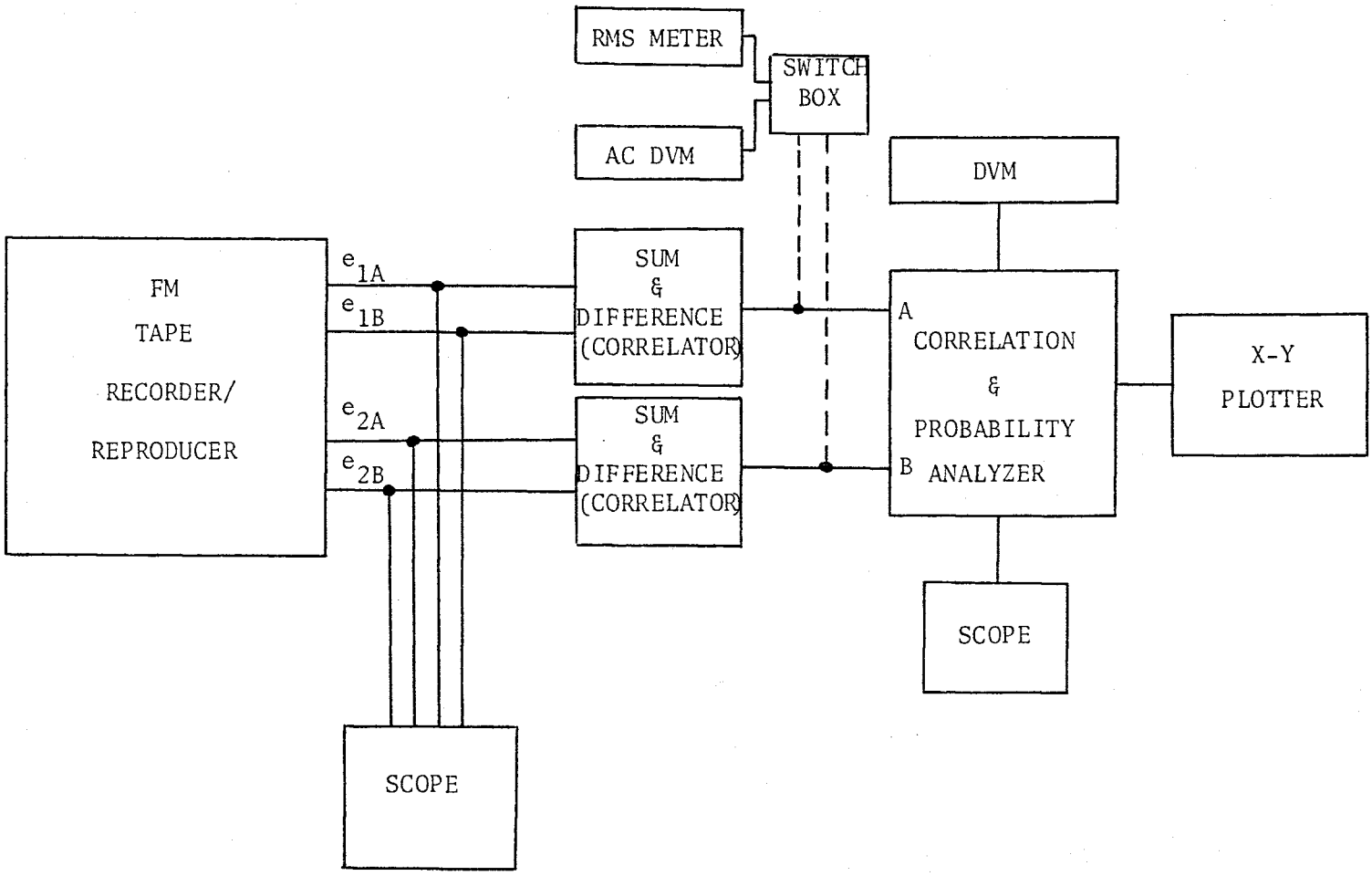

Figure 3.3-1: Two-Point 'X' Sensor Probe Signals Processing Instrumentation

Sum and Difference Correlators were used between the Tape Recorder and the Analyser. If e_{A_1}, and e_{A_2} are the signals from the two sensors in the 'X' probe located at point A, we have

$$e_{A1} = S_{A_1}(u_1 + u_2)_A \tag{3.3-1}$$

$$e_{A_2} = S_{A2}(u_1 - u_2)_A \tag{3.3-2}$$

With an appropriate adjustment of the input gains (G_{A_1}, G_{A_2}) in the 1015C correlator and by operating it in the sum (difference) mode we can generate an output signal proportional to the u_1 (u_2) component of the fluctuating velocity as follows

$$G_{A_1}e_{A_1} \pm G_{A_2}e_{A_2} = \left(G_{A_1}S_{A_1} \pm G_{A_2}S_{A_2}\right)u_{1,A} + \left(G_{A_1}S_{A_1} \mp G_{A_2}S_{A_2}\right)u_{2,A} \tag{3.3-3}$$

If $$G_{A_1}S_{A_1} = G_{A_2}S_{A_2} = S_A \tag{3.3-4}$$

Then $$G_{A_1}e_{A_1} + G_{A_2}e_{A_2} = 2S_A u_{1,A} \tag{3.3-5}$$

$$G_{A_1}e_{A_1} - G_{A_2}e_{A_2} = 2S_A u_{2,A} \tag{3.3-6}$$

The same procedure can be applied to the 'X' probe placed at point B. Equation (3.3-4) shows the importance of the accurate knowledge of the ratio between the velocity sensitivities for the two sensors in an 'X' probe. This justifies the procedure of several checks on calibration coefficients, mentioned in Section 3.2, during the same experimental run.

For the single sensor measurements (axial velocity and temperature) the instrumentation used was the same as shown in Fig. 3.3-1, the only difference being the mode of operation of the 1015C. For single sensor

signals they were used only as AC couplers.

The pre-processed signals were then passed to the 1065A Analyser which, after sampling and digitizing them, produced and stored in 100 bins product type sums for auto and cross-covariances as functions of delay time. A hard copy output for those covariances was obtained by plotting them on a Houston Model 2000 X-Y plotter. In addition to this output the zero lag time and peak values were read on a Hewlett Packard Model 34702A Digital Multimeter.

The 1065A Analyzer can digitize signals with 100 mV RMS (sine wave) to an accuracy of one part in 256. In order to bring the input signals to this operational range, attenuation controls are provided in the front panel of the instrument. The proper setting of these controls is very important since if the attenuation is too high, the resolution is poor; if it is too low, a significant part of the signal can be lost. The setting of the input attenuators was then made by running the Analyser in the probability density function (PDF) mode. In this mode of operation a PDF centered about the center bin (49) is generated. The attenuators were then set so that bin (0)/ bin (49) $\approx$ 0.25 which would indicate that had the signals been Gaussianly distributed, less than 10% of the signal would have been clipped off.

The cross covariances were normalized with the square roots of the zero time delay auto-covariances to generate the correlation functions shown in Chapters 4 and 5. For example, for the axial component of the fluctuating velocity at points A and B, we have,

$$C_{1_A 1_B}(\tau) = K_A K_B \, \overline{u_{1_A}(t) u_{1_B}(t+\tau)} \qquad (3.3\text{-}7)$$

for the cross covariance, and

$$C_{1_A 1_A}(\tau) = K_A^2 \, \overline{u_{1_A}(t) u_{1_A}(t+\tau)} \qquad (3.3\text{-}8)$$

and

$$C_{1_B1_B}(\tau) = K_B^2 \, \overline{u_{1_B}(t)\, u_{1_B}(t+\tau)} \qquad (3.3\text{-}9)$$

for auto-covariances. K_A and K_B are Analyser operational constants, dependent upon the attenuation settings. For the correlation function we have

$$R_{1_A1_B}(\vec{x};\tau) = \frac{C_{1_A1_B}(\tau)}{\left[C_{1_A1_A}(0)\, C_{1_B1_B}(0)\right]^{1/2}} \qquad (3.3\text{-}10)$$

with $\vec{x}$ being the separation vector between points A and B.

For the axial separation measurements, for both velocity and temperature, a radial offsetting procedure was used to account for interference effects on the signal from the downstream probe as outlined in Section 3.2. For those measurements after the normalization was made, a correction factor was applied to the correlation functions corresponding to small separations. The offset correction factors (OCF) were obtained from on-line correlation measurements as shown in Fig. 3.2-6 and defined as

$$\text{OCF} = \frac{\text{(zero offset extrapolated correlation value)}}{\text{(value at the offset used for recording)}}$$

Table 3.3-1 presents a typical set of correction factors.

Subsequent digital analysis of the correlation functions was done on an IBM 360/75 Digital computer, via a time sharing system (initially PLORTS and later DEC-10 systems). Those systems allowed programs as well as data to be stored on magnetic disks and handled through an accoustic telephone link and a teletype terminal. This procedure was also used during the experiments to calculate calibration coefficients and operational constants for the instruments.

	y/R	x_1/R	OFFSET (in)	OCF
VELOCITY		0.125	0.025	1.089
	0.772	0.250	0.025	1.076
		0.400	0.050	1.099
TEMPERATURE	0.787	0.130	0.025	1.102
		0.255	0.050	1.163

Table 3.3-1

Offset Correction Factors for Axial Separation Correlation Functions

4. VELOCITY FIELD RESULTS

4.1 One-point Intensity and Mean Velocity Distributions

Mean velocity measurements were taken with a single sensor probe under isothermal conditions at a section 80 diameters from the test section entrance, thus providing fully developed conditions at that location. These results are presented in Fig. 4.1-1 in dimensionless form

$$U^+ = \frac{\overline{U}}{U_\tau} \tag{4.1-1}$$

with the shear velocity defined by

$$U_\tau = \left(\frac{f U_b^2}{2}\right)^{1/2} \tag{4.1-2}$$

The dimensionless wall distance is given by

$$y^+ = \frac{y U_\tau}{\nu} \tag{4.1-3}$$

By using Blasius' law of friction (see Schilichting (1968)) (4.1-2) is modified to read

$$U_\tau = .1989 \left(\frac{\nu}{D}\right)^{1/8} U_b^{7/8} \tag{4.1-4}$$

which was used in the course of the present research. Also in Fig. 4.1-1 a comparison is made between the present data and two well known correlations, namely

$$U^+ = 5.5 + 5.75 \log y^+ \tag{4.1-5}$$

suggested by Nikuradse (see Knudsen and Katz (1958)) and

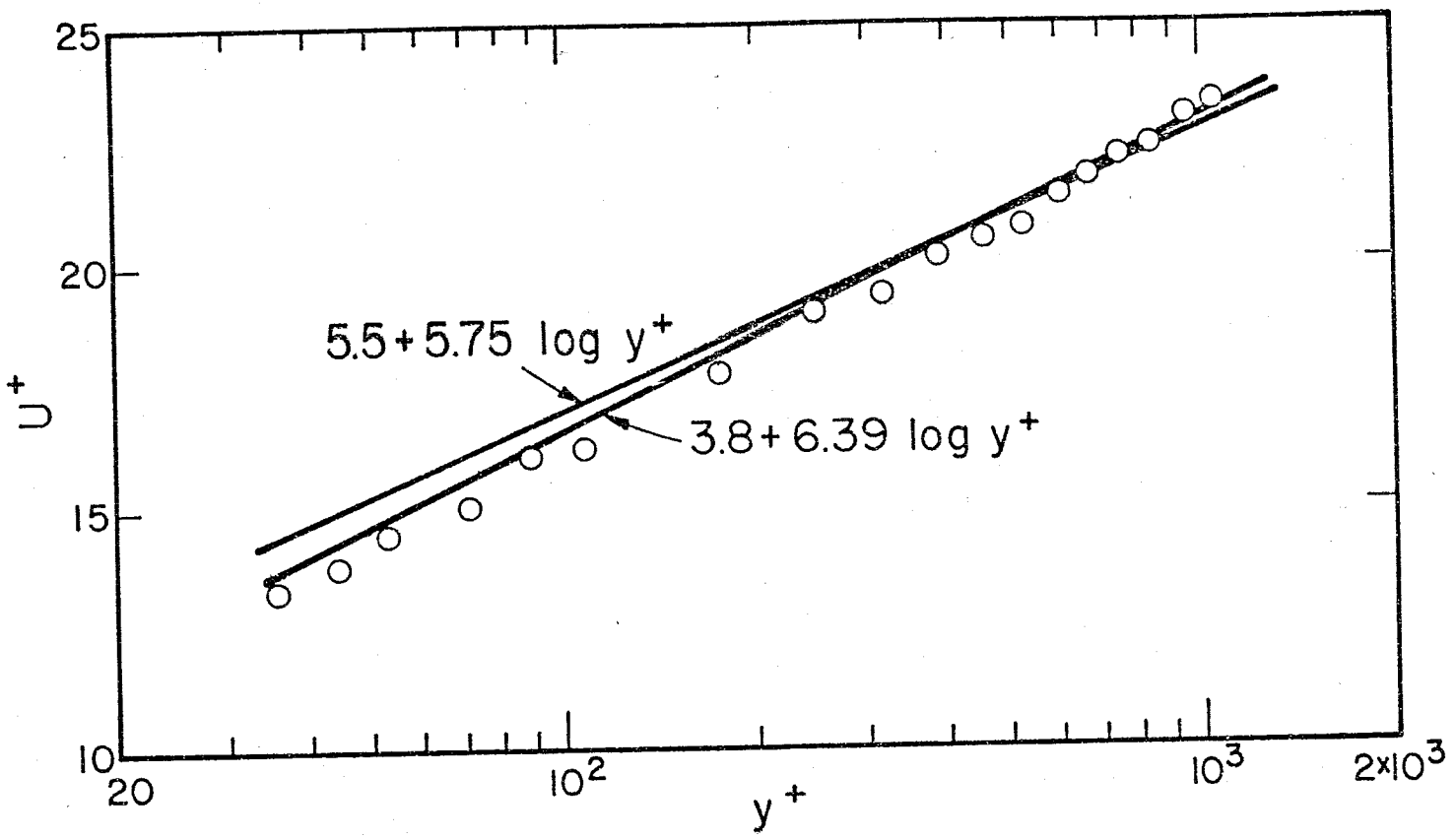

Figure 4.1-1: Mean Velocity Profiles
Re = 56,590

$$U^+ = 3.8 + 6.39 \log Y^+$$

proposed by Deissler (1951). The best agreement is obtained with Deissler's relation. Burchill (1970) has reported the same conclusion with his measurements in the same loop.

Single-point normalized velocity intensities, for both axial and normal components, are presented in Figs. 4.1-2 and 4.1-3, along with experimental results reported by Burchill (1970), Laufer (1954) and Sabot and Comte-Bellot (1974). In the present study these single point measurements were not taken very near the wall so that the normal decrease of the intensities in this region was not observed.

4.2 Two-Point Velocity Field Structure

Following the procedures previously outlined for two-point data acquisition and processing techniques, two groups of experiments were conducted, namely, two-point transverse separation measurements with 'x' probes and two-point axial separation with single sensor measurements. For all runs the flow rate was set such as to give a pipe Reynolds number of 56,590 and the water temperature was kept approximately constant and equal to 80°F, with an average deviation of less than 0.8%. In Figs. 4.2-1 and 4.2-2 space-time correlations are presented for the axial component of the velocity obtained, respectively, from transverse and axial separation measurements.

Integral time-scales in the convected frame for the axial velocity component were calculated by a least squares exponential fit to the envelope of the space-time curves at all axial separations (Fig. 4.2-2). These results are presented in Table 4.2-1, together with estimated values of the time scales for the normal component of the velocity obtained by using the ratios between these scales as reported by Sabot and Comte Bellot (1974).

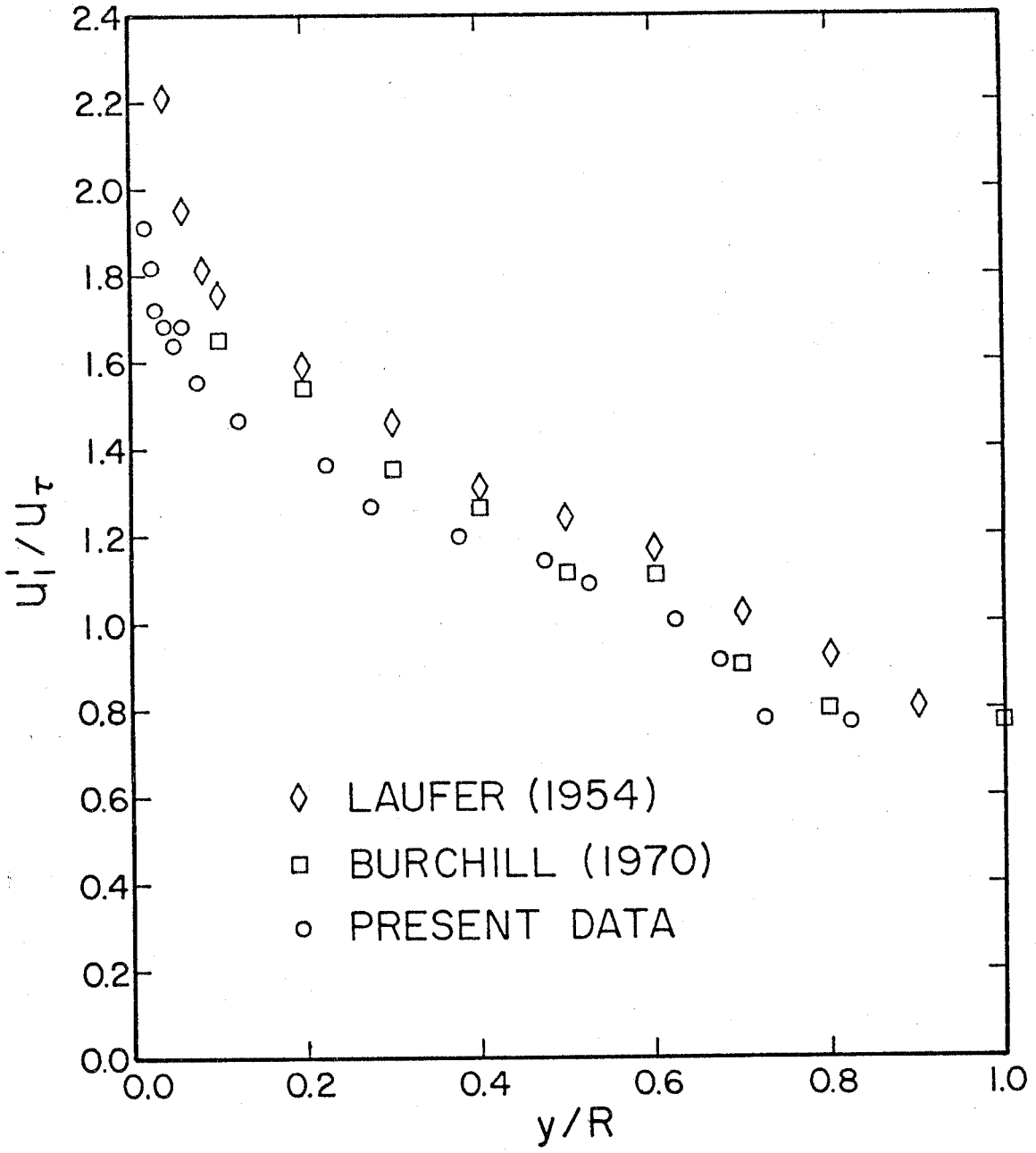

Figure 4.1-2: Normalized Intensities of the Axial Velocity Component

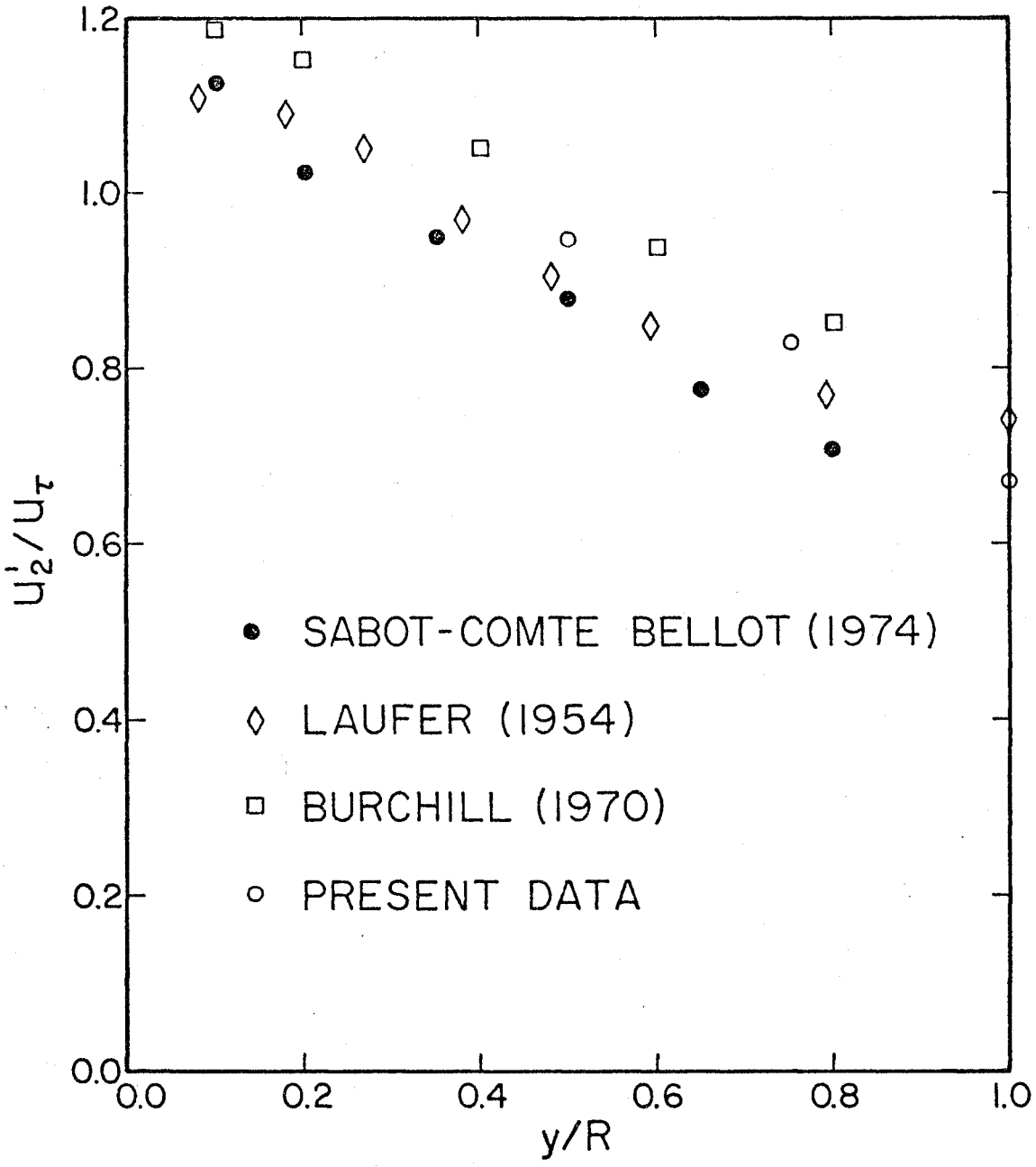

Figure 4.1-3: Normalized Intensities of the Normal Velocity Component

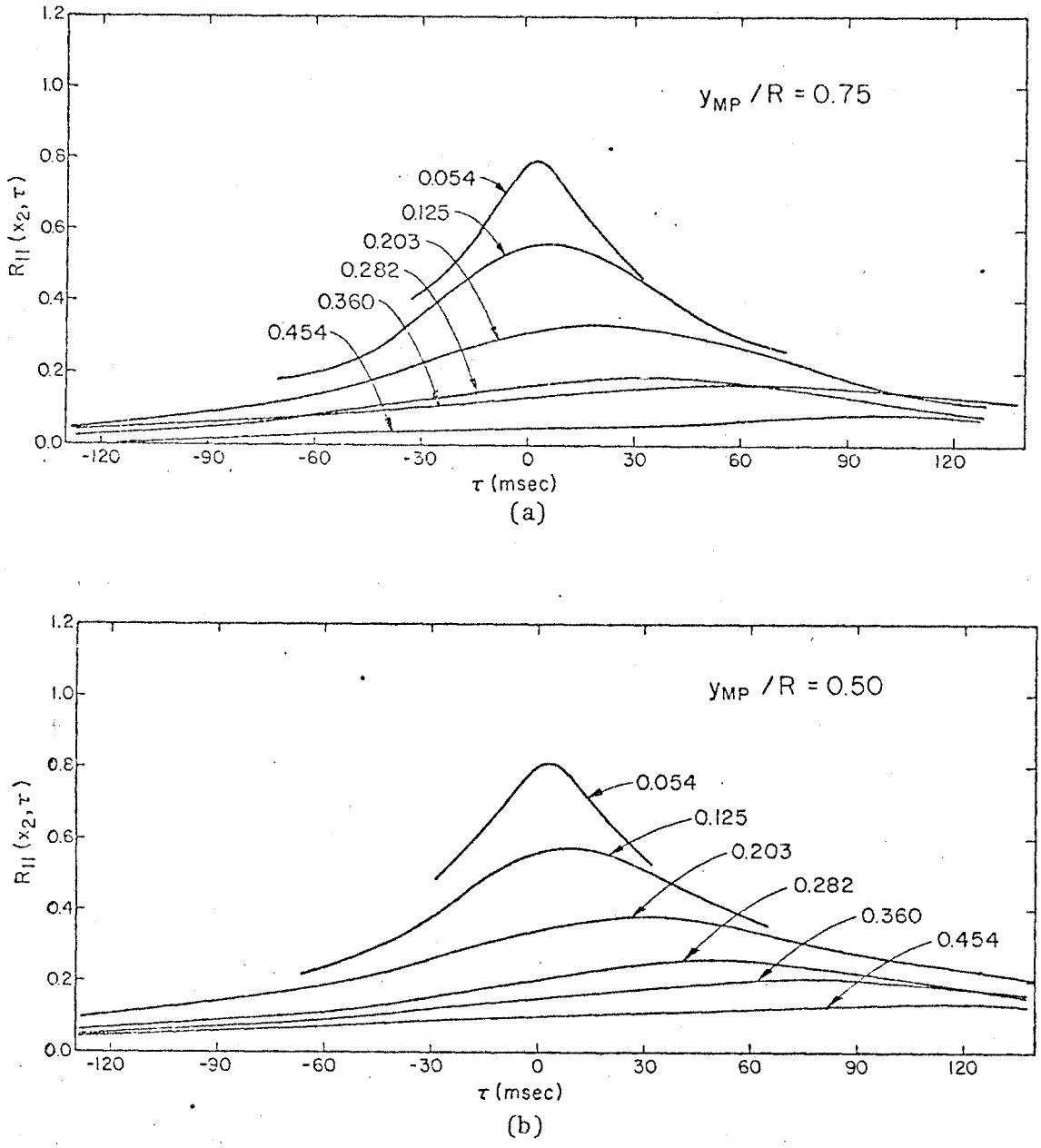

Figure 4.2-1: Space-time Correlations - Axial Velocity Component, Transverse Separations

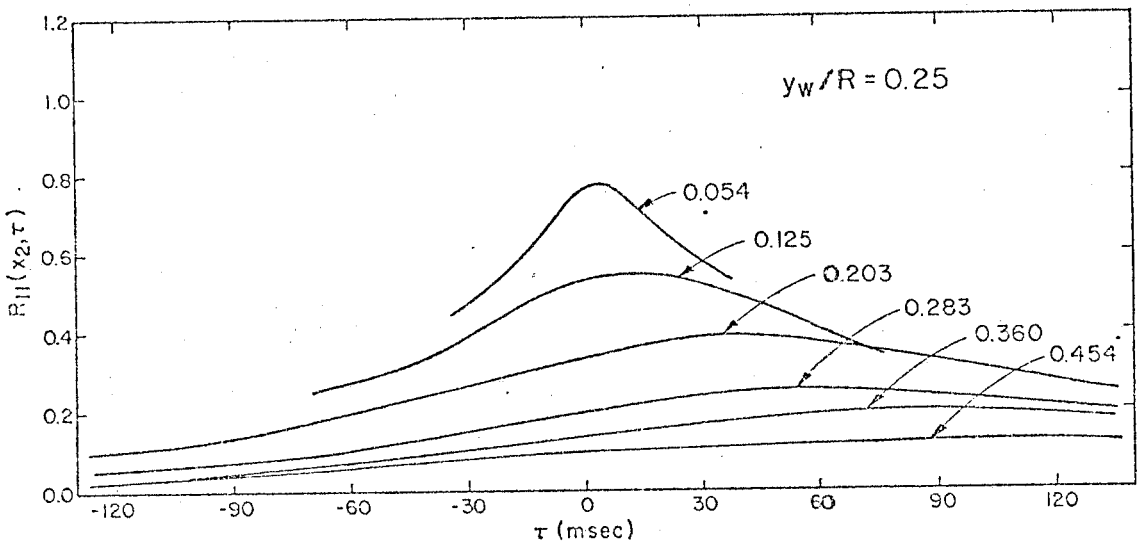

(c)

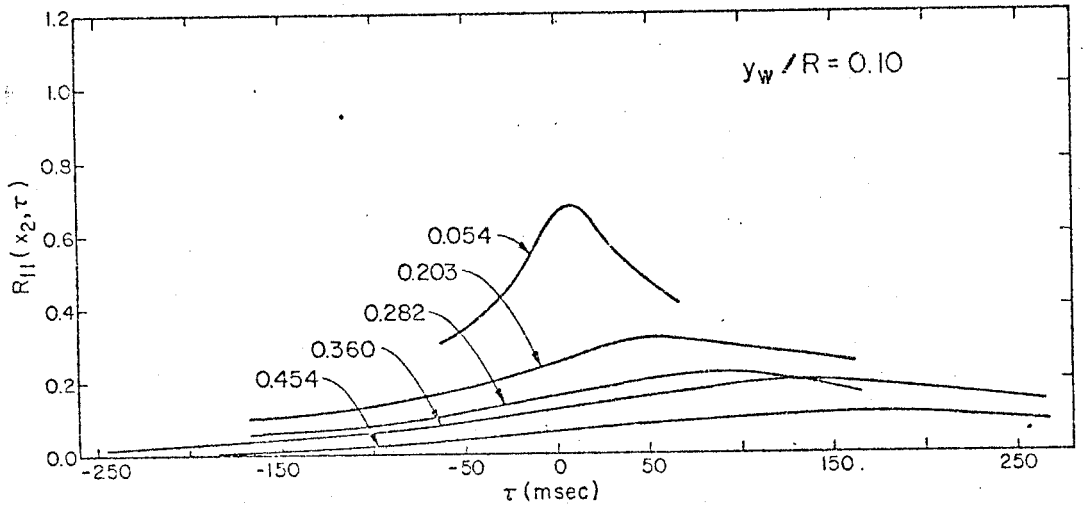

(d)

Figure 4.2-1

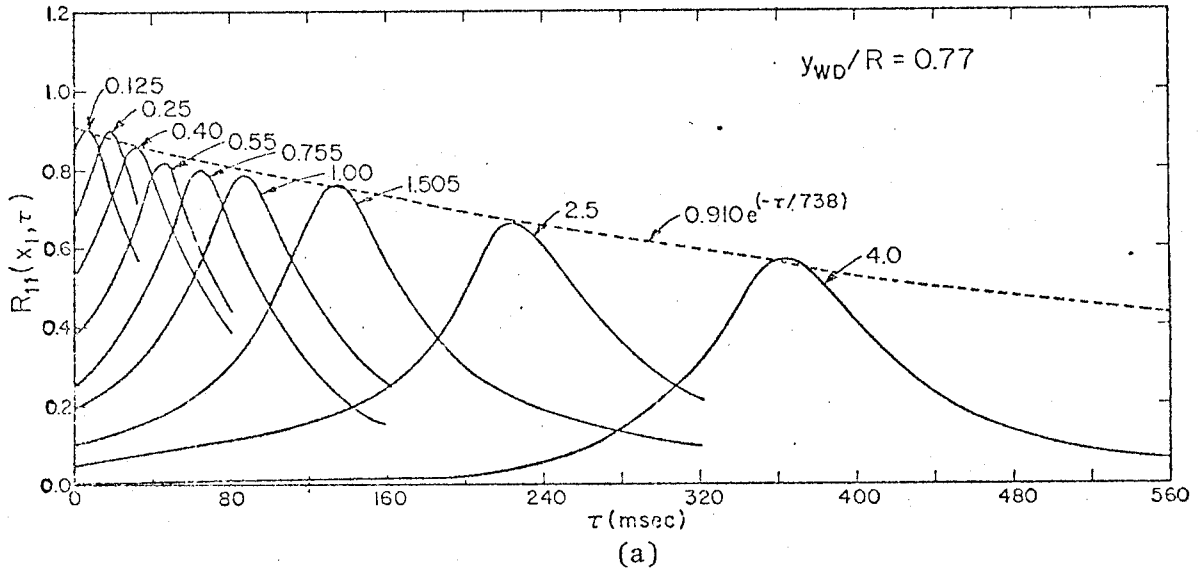

(a)

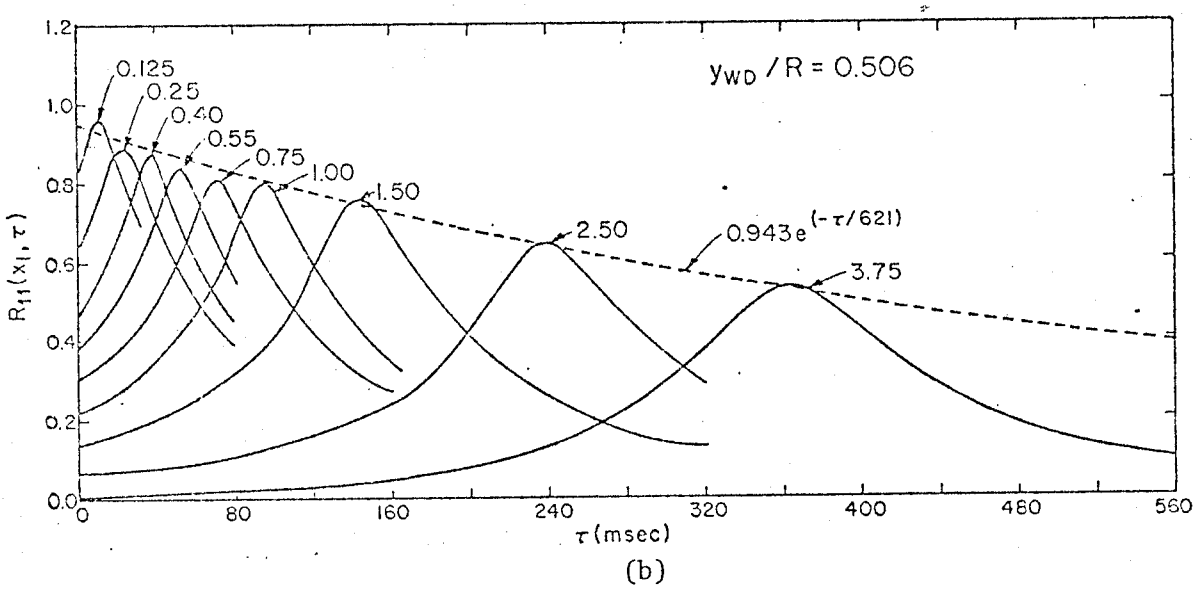

(b)

Figure 4.2-2: Space-time Correlations - Axial Velocity Component, Axial Separations

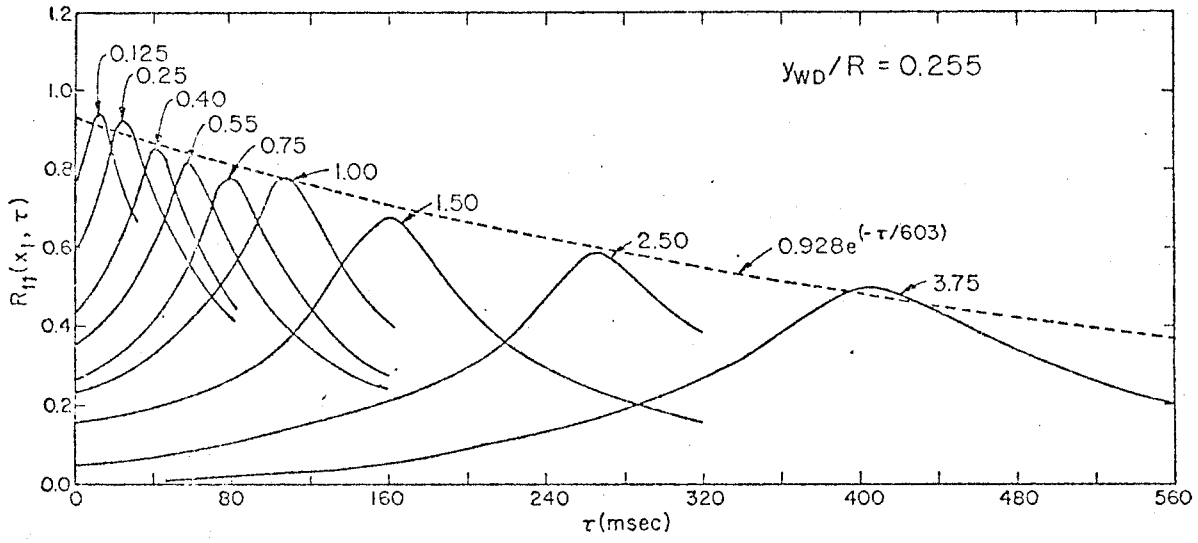

(c)

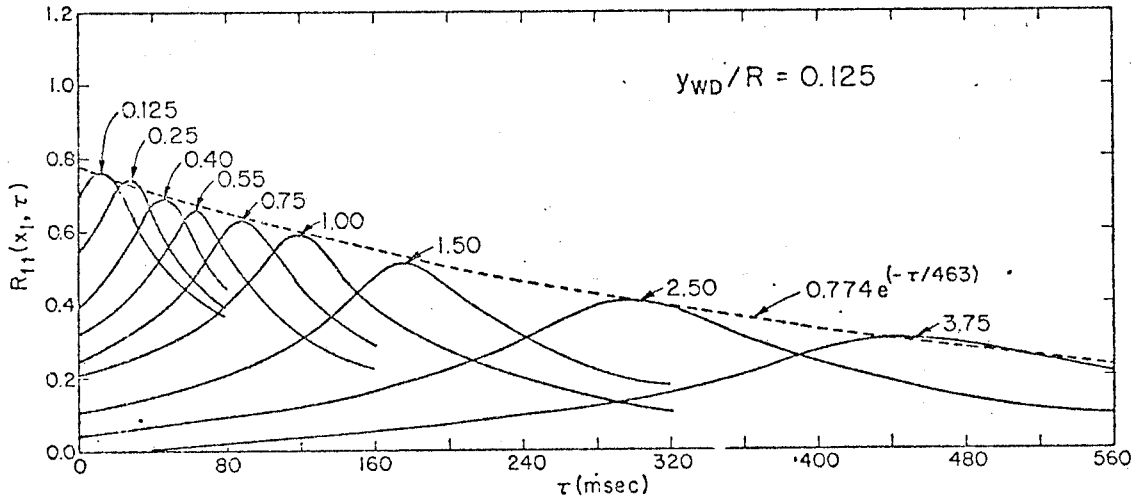

(d)

Figure 4.2-2

Y/R	$\mathcal{J}_{11}^{(1)}$ (msec)	$\mathcal{J}_{22}^{(1)}$ (est) (msec)
0.75	668	227
0.50	585	133
0.25	560	88
0.10	358	43

Table 4.2-1: Integral Time-Scales in the Convected Frame

In Figs. 4.2-3 through 4.2-5 are presented space-correlation results from x_2-separation measurements for, respectively, axial velocity component, normal velocity component and shear coefficients. The correlation curves $R_{11}(o,x_2)$ and $R_{22}(o,x_2)$ were then integrated to yield the integral length scales shown in Figs. 4.2-6 and 4.2-7. In these figures it is clear that depending upon the way the correlation functions are integrated (or the two-point measurements taken) different results are obtained for the length scales. In both figures open symbols were used whenever the integral length scales were calculated as

$$L_{ii}^{(2)}(y) = \int_0^{x_{2_o}} R_{ii}\left[\left(y - \frac{x_2}{2}\right),\left(y + \frac{x_2}{2}\right)\right] dx_2 \qquad (4.2\text{-}1)$$

For the dark symbols the scales were given by

$$L_{ii}^{(2)}(y) = \int_0^{x_{2_o}} R_{ii}\left[y, y + x_2\right] dx_2 \qquad (4.2\text{-}2)$$

with x_{2_o} being the first zero crossing of the correlation function. In both (4.2-1) and (4.2-2) the argument of R_{ii} indicates the positions of the two 'X' probes when the two-point measurements were taken. This effect of the way the experimental data are treated has been generally overlooked in the

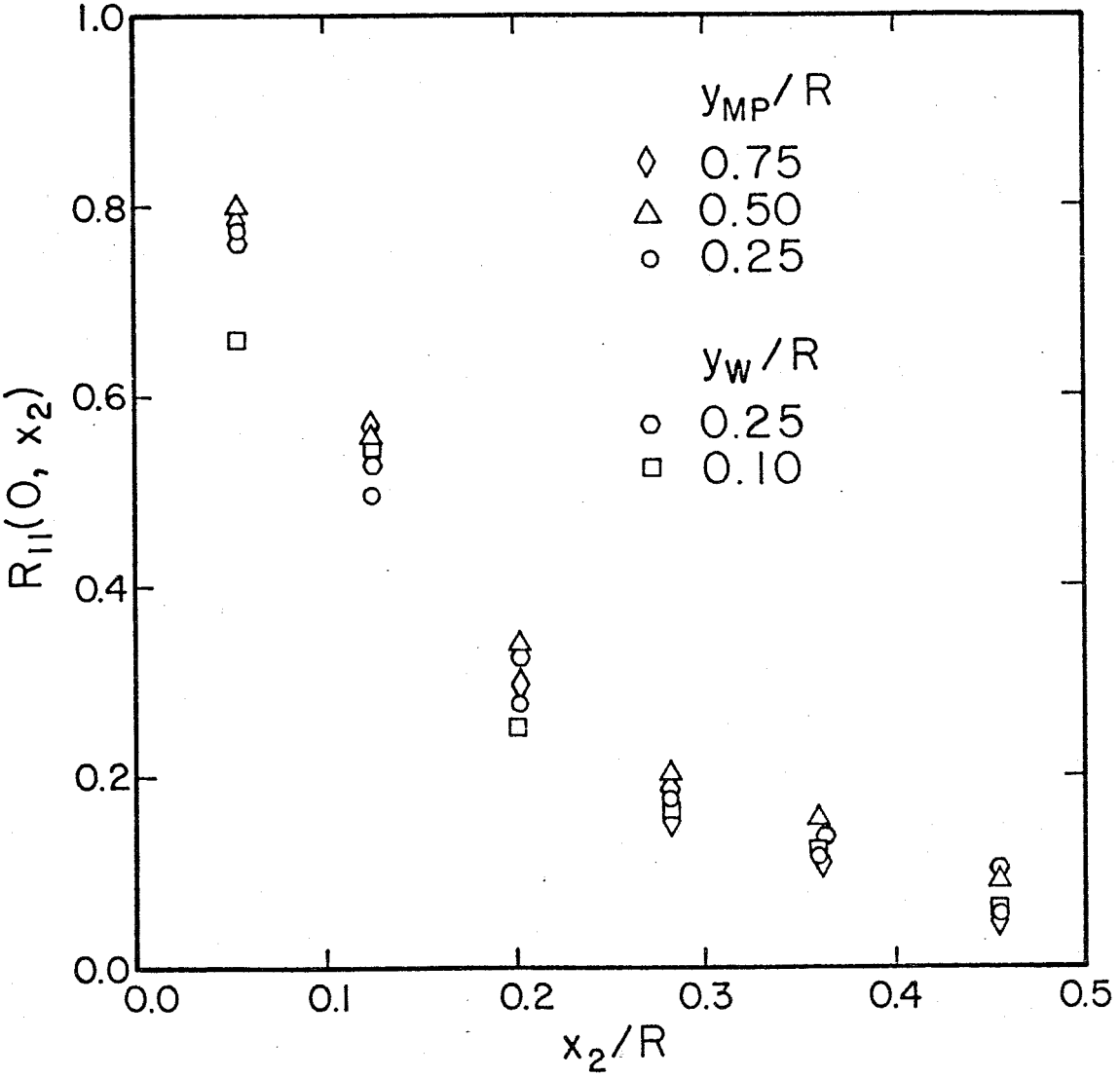

Figure 4.2-3: Space Correlations-Axial Velocity Component, Transverse Separations

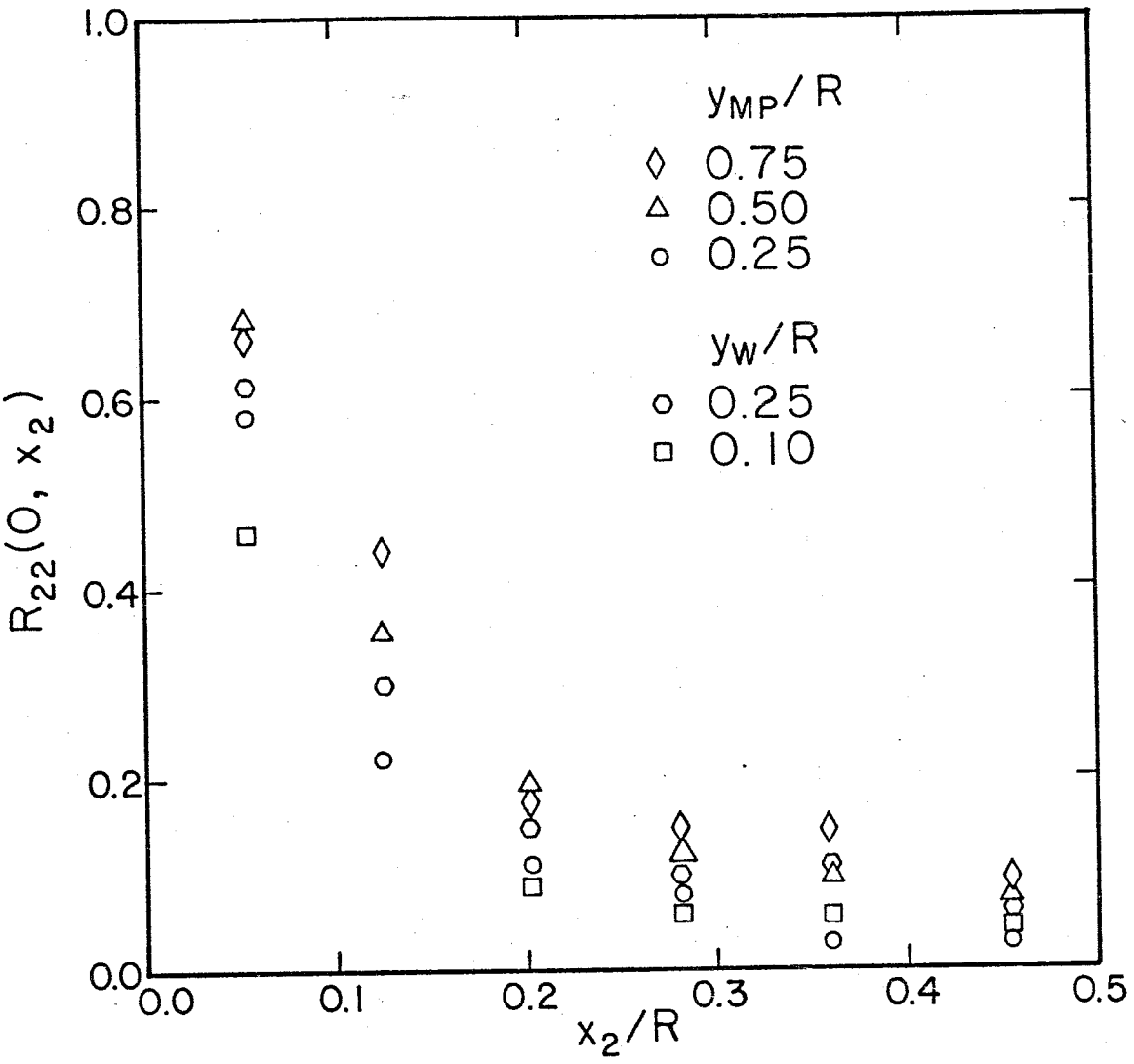

Figure 4.2-4: Space Correlations-Normal Velocity Component, Transverse Separations

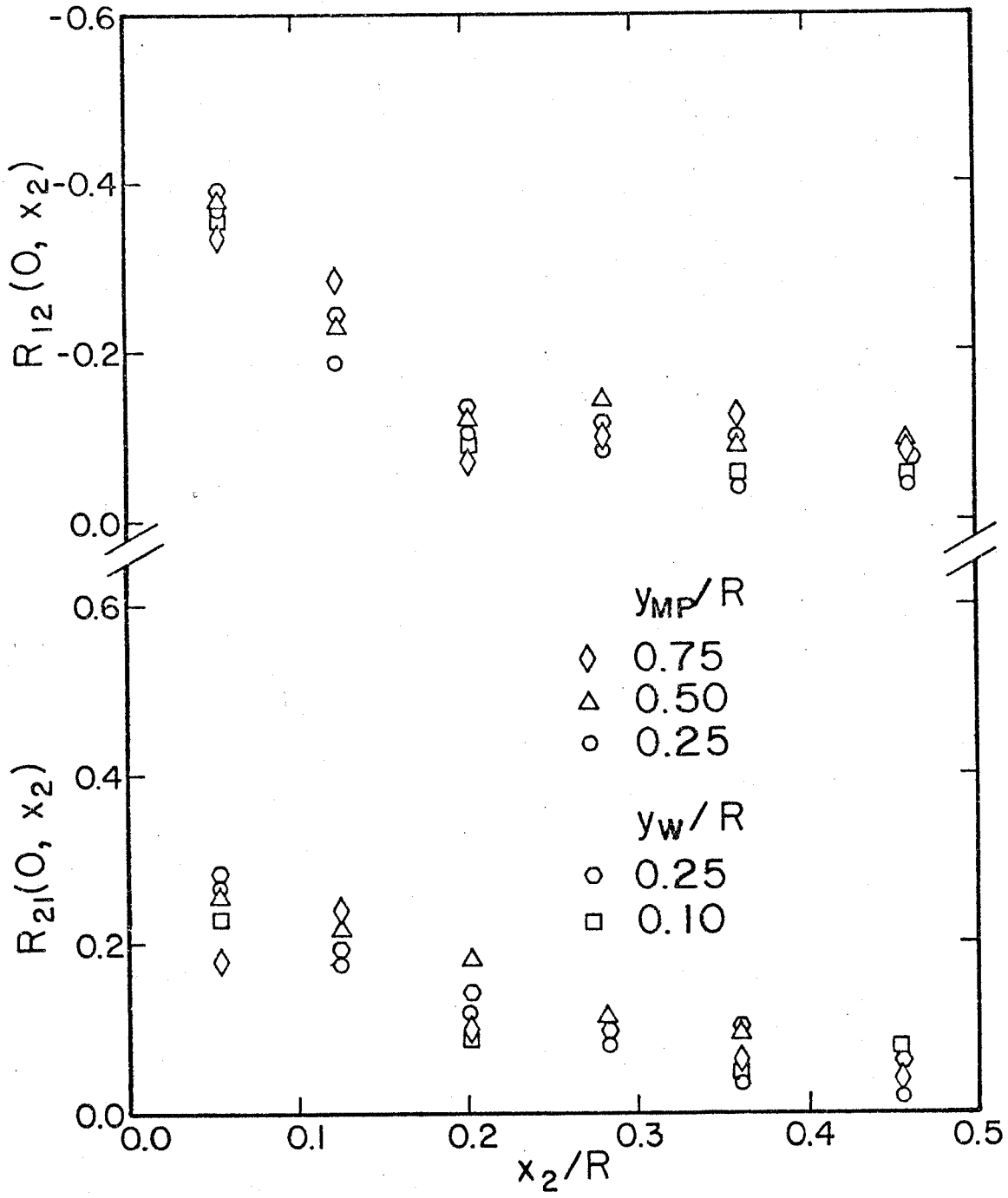

Figure 4.2-5: Space Correlations-Shear Coefficient, Transverse Separations

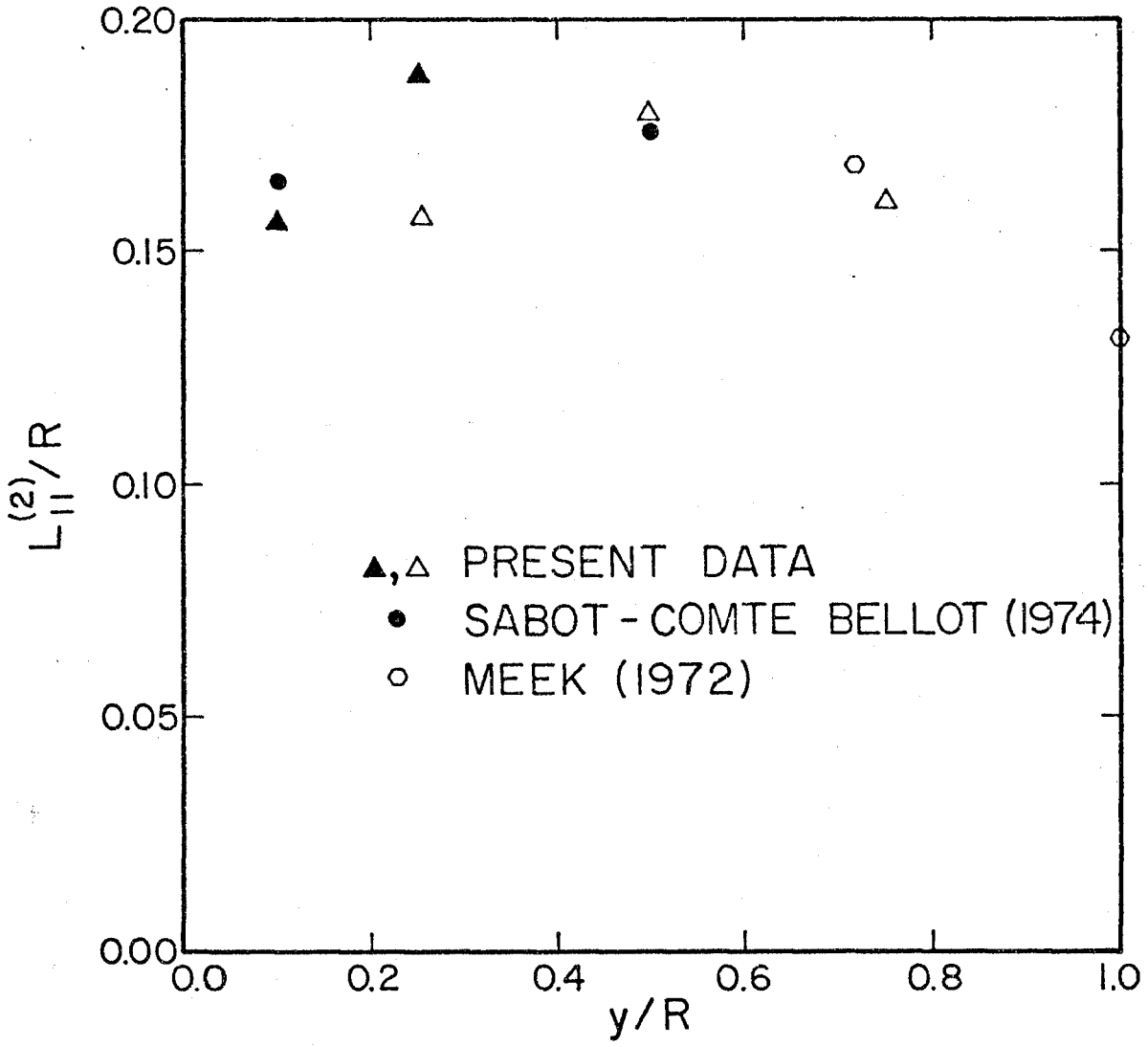

Figure 4.2-6: Integral Transverse Length Scales
Axial Velocity Component
Open Symbols - Centered Correlations
Dark Symbols - One-Sided Correlations

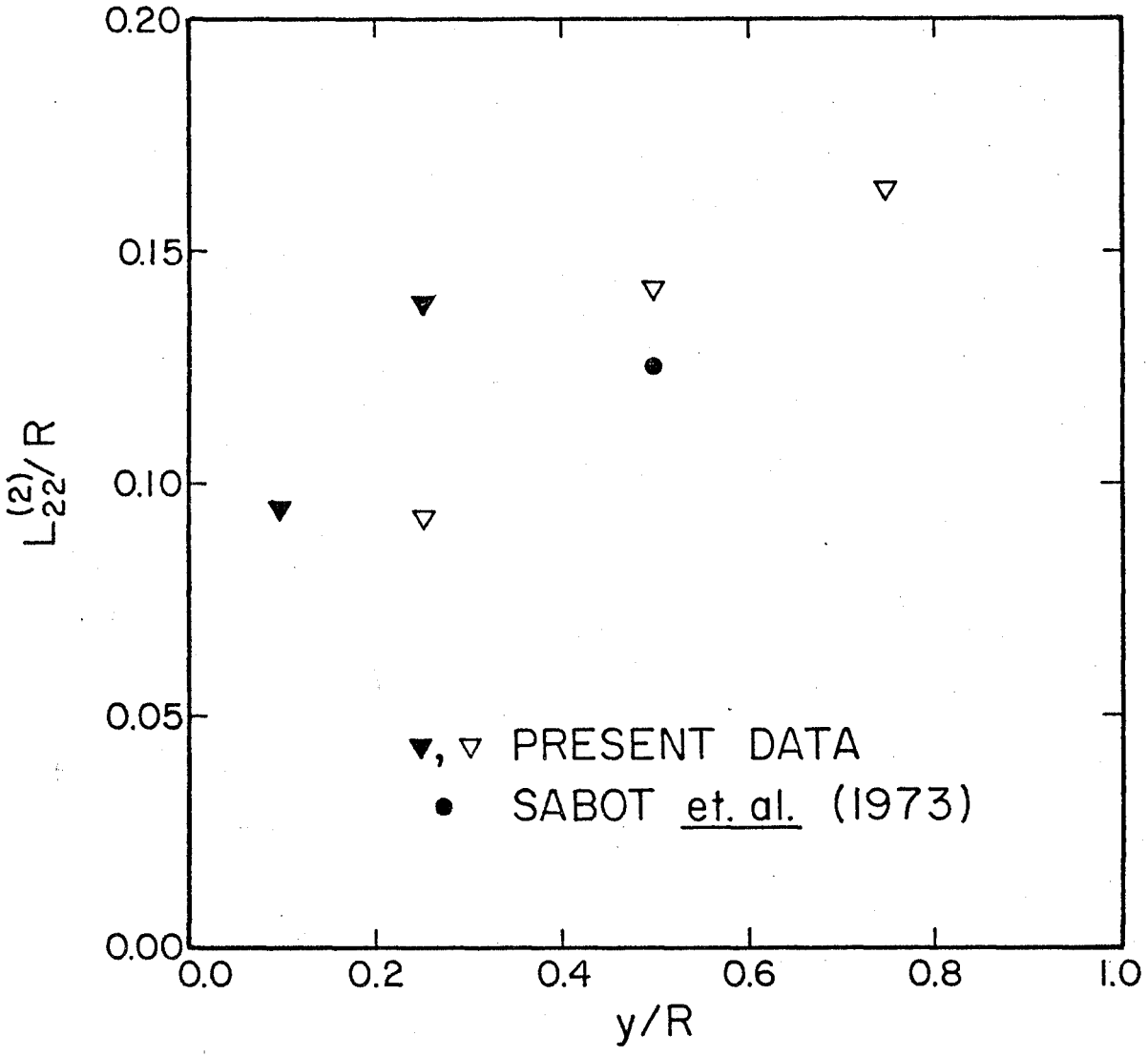

Figure 4.2-7: Integral Transverse Length Scales
Normal Velocity Component
Open Symbols - Centered Correlations
Dark Symbols - One-Sided Correlations

literature, perhaps because in the core region the difference in the results from (4.2-1) and (4.2-2) is not expected to be large. However, close to the wall the difference is significant and care must be taken when evaluating and making use of these scales. For example, none of the eddy diffusivity models based on length scales, which were examined in the course of this research, has clearly taken into account this point. A third way of calculating transverse length scales from space correlation functions was suggested by Bobkov et.al. (1966). The integral scale is given by

$$L_{ii}^{(2)} = \frac{L_{ii}^{(2)+} + L_{ii}^{(2)-}}{2} \tag{4.2-3}$$

where

$$L_{ii}^{(2)+} = \int_0^{x_{2_o}^+} R_{ii}(y, y+\eta)\, d\eta \tag{4.2-4a}$$

$$L_{ii}^{(2)-} = \int_0^{x_{2_o}^-} R_{ii}(y, y-\eta)\, d\eta \tag{4.2-4b}$$

with $x_{2_o}^+$, $x_{2_o}^-$ = first zero crossings of the correlation functions. They pointed out that this method, which gives values in between the results from (4.2-1) and (4.2-2), should be used whenever the correlation functions are strongly asymmetric. This is the case of the wall region in a pipe flow.

In the present work two-point measurements were taken only for $R_{ii}(y-\frac{x_2}{2}, y+\frac{x_2}{2})$ and $R_{ii}(y, y+x_2)$ calculations. Therefore no application was made of the Bobkov et.al. (1966) method.

In Fig. 4.2-8 are presented space-correlation results from x_1-separation measurements and for the axial component of the velocity. As before the

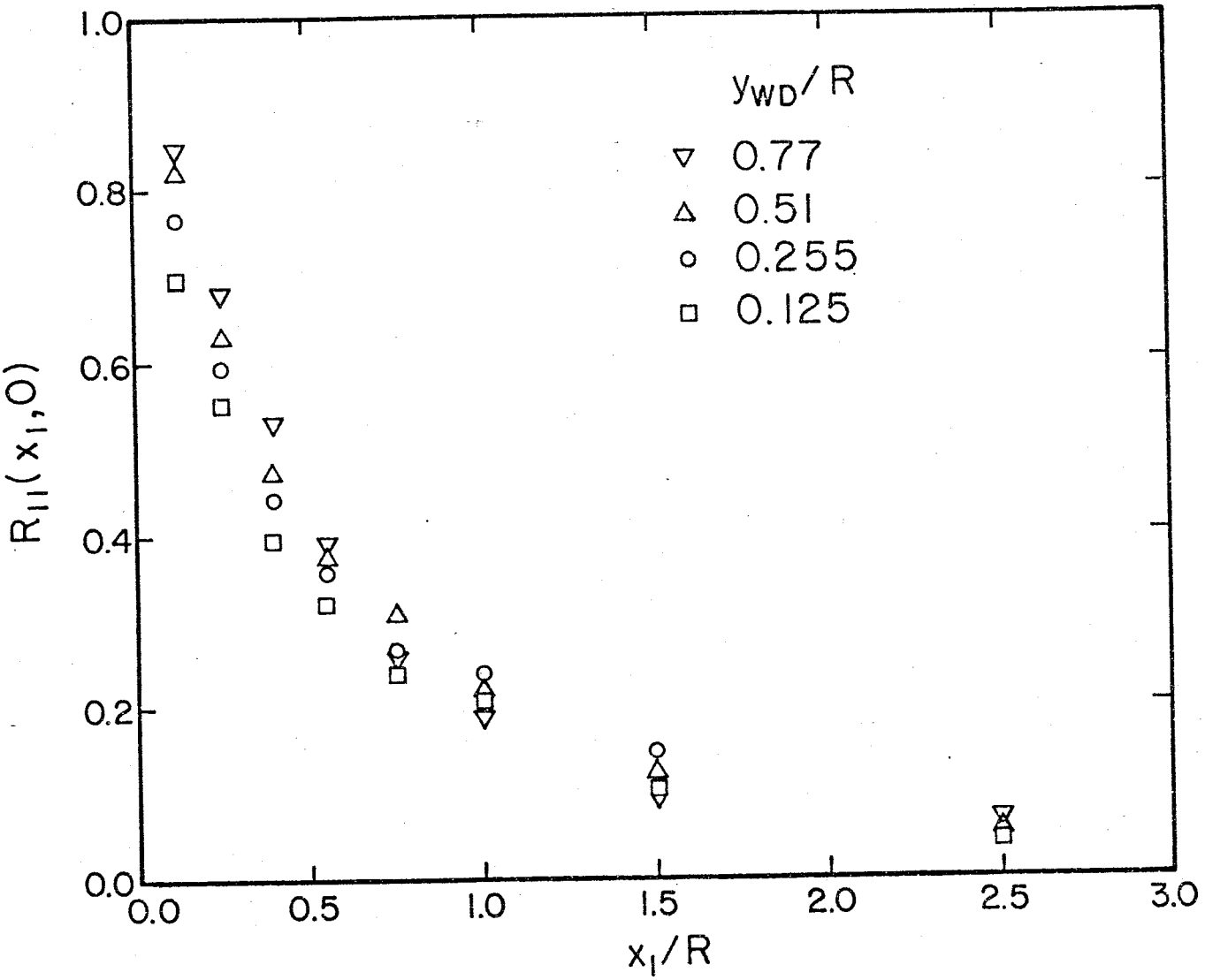

Figure 4.2-8: Space Correlations-Axial Velocity Component, Axial Separations

correlation functions were integrated to yield the longitudinal length scales shown in Fig. 4.2-9. In this figure the dark symbols mean that the scales were obtained from single-point auto-correlation functions through the Taylor's Hypothesis. The reasonable agreement between the present data and the results reported by Burchill (1970) shows the appropriateness of this hypothesis in which the length scale is related to the Eulerian integral time-scale by

$$L_{ii}^{(1)} = \overline{U}_1 \, J_{ii}^{E} \tag{4.2-5}$$

The Eulerian time scale can be obtained from the autocorrelation function by integration, i.e.

$$J_{ii}^{E} = \int_0^{\infty} R_{ii}(0;\tau)\, d\tau \tag{4.2-6}$$

with

$$R_{ii}(0;\tau) = \frac{\overline{u_i(\vec{x};t)\, u_i(\vec{x};t+\tau)}}{\overline{u_i^2}} \tag{4.2-7}$$

The high value of the longitudinal length scale obtained by Sabot et.al. (1973) may be partially explained by the larger Reynolds number used (138,000 vs. 56,000 in the present work). Bobkov et.al. (1966) have studied the dependence of the scales, for temperature fluctuations, upon the Reynolds number. They found that this dependence is stronger the further one gets away from the wall. At the centerline an asymptotic value is reached only at about Re = 100,000 (as shown in Fig. 4.2-10). The lower values reported by Howard (1974) seem to show some sort of developing characteristic. In this case scales are expected to be smaller, at each radial location, than the corresponding ones in the fully developed region. Finally the straight line

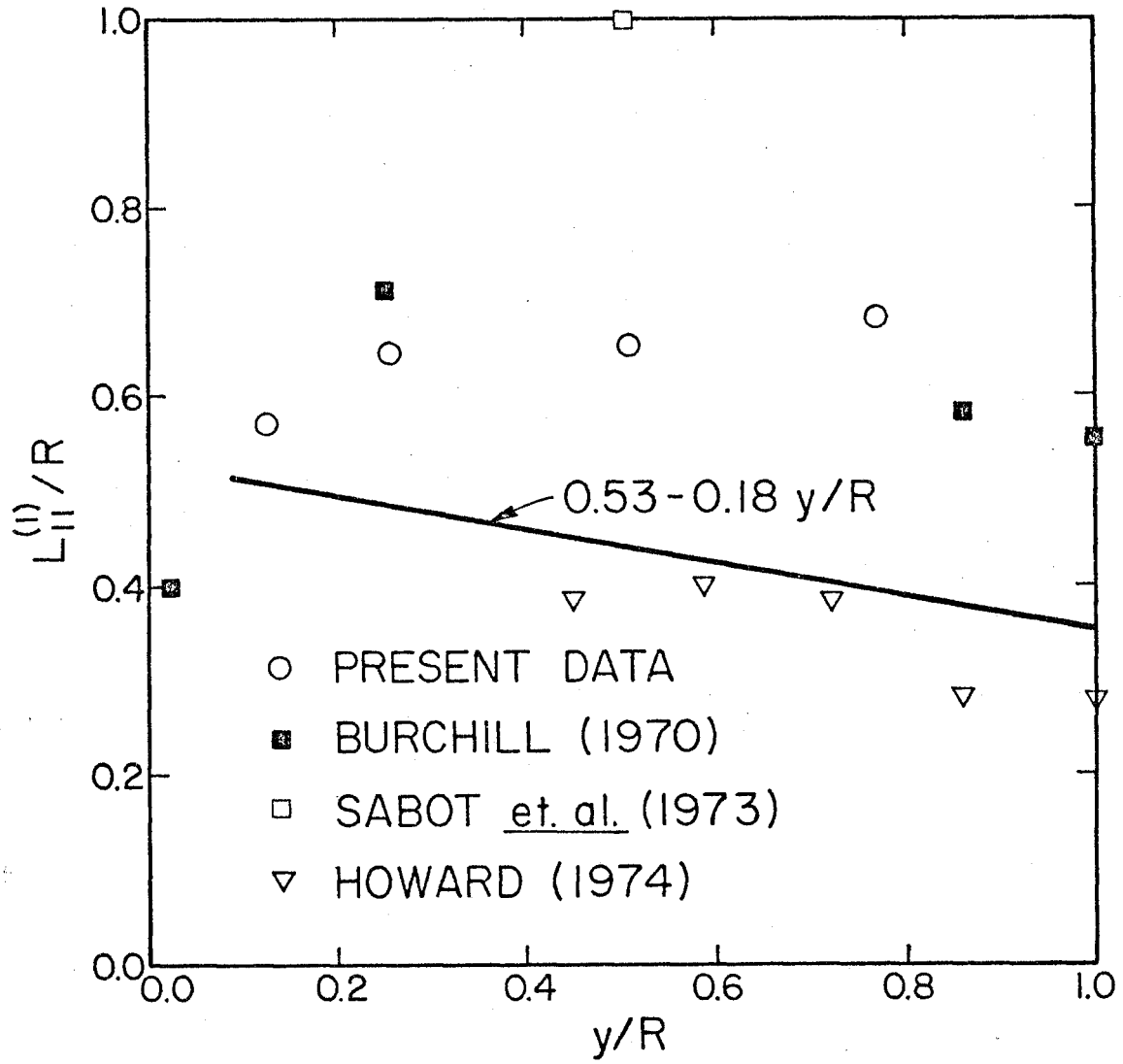

Figure 4.2-9: Integral Longitudinal Length Scales
Axial Velocity Component
Open Symbols - Two Point Meas.
Dark Symbols - Single Point Meas.

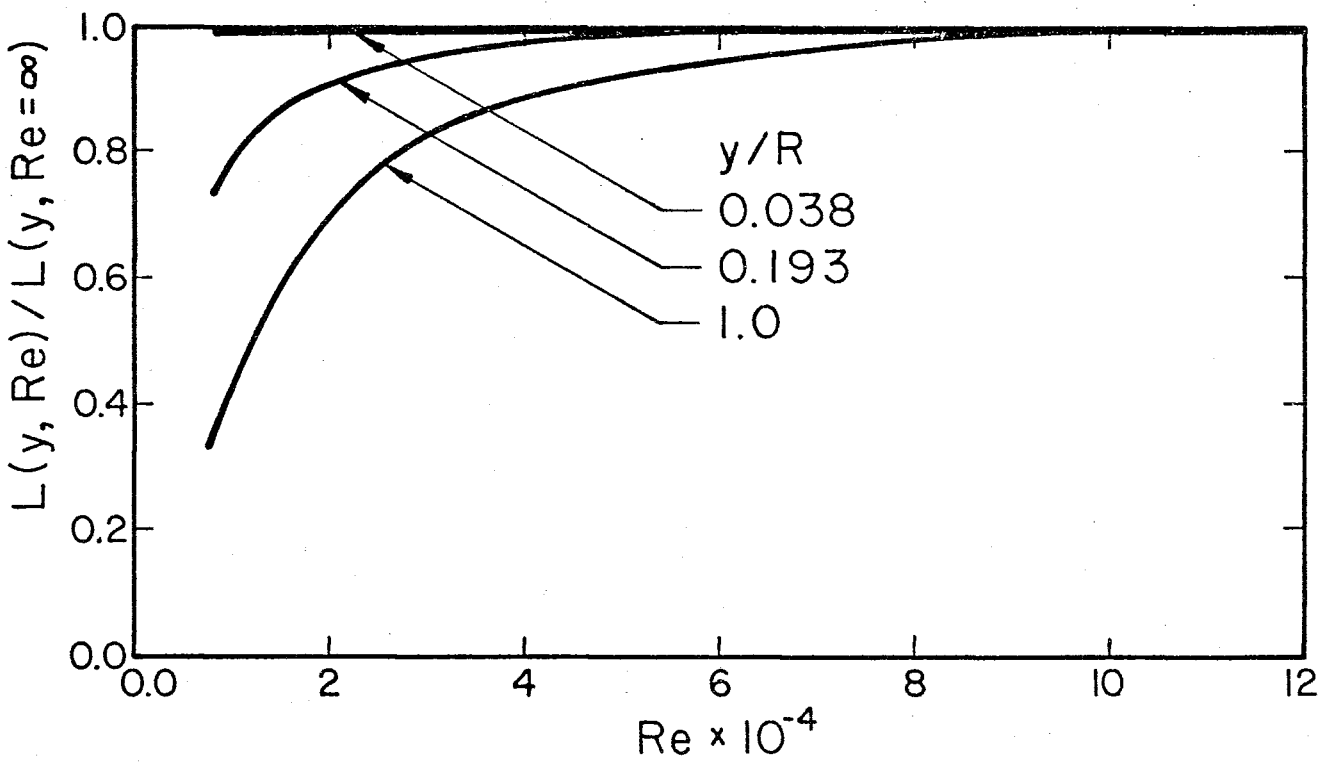

Figure 4.2-10: Scales of the Temperature Fluctuations as a Function of Re Number (Babkov et.al. High Temperature Vol. 4, 3, p. 373, 1966)

in Fig. 4.2-9 is the equation proposed by Bose (1963)

$$\frac{L_{11}^{(1)}}{R} = 0.53 - 0.18\,\frac{y}{R} \qquad (4.2\text{-}8)$$

to represent the radial dependence of the axial elngth scale in a pipe flow. His scales were evaluated by using auto-correlation functions plus the Taylor's Hypothesis. His measurements were taken at three different Reynolds numbers in the range $1.28\text{-}2.32 \times 10^5$ and the results showed practically no more Reynolds number dependence thus corroborating Bobkov et.al. findings.

5. TEMPERATURE FIELD RESULTS

5.1 One-Point Intensity and Mean Temperature Distributions

Mean temperature measurements were taken with a single sensor probe, a flow rate set to give a pipe Reynolds number of 56,590, a wall heat flux of 3820 BTU/hr ft^2 and an average outlet bulk water temperature of 80°F. The results for a radial traverse done at a section 24 diameters downstream from the beginning of the heated section are presented in Fig. 5.1-1. These results are presented in a dimensionless form

$$T^+ = \frac{T_w - \overline{T}}{T^*} \tag{5.1-1}$$

with the friction temperature T* defined by

$$T^* = \frac{q_w}{\rho c_p \sqrt{\tau}} \tag{5.1-2}$$

Also in Fig. 5.1-1 are presented results reported by Burchill (1970) for Re = 50,000 and the same wall heat flux (3820 BTU/hr ft^2) along with a correlation for water

$$T^+ = 34.5 + 5.93 \log Y^+ \tag{5.1-3}$$

suggested by Gowen and Smith (1967). Although there is large disagreement in the absolute values, the present data showed approximately the same slope as Gowen's correlation. This parametrization of mean temperature results as $T^+ = A + BY^+$, has some limitations. It is not supposed to collapse data for different fluids. Even for the same fluid but different flow and/or heat transfer conditions, values of T^+, for the same Y^+, may be quite different, as verified by Burchill (1970). However the slope seems to be independent of these conditions, which brings some meaning to this kind of parametrization.

Another way of presenting mean temperature results would be as a temperature defect law, analogous to the velocity defect law. In the present

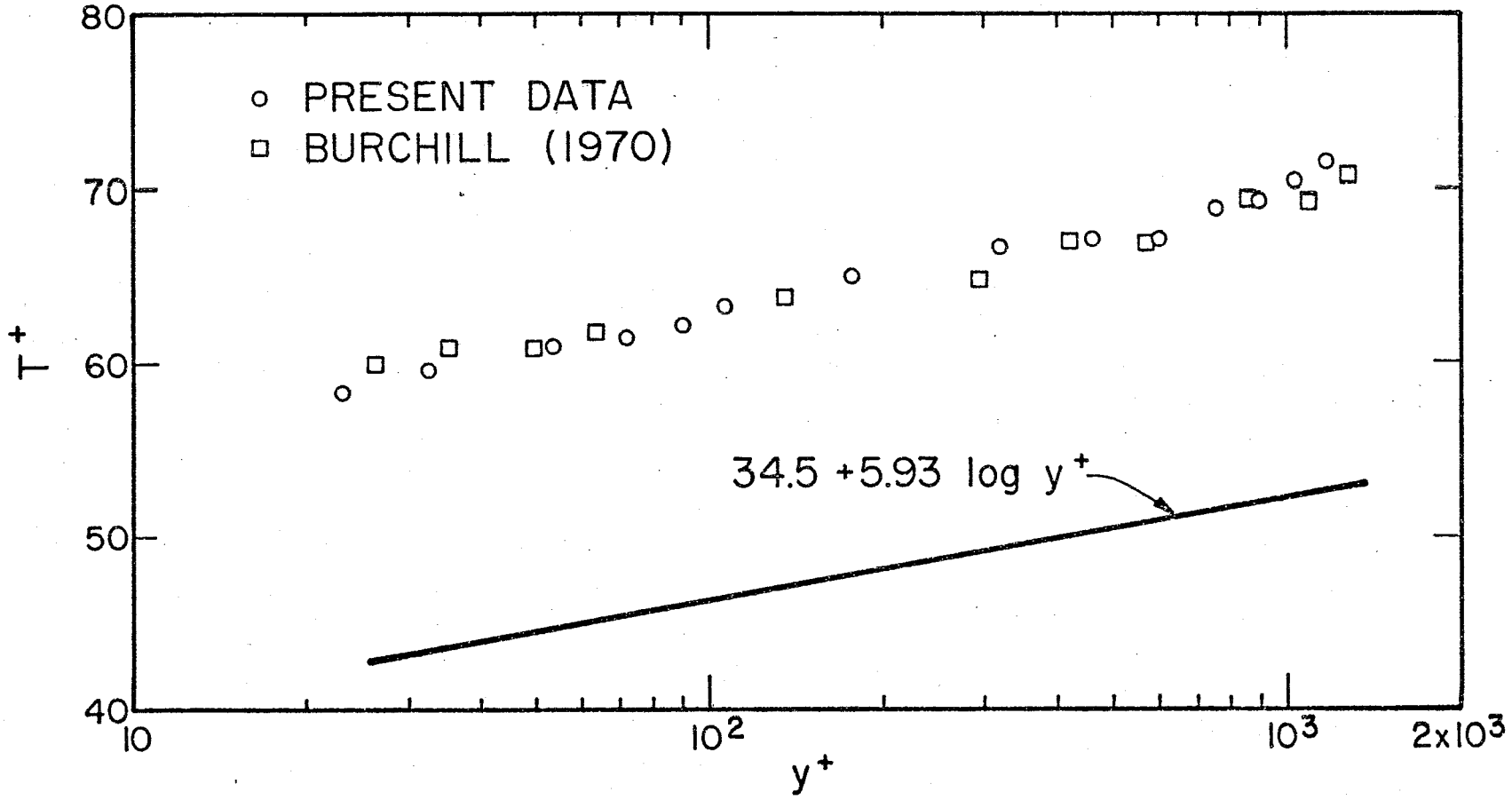

Figure 5.1-1: Mean Temperature Profiles - $X_{th}/D = 24$
$q''_w = 3820$ BTU/hr ft^2
$Re = 56,590$

research, with single sensor curved probes, the maximum wall distance allowed was approximately 1.7 inches (Y/R=0.85). Therefore no attempt was made of correlating mean temperature data using this position as centerline.

Single-point normalized temperature intensities, for $X_{th}/D = 24$, are presented in Fig. 5.1-2 along with experimental data from Burchill (1970) (water, Re=50,000 and q''_w = 3820 BTU/hr ft^2) and Bremhorst and Bullock (1970) (air, Re=34,700 and q''_w=56 BTU/hr ft^2).

In Fig. 5.1-3 is shown the dependence of the intensity of the temperature fluctuations on both radial and axial location in the thermal entrance region. It is interesting to note that the temperature fluctuations, plotted as Θ'/T^* vs Y/R, still show some developing characteristics between $X_{th}/D = 19$ and $X_{th}/D = 24$. For air flow, Tanimoto and Hanratty (1963) have observed marked differences in the temperature intensities at $\frac{X_{th}}{D} = 12.6$ and $\frac{X_{th}}{D} = 45.3$, unlike the mean temperatures. As a result they pointed out that "it appears that temperature fluctuation measurements are a more sensitive test as to when a temperature field is fully developed".

Finally, an attempt was made to obtain mean temperature profiles in the thermal entrance region. However, the normalization of the results for plotting as T^+ vs. (Y^+ and X_{th}/D), was not possible due to a considerable scatter among the different wall thermocouple readings. Mounting and/or thermal contact problems could be the cause for this scatter. In addition, the fluid mean temperature gradients in the beginning of the thermal entrance were very small and could not be detected accurately due to slow oscillations still present in the filtered signals. Perhaps another method for mean temperature measurements, for example, the voltage-to-frequency conversion technique used by Pessoni (1974) could yield usable results.

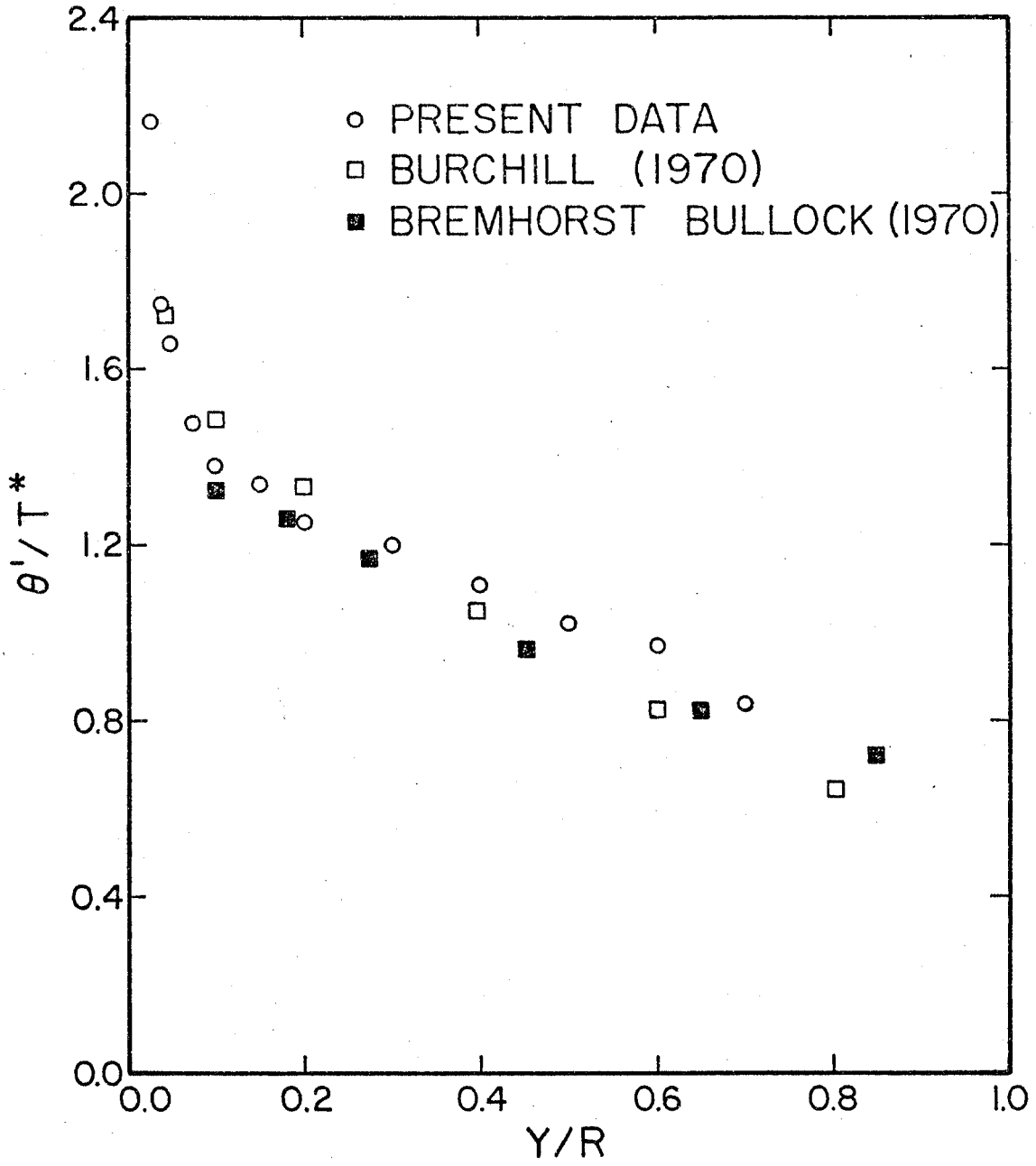

Figure 5.1-2: Normalized Intensities of Temperature Fluctuations
$X_{th}/D = 24$

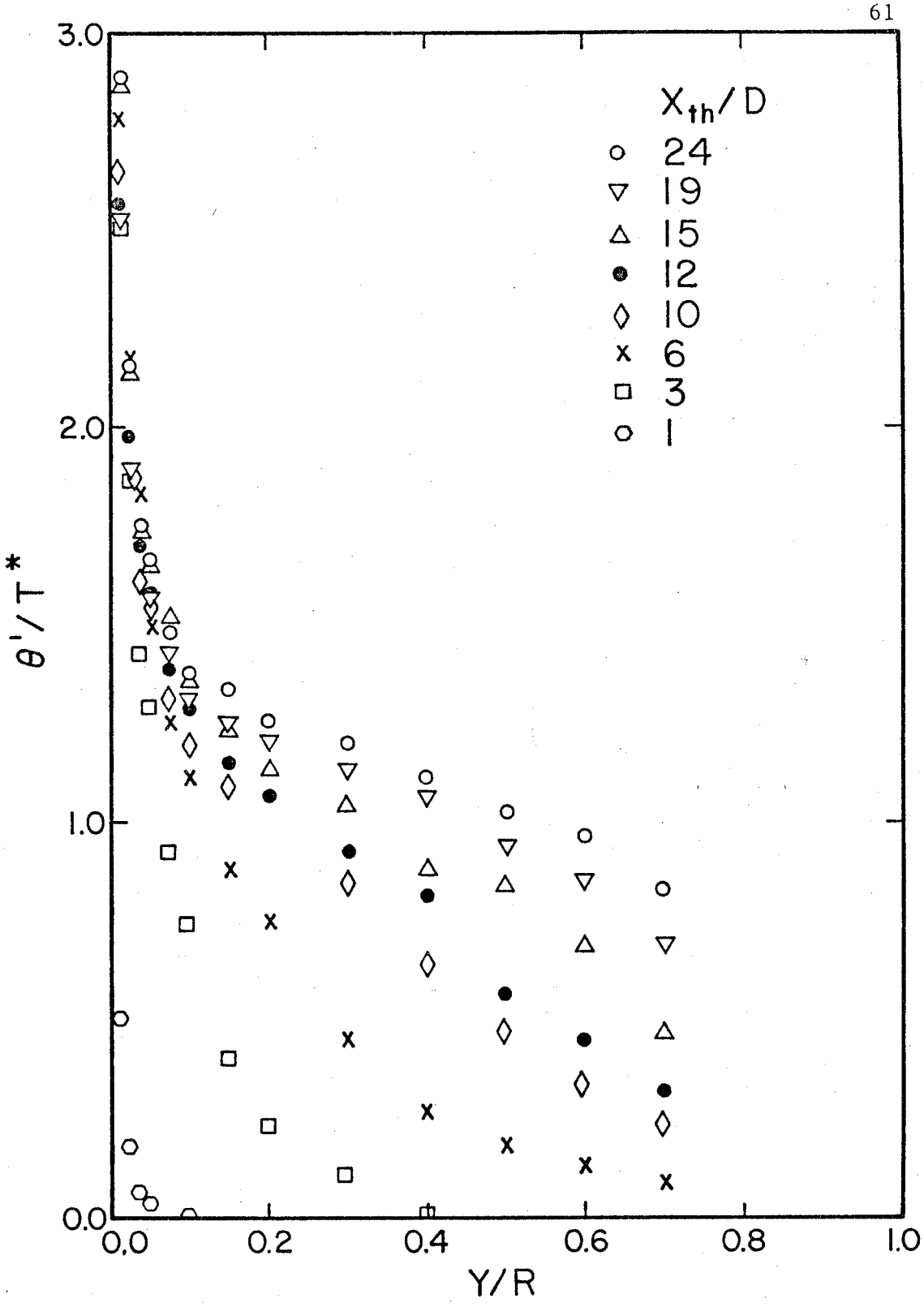

Figure 5.1-3: Normalized Intensities of Temperature Fluctuations-Thermal Entrance Region

5.2 Two-Point Temperature Field Structure

For the temperature field structure again two-groups of experiments were carried out, namely; two-point transverse and axial separation measurements, both with two single sensor probes.

The flow rate, the water temperature and the heat flux were the same as used in the one-point measurements. A full set of data points was taken at $X_{th}/D = 23.5$ and a smaller number of points at both $X_{th}/D = 14.5$ and 5.5, X_{th} being the distance from the beginning of the heated portion of the test section to the point of measurement.

In Figs. 5.2-1 and 5.2-2 are presented space time correlations for temperature fluctuations obtained, respectively, from transverse and axial separation measurements.

Space-correlation results at $X_{th}/D = 23.5$ are presented in Figs. 5.2-3 and 5.2-5 from, respectively, x_2 and x_1 separation measurements. The dependence of these space correlation results upon axial location in the thermal entrance region is shown in Figs. 5.2-4 and 5.2-6. However, this dependence is better seen in Figs. 5.2-7 and 5.2-8 where integral length scales are plotted. These scales were obtained from the correlation curves $R_{tt}(o,x_2)$ and $R_{tt}(x_1,o)$ by graphical integration, up to the first zero crossing. The transverse scales (Fig. 5.2-7) seem to be more sensitive to the axial location in the thermal entry region than the longitudenal scales (Fig. 5.2-8). This was expected since, depending upon the radial location of the center probe, intermittency effects come into play in the transverse measurements. Beyond X_{th}/D approximately equal to 15 the longitudinal scales, for the two radial locations examined, showed only slight increases with the distance from the beginning of the heated section. For the transverse scales close to the wall ($Y_w/R=0.10$) some sort of asymptotic value was already

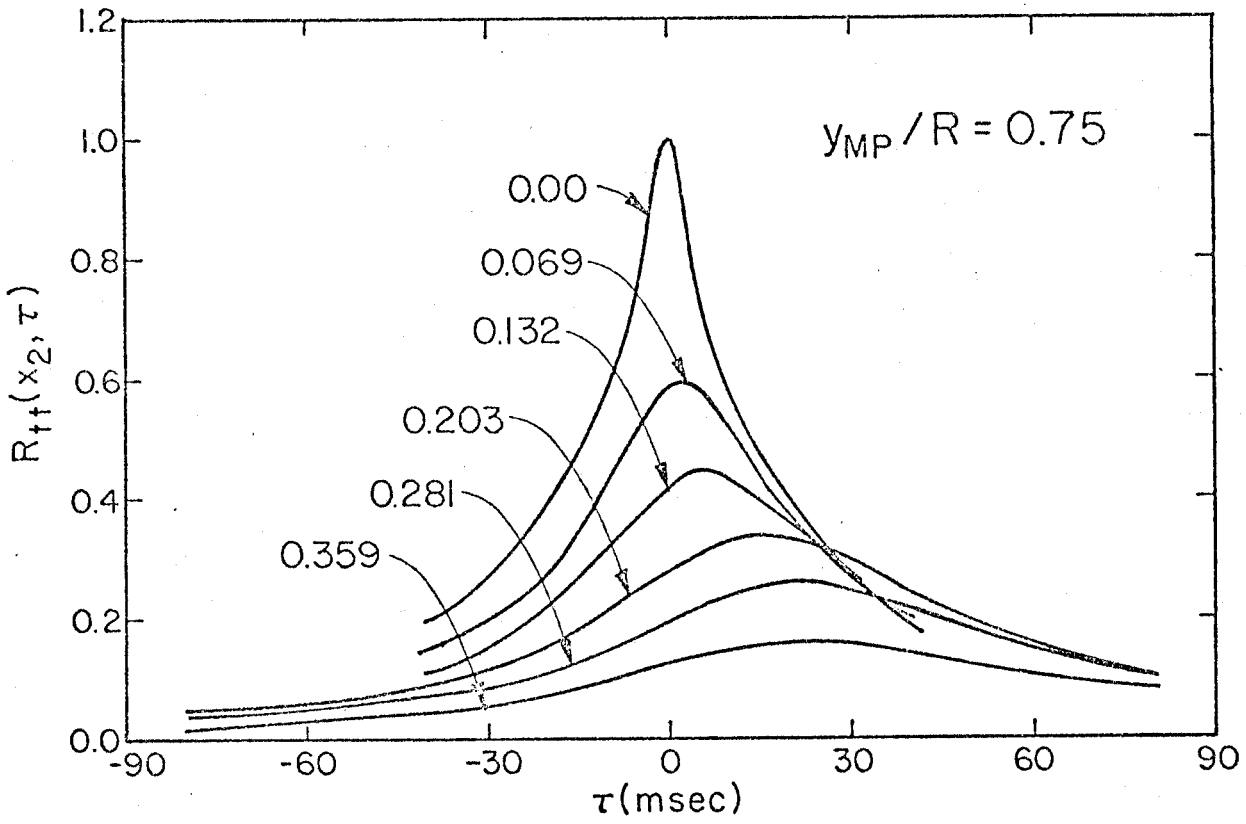

(a)

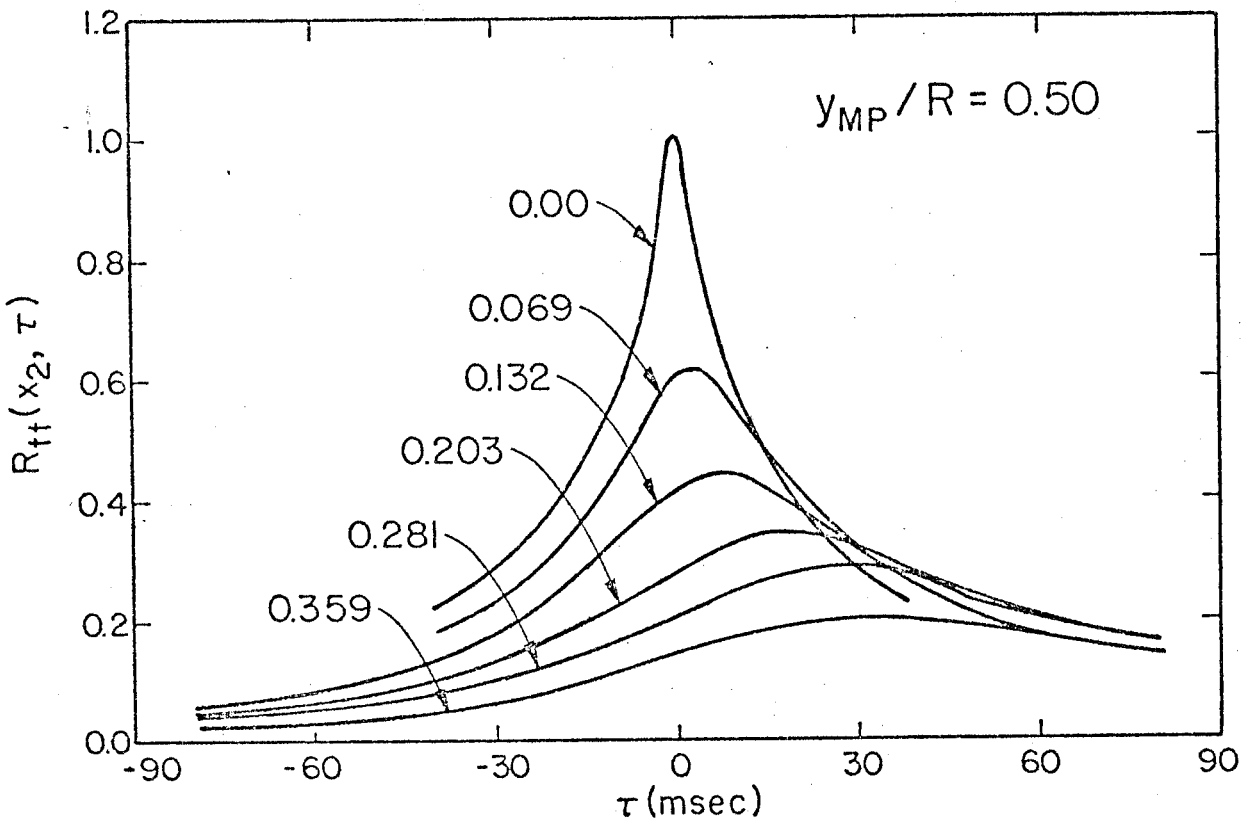

(b)

Figure 5.2-1: Space-time Correlations for Temperature Fluctuations-Transverse Separations

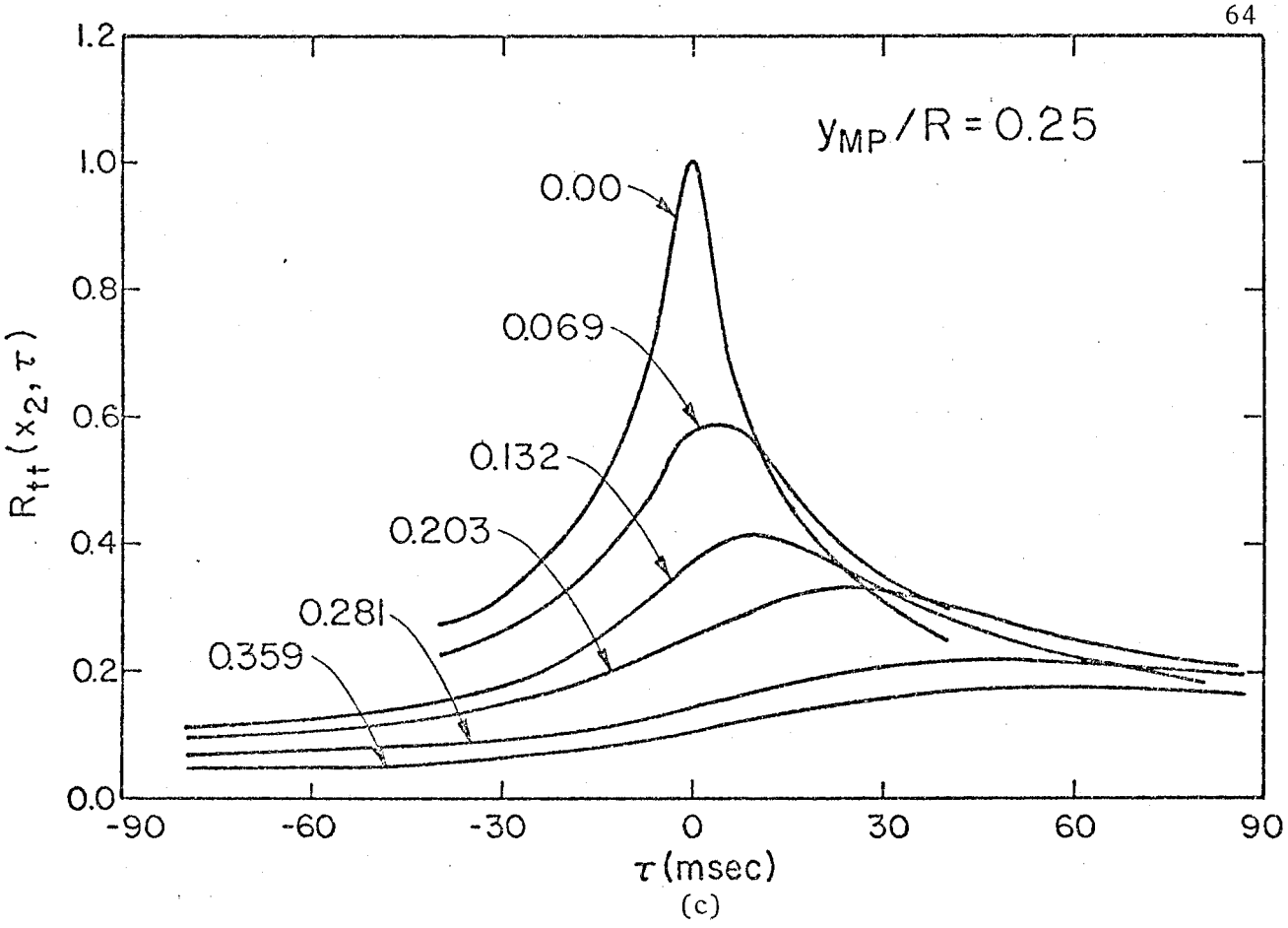

(c)

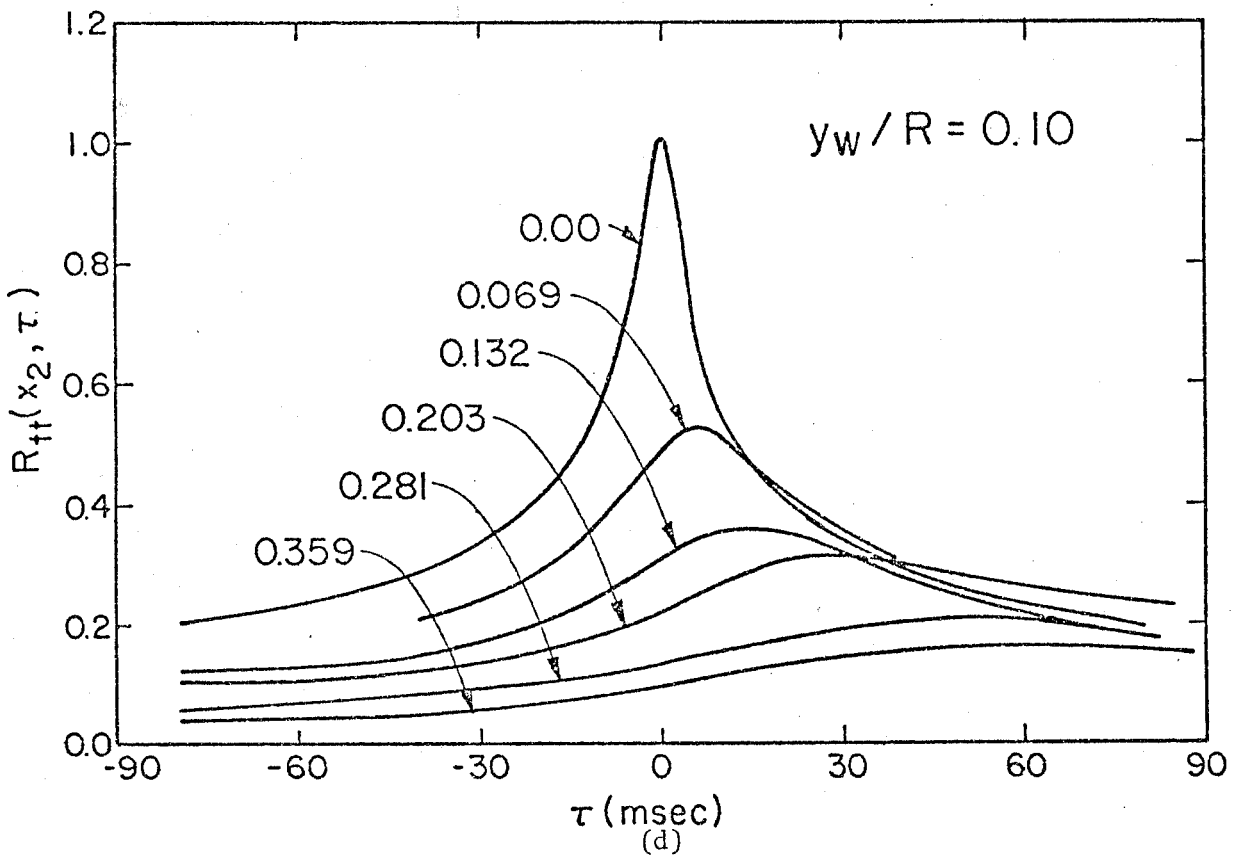

(d)

Figure 5.2-1

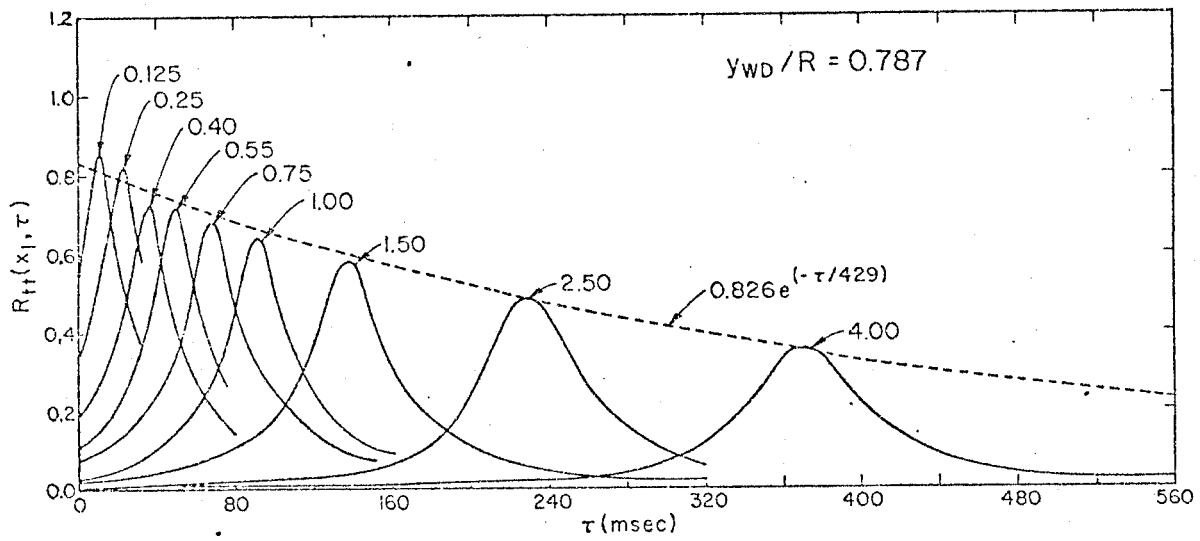

(a)

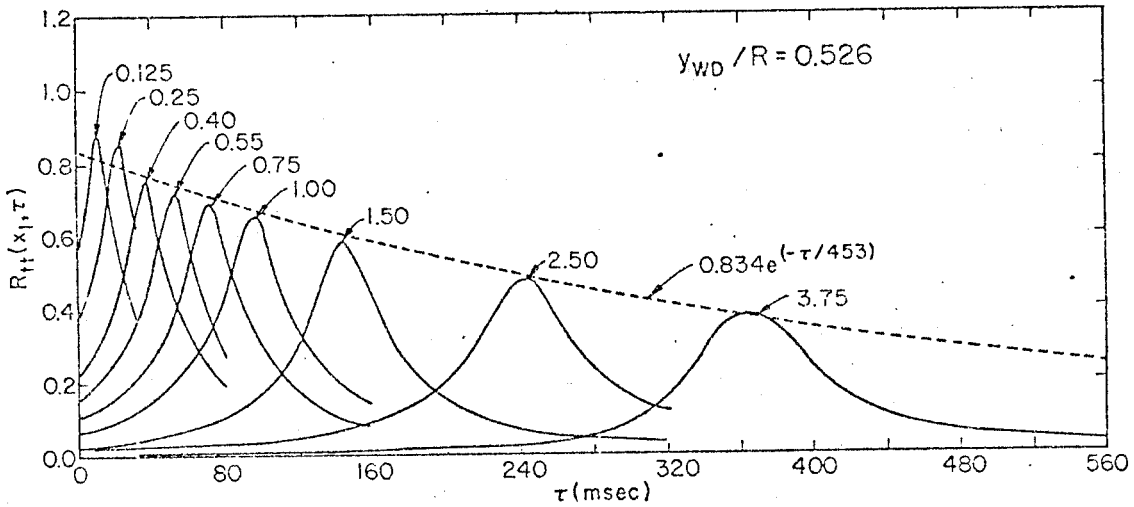

(b)

Figure 5.2-2: Space-Time Correlations for Temperature Fluctuations-Longitudinal Separations

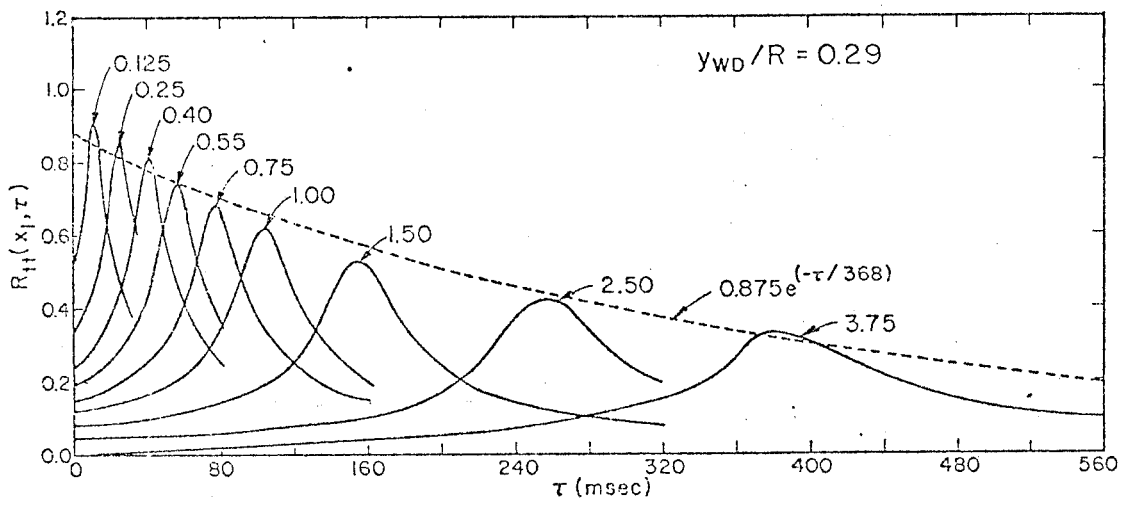

(c)

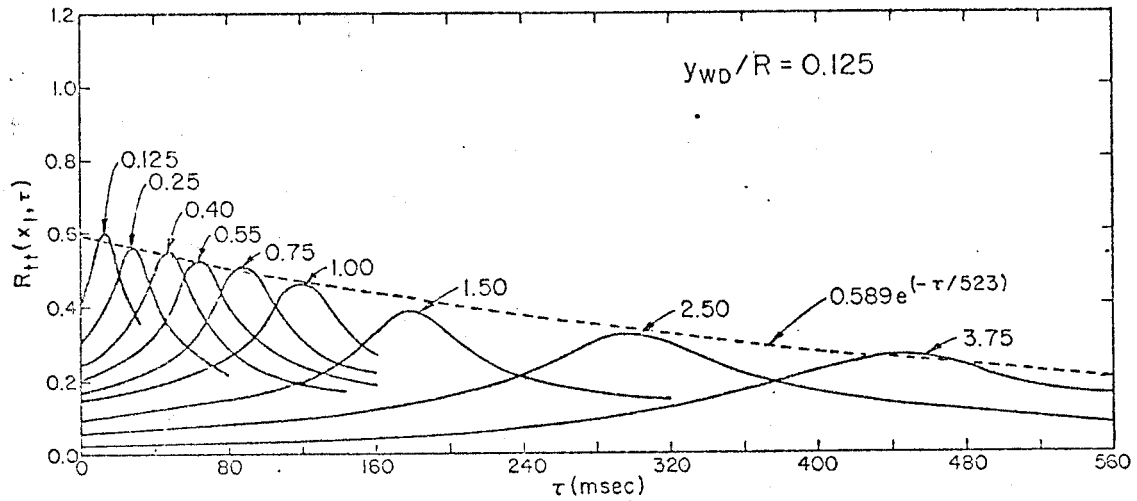

(d)

Figure 5.2-2

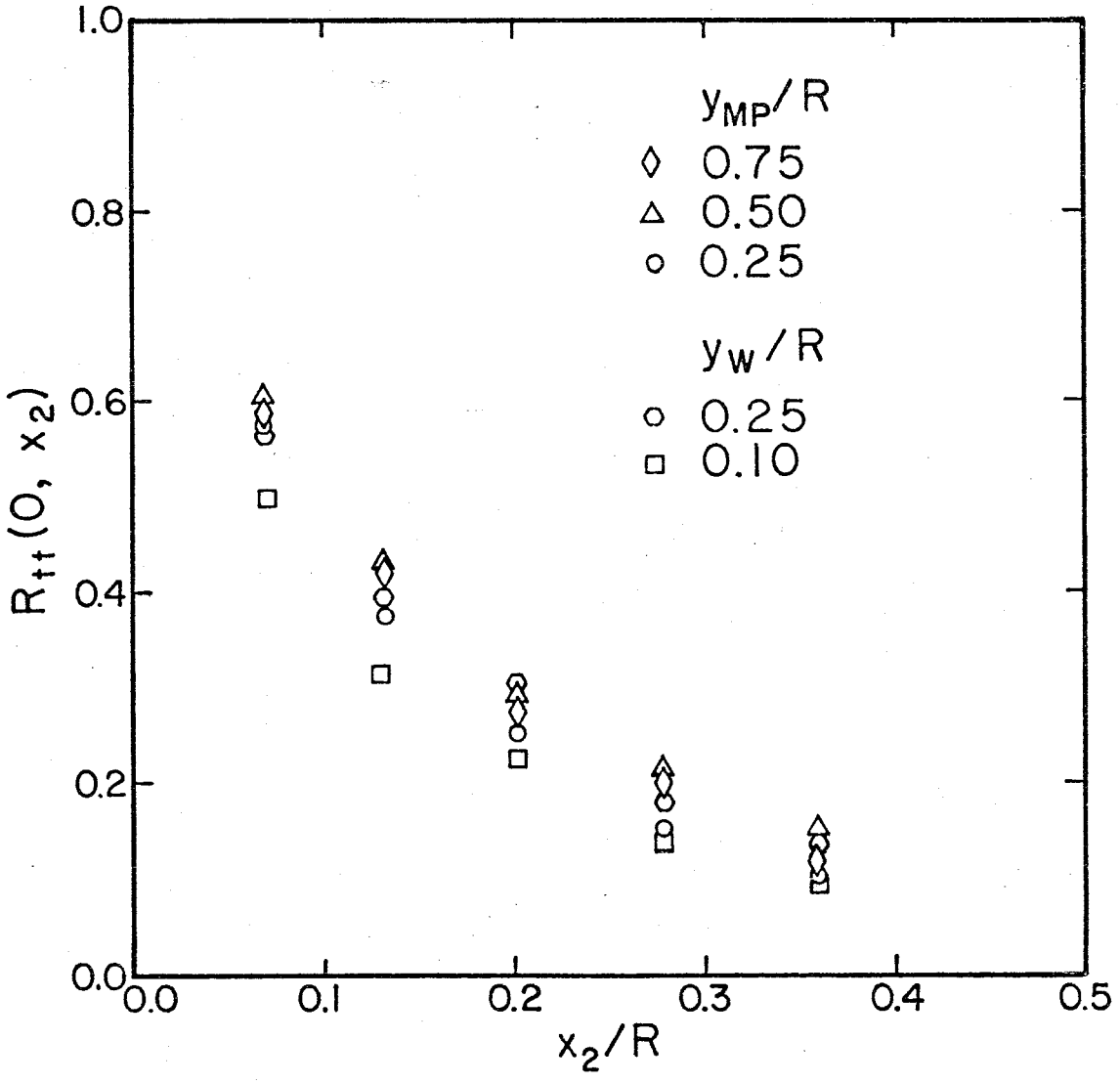

Figure 5.2-3: Space Correlations-Temperature, Transverse Separations

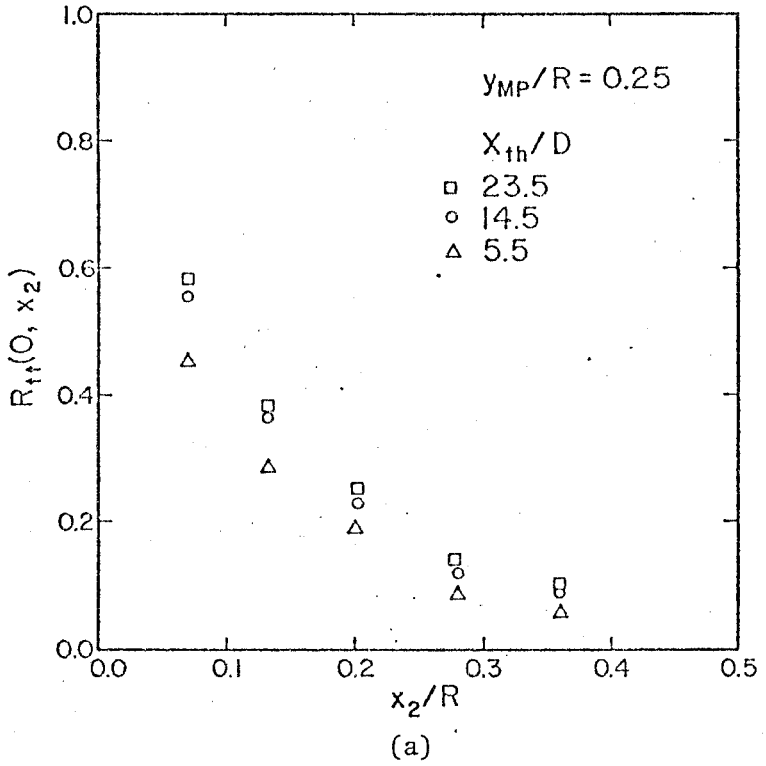

(a)

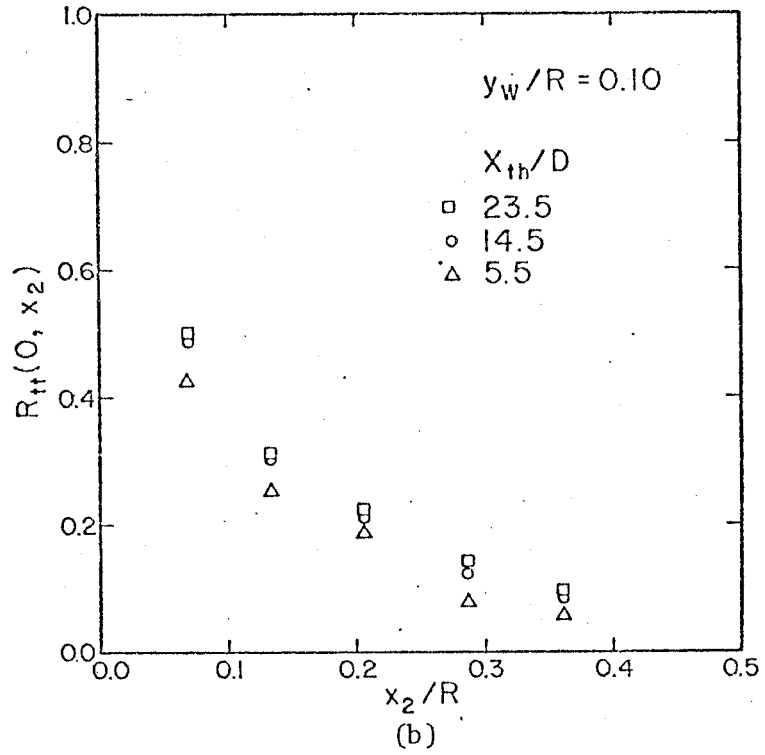

(b)

Figure 5.2-4: Temperature Space Correlations-Transverse Separations-Thermal Entrance Region

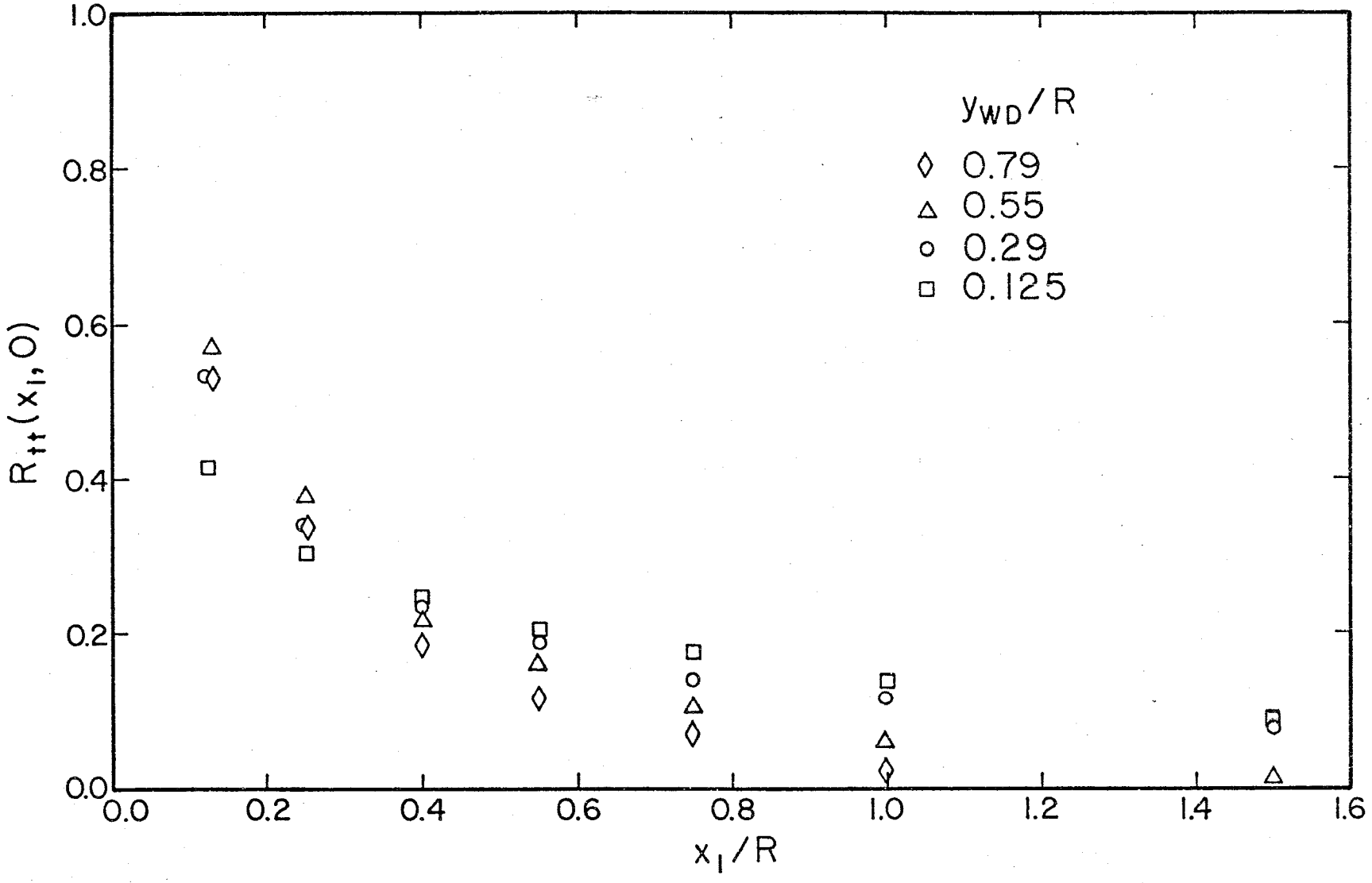

Figure 5.2-5: Space Correlations-Temperature, Axial Separations

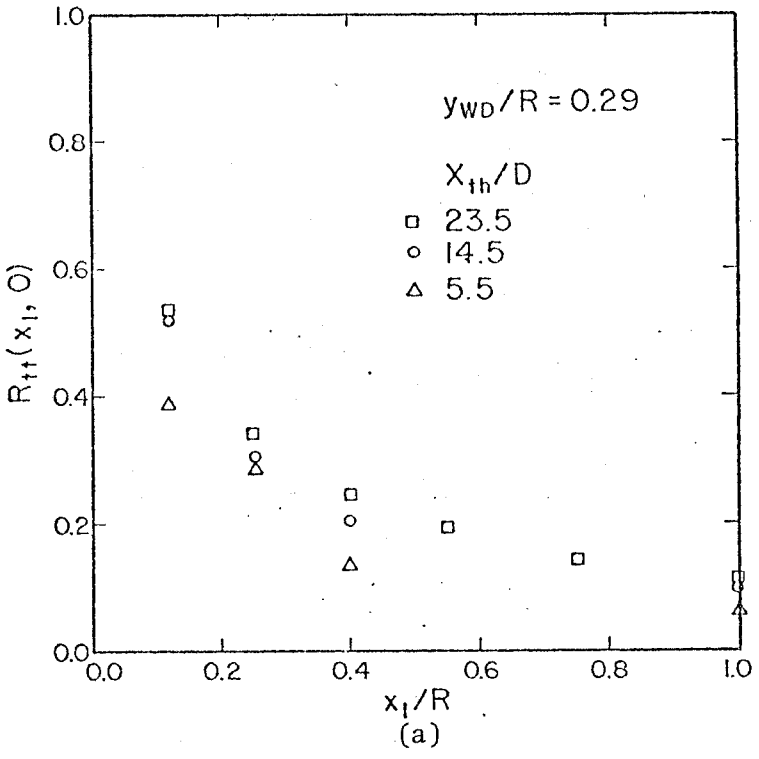

(a)

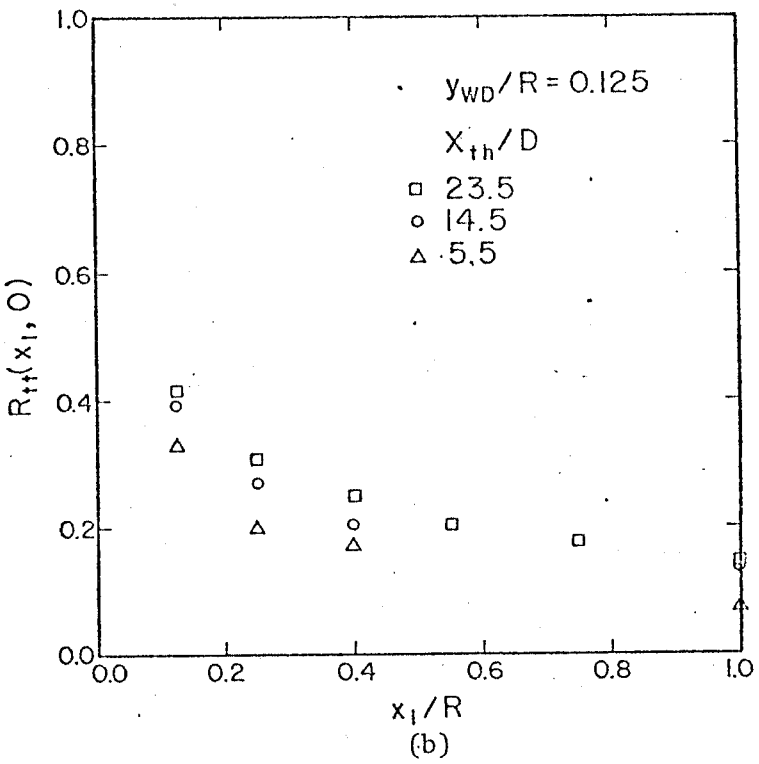

(b)

Figure 5.2-6: Temperature Space Correlations-Axial Separations-Thermal Entrance Region

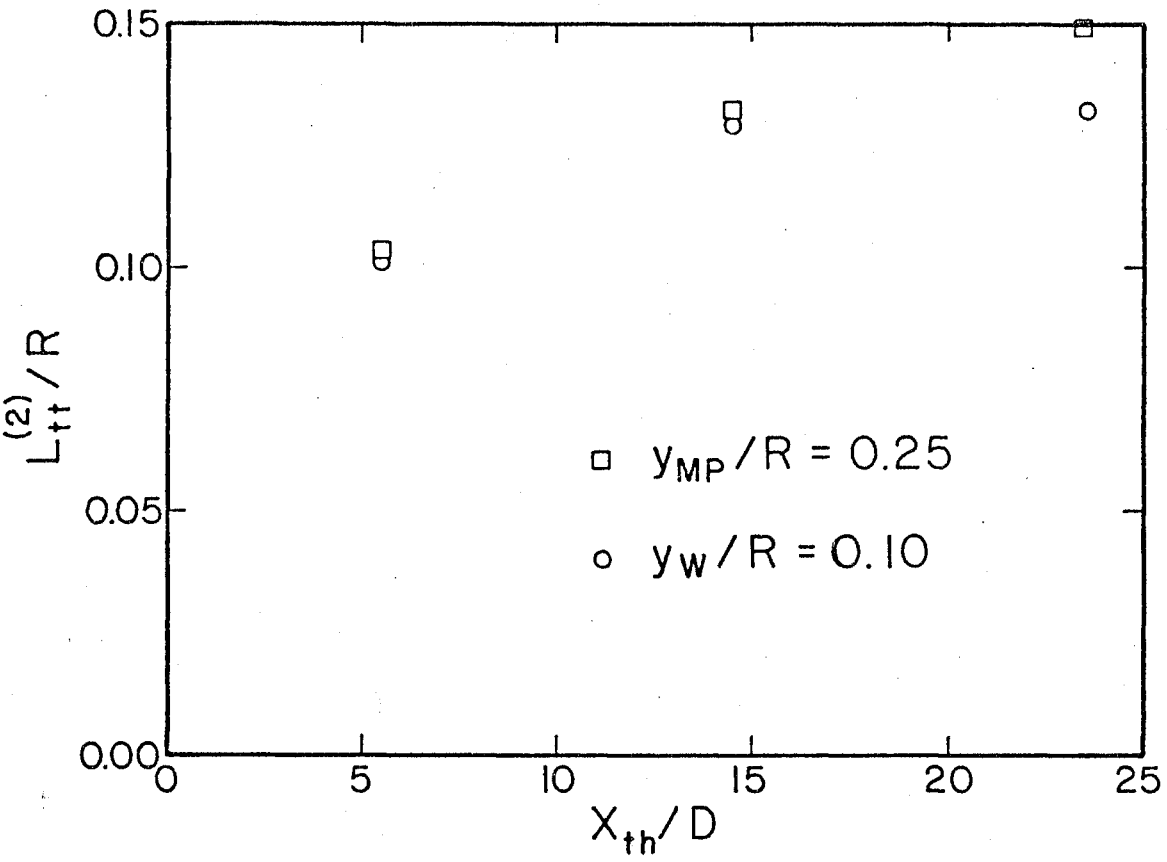

Figure 5.2-7: Transverse Temperature Length Scales
Thermal Entrance Region

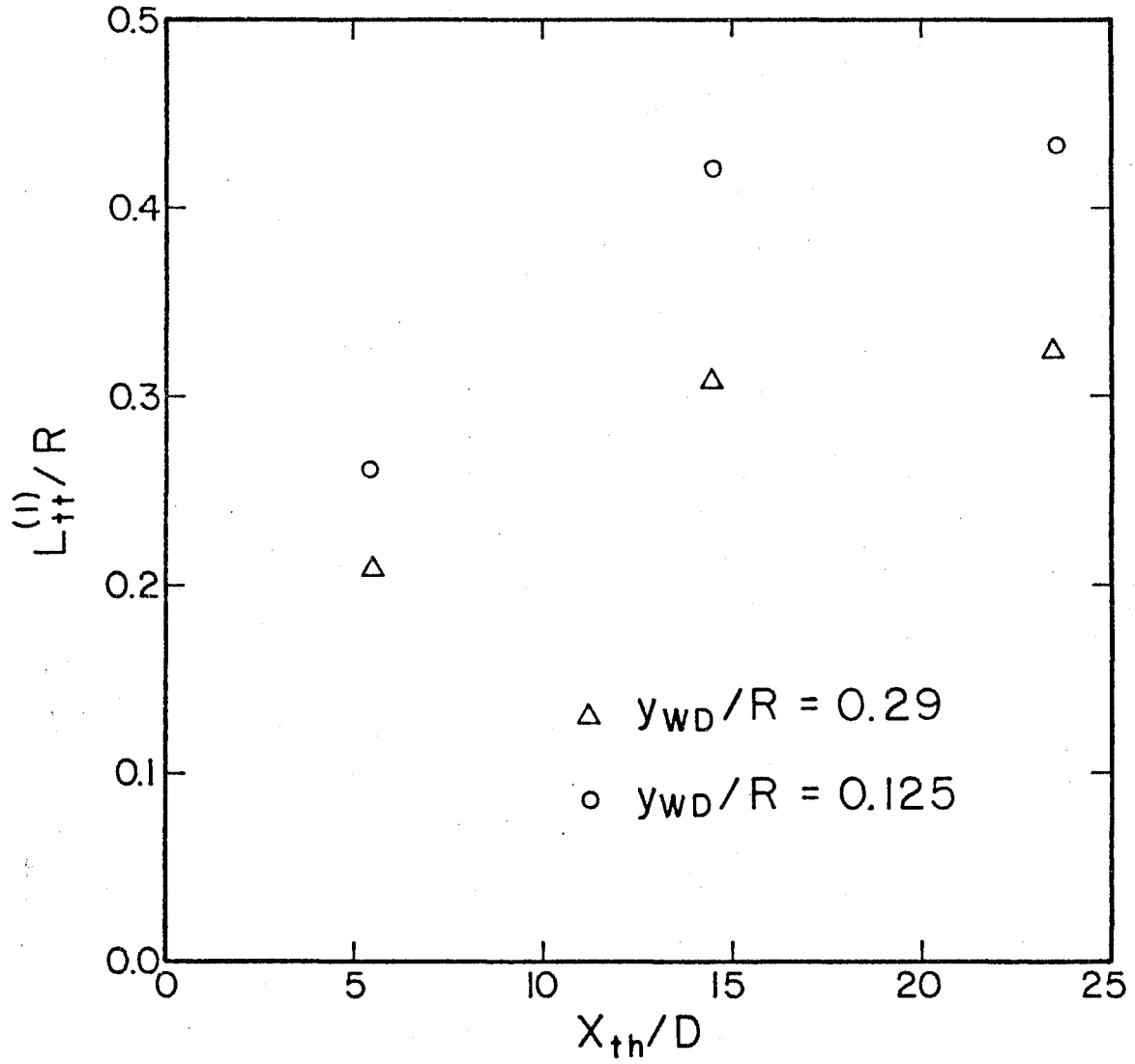

Figure 5.2-8: Longitudinal Temperature Length Scales Thermal Entrance Region

reached at about $X_{th}/D = 15$ but for the other radial location ($Y_w/R=0.25$) a significant increase in the scale was still observed for X_{th}/D going from 14.5 to 23.5.

In Fig. 5.2-9 temperature transverse length scales for $X_{th}/D = 23.5$ were plotted together with the corresponding velocity scales of both axial and normal components. As before, in this figure the open and dark symbols were used whenever the integral scales were calculated, respectively, with (4.2-1) and (4.2-2). Fig. 5.2-9 shows; firstly, that the way correlation data are handled near the wall affects the temperature scales in the same way that the velocity scales were affected and secondly, that some sort of trend toward isotropy (which would mean equal scales for all velocity components as well as passive scalar quantities like temperature) can be observed near the center of the pipe. Finally it also shows that for all four radial locations examined $L_{22}^{(2)} < L_{tt}^{(2)} < L_{11}^{(2)}$ holds.

In Fig. 5.2-10 temperature longitudinal length scales ($X_{th}/D=23.5$) from the present two-point measurements (open symbols) are presented along with other scales obtained by other experimenters from single sensor measurements (dark symbols). Burchill's (1970) results are for water and were calculated from spectral functions. Hochreiter's (1971) results are for mercury and also were obtained by extrapolating the temperature spectrum to zero wave number. Their Eulerian scales were given by

$$L^{E}_{tt} = \frac{\pi}{2\,\overline{\theta^2}} \lim_{k \to 0} E_T(k) \qquad (5.2\text{-}1)$$

where $E_T(k)$ is the temperature power spectrum and k is the wave number. This procedure implicitly assumes that the Taylor's hypothesis is valid since the wave number k is related to the frequency f through

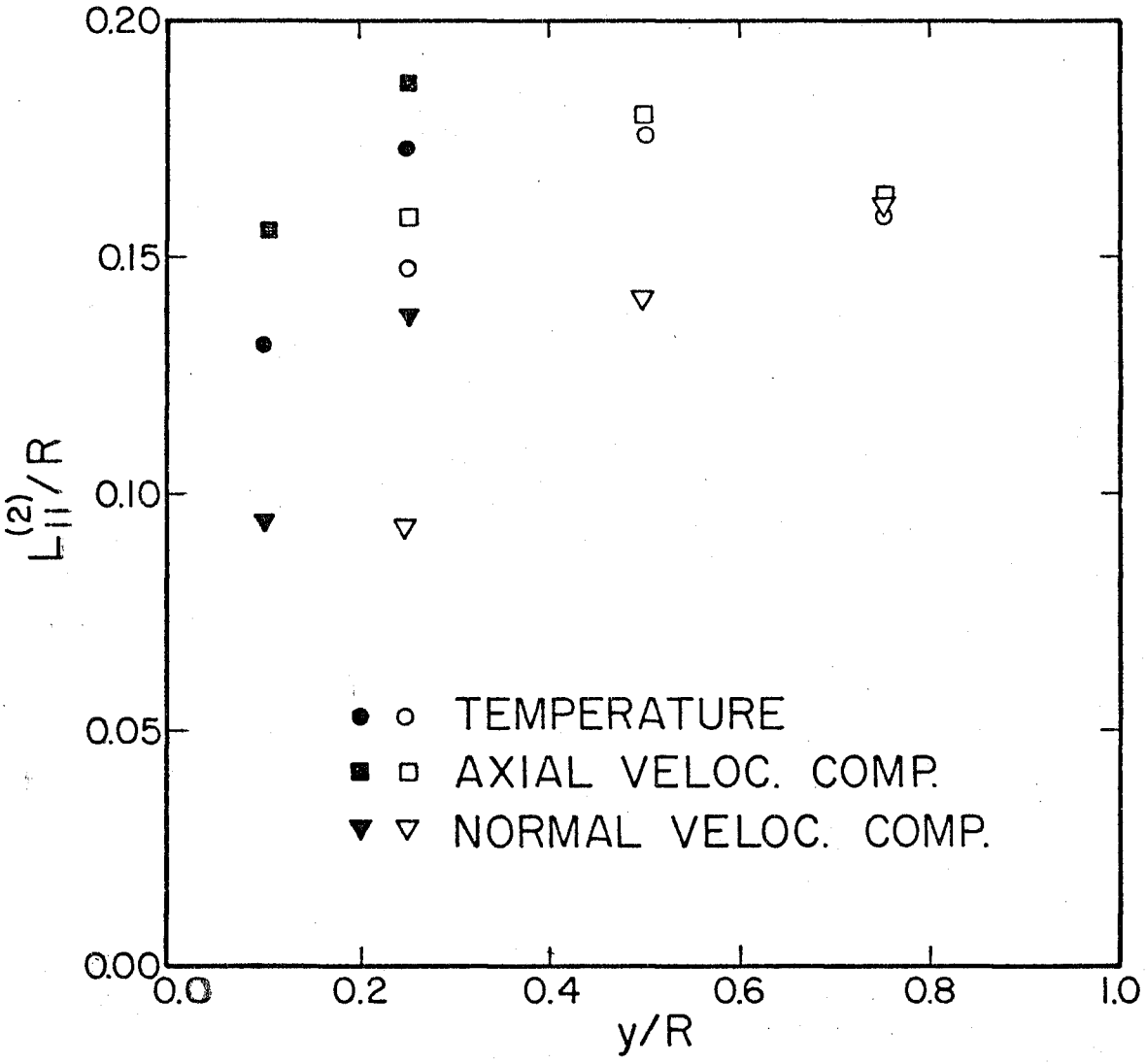

Figure 5.2-9: Integral Transverse Length Scales Velocity and Temperature

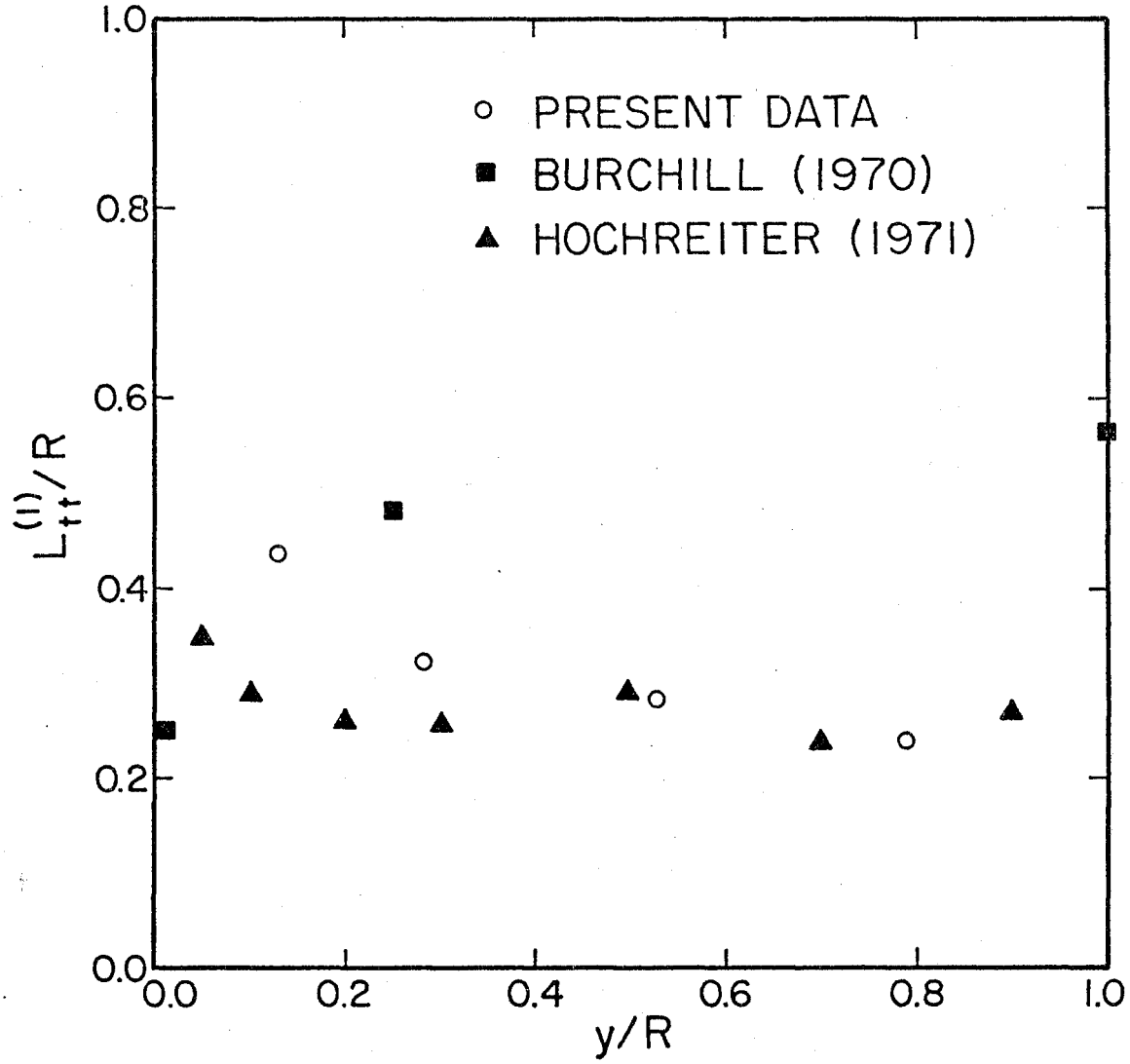

Figure 5.2-10: Temperature Longitudinal Length Scales
Open Symbols - Two-Point Meas.
Dark Symbols - Single Point Meas.

$$k = \frac{2\pi f}{\overline{U}} \qquad (5.2\text{-}2)$$

where $\overline{U}$ is the local mean fluid velocity.

The agreement between the present data and Hochreiter's results in the core region is good. Also the trends for the radial dependence are the same, unlike Burchill's results which show scales increasing with the distance from the wall. The smaller values reported by Hochreiter near the wall seem to show the effect of the existence, in the case of mercury, of a significant axial mean temperature gradient. This gradient in water flows is usually very small and usually neglected. Therefore, the decorrelation rate with axial separation in water will be smaller than for the case of mercury, thus corresponding to bigger scales.

Figure 5.2-11 shows a comparison between temperature and velocity (both axial and normal components) longitudinal scales. The temperature and the axial velocity component scales were obtained directly from the present two-point measurements. The normal velocity component scales were calculated by using

$$L_{22}^{(1)} \simeq \overline{u_2^2}\, \mathcal{J}_{22}^{(1)} \qquad (5.2\text{-}3)$$

from the corresponding values of the integral convected time scales (estimated in section 4.2).

It is interesting to note that, once more, for all radial locations examined $L_{22}^{(1)} < L_{tt}^{(1)} < L_{11}^{(1)}$ holds. This shows that the fluctuating temperature field is determined by both (certainly all) components of the velocity field. In addition, the relative influence of the different velocity components on the behavior of the temperature fluctuations appears to be radially dependent. For example, close to the wall, the temperature fluctuations seem to follow more closely the axial velocity component than the normal component. In the

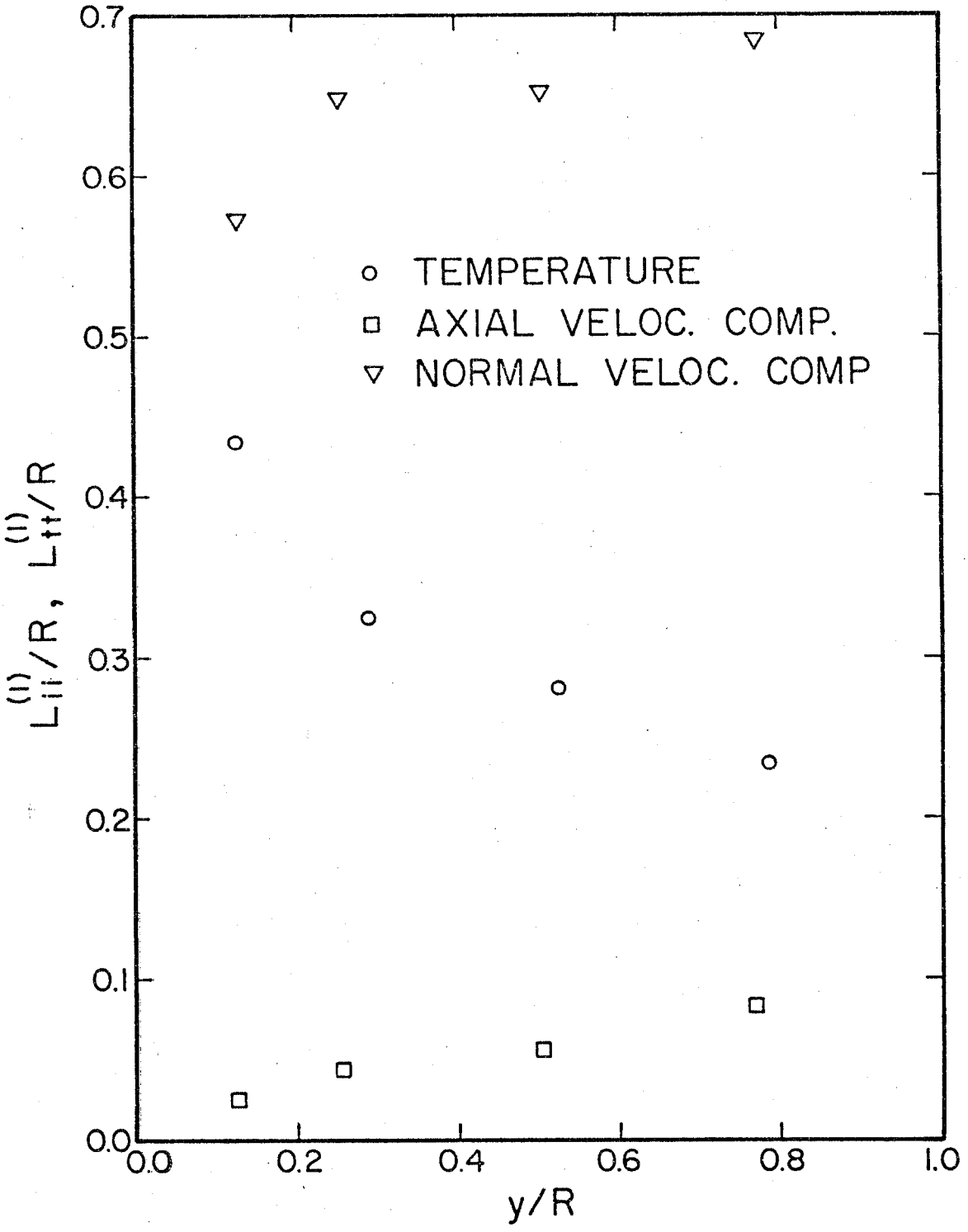

Figure 5.2-11: Integral Longitudinal Length Scales Velocity and Temperature

center region both components of the velocity field seem to affect equally the temperature field. In order to examine this point one step further, characteristic frequencies (i.e. the frequency corresponding to maximum energy) for all three fluctuating signals (u_1, u_2 and Θ) were obtained from spectral functions reported by Burchill (1970). The radial dependence of these frequencies is shown in Fig. 5.2-12. The large difference between the characteristic frequencies for the temperature and normal velocity component fluctuations near the wall may explain why the fluctuating temperature field follows more closely the axial rather than the normal velocity component field in this region. Near the centerline the normal velocity component shows smaller characteristic frequencies and, therefore, it begins to affect more strongly the behavior of the temperature fluctuations. It is interesting to note that the previous discussion may be applied, without modifications, to explain the radial variation of the integral convected time scales for the three fluctuating signals (u_1, u_2 and Θ). These time scales are shown in Fig. 5.2-13.

Due to the availability of complete sets of space-time correlation curves from axial separation measurements for both temperature and axial velocity component signals, a comparative study was made on the convection velocities for these two turbulent fields. In connection with space-time, axial separation, correlation curves two definitions of a convection velocity can be used. In the first one the convection velocity, for a fixed separation x_1, would be given by

$$U_c = \frac{x_1}{\tau_m} \tag{5.2-4}$$

where the time delay τ_m satisfies

$$\left.\frac{\partial R(x_1;\tau)}{\partial \tau}\right|_{\tau=\tau_m} = 0 \tag{5.2-5}$$

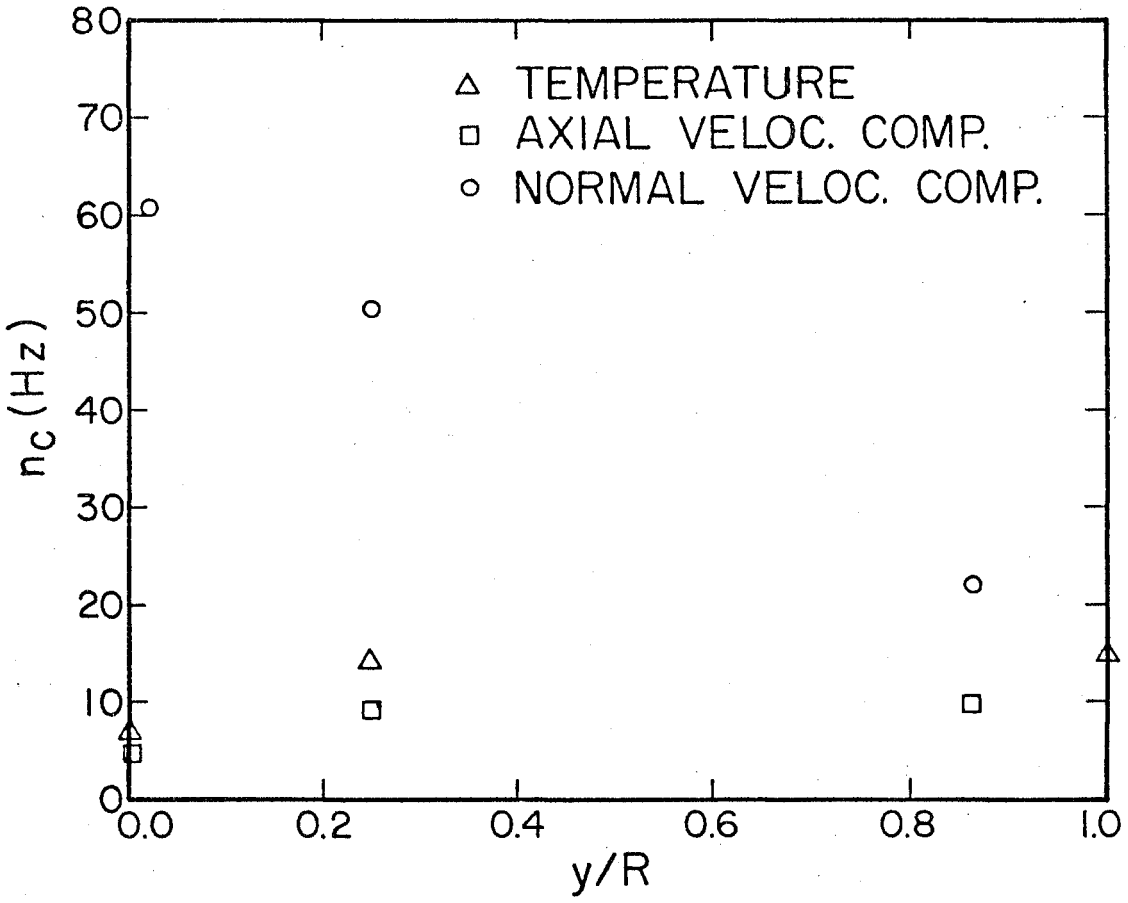

Figure 5.2-12: Characteristic Frequencies-Temperature and Velocity Fluctuating Signals

In a similar manner we can also define a convection velocity for a fixed time delay τ_1 and a varying separation as

$$V_c = \frac{x_{1m}}{\tau_1} \tag{5.2-6}$$

where x_{1m} satisfies

$$\left.\frac{\partial R(x_1;\tau_1)}{\partial x_1}\right|_{x_1=x_{1m}} = 0 \tag{5.2-7}$$

The difference between the convection velocities calculated with (5.2-4) and (5.2-6) is a measure of how much the turbulent flow being examined deviates from the perfectly frozen Taylor's model. A detailed discussion on this point can be found, among others, in Wills (1964) and in Cliff and Sandborn (1973). In the present study definition (5.2-4) was used. This was done since measurements were taken for a small number of separations and thus the accuracy in the convection velocity would be very poor had (5.2-6) been used. In addition to that, by looking at the shapes of the peaks in the correlation curves shown in Figs. 4.2-2 and 5.2-2 it appears that no significant difference would be obtained by using (5.2-6) instead of (5.2-4). The resulting convection velocities, normalized with the local mean velocity, are presented in Fig. 5.2-14 for both temperature and axial velocity component signals. Within the experimental errors involved there is no difference whatsoever between the convection and the local mean velocity. This result holds for both temperature and axial velocity component measurements and all radial locations examined. The same result holds for axial separation measurements for temperature in the thermal entrance region. The reason this occurred may be found in the fact that only relatively small axial separations

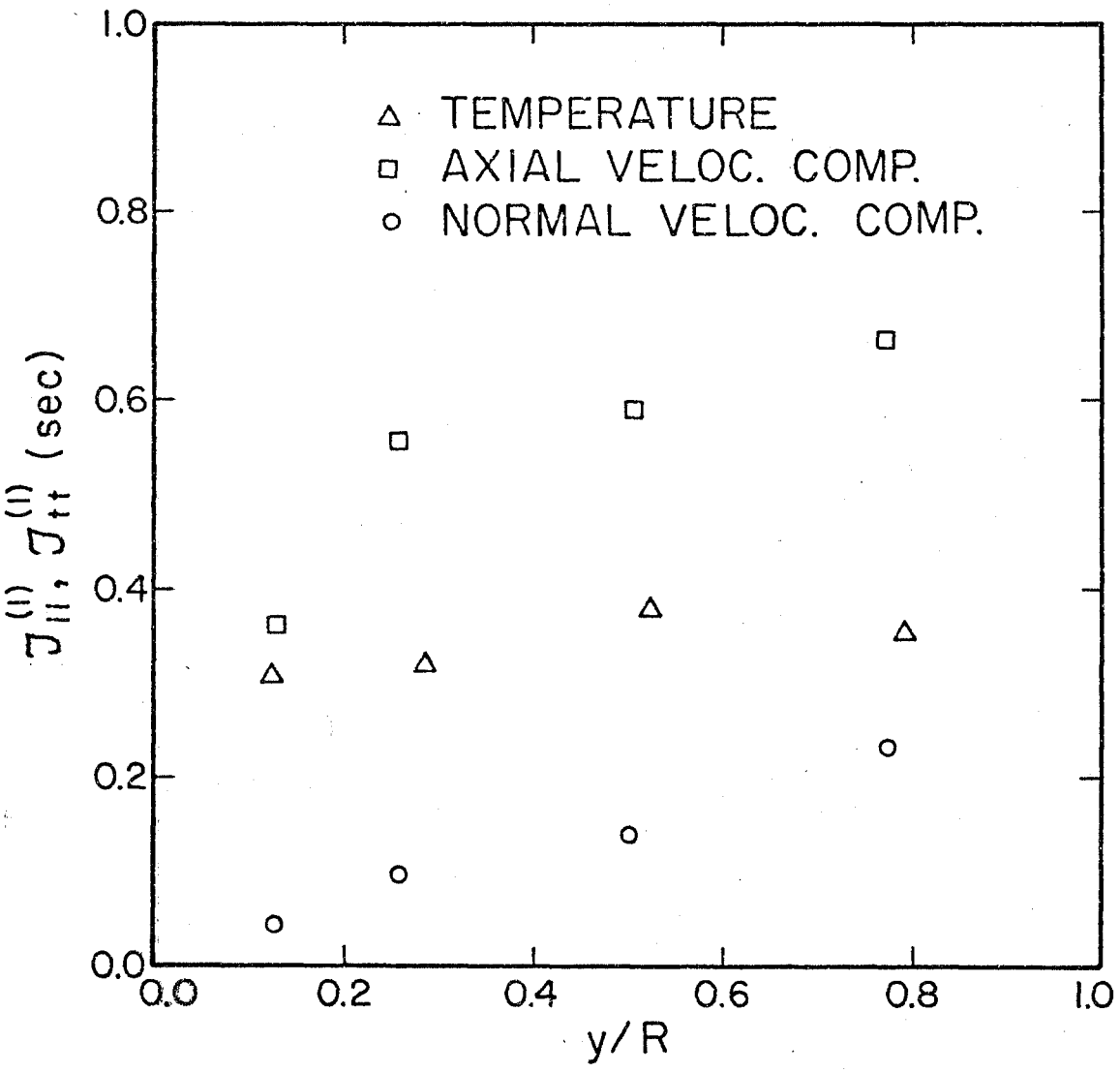

Figure 5.2-13: Integral Convected Time Scales
Velocity and Temperature

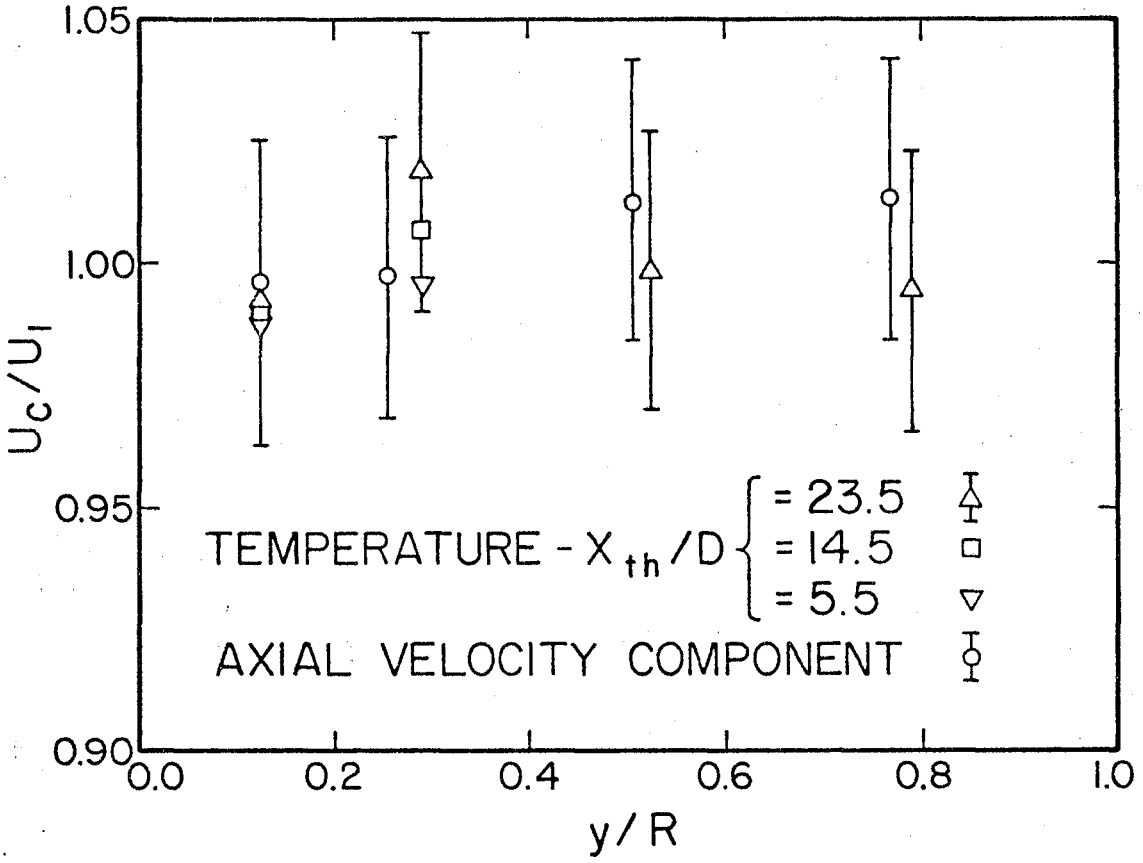

Figure 5.2-14: Normalized Convection Velocities-Temperature and Axial Velocity Component

(maximum x_1=4R) were used in the present work. Sabot and Comte-Bellot (1971) have reported convection velocities slightly smaller than the corresponding mean velocities, but for x_1 = 10 R. Their results also have shown a ratio $U_c/\overline{U}$, decreasing with x_1/R for $0.16 < Y/R < 1.0$. Close to the wall they have obtained convection velocities larger than the local mean fluid velocities. This last result seems to be consistent with the model for convection velocities proposed by Cliff and Sandborn (1973).

6. ANALYSIS OF THE RESULTS AND INTERPRETATIVE MODELS

6.1 Modeling Two-Point Velocity Correlations

The inappropriateness of the isotropic models to represent confined shear flows can readily be seen by looking at the differences between the intensities for the various velocity components or the existence of non-zero shear coefficients. Therefore, to represent two-point correlations we have examined somewhat more complicated forms, namely, the ones from axisymmetric models.

6.1.1 Axisymmetric Turbulence - Introduction

The theory of axisymmetric turbulence was first derived by Batchelor (1946) and extended by Chandrasekhar (1950). In this theory the two-point correlation tensor defined by

$$Q_{ij} = \overline{u_i(\vec{x})\, u_j(\vec{x}+\vec{r})} \qquad (6.1\text{-}1)$$

is invariant only for rotations with respect to a preferred axis $(\vec{\lambda})$ and for reflections in planes containing this axis. This theory assumes homogeneity which makes it applicable only to regions in the flow field where the length scales are small compared to the spatial variation of the turbulence intensities. The end result of this theory is that the correlation tensor Q_{ij} can be fully represented by the knowledge of two scalar functions Q_1 and Q_2 of the variables r^2 and r_μ such that the following equations are satisfied

$$Q_{ij} = A\xi_i\xi_j + B\delta_{ij} + C\lambda_i\lambda_j + D\left[\lambda_i\xi_j + \xi_i\lambda_j\right] \qquad (6.1\text{-}2)$$

where

$$A = \left(D_r - D_{\mu\mu}\right)Q_1 + D_r Q_2 \qquad (6.1\text{-}3a)$$

$$B = \left[-\left(r^2 D_r + r\mu D_\mu + 2\right) + r^2\left(1-\mu^2\right) D_{\mu\mu} \right. \tag{6.1-3b}$$

$$C = -r^2 D_{\mu\mu} Q_1 + \left(r^2 D_r + 1\right) Q_2 \tag{6.1-3c}$$

$$D = \left(r\mu D_\mu + 1\right) D_\mu Q_1 - \mu r D_r Q_2 \tag{6.1-3d}$$

with $r^2 = \vec{\xi}\cdot\vec{\xi}$, $r\mu = \vec{\xi}\cdot\vec{\lambda}$ (as shown in Fig. 6.1-1)

$$D_r = \frac{1}{r}\frac{\partial}{\partial r} - \frac{\mu}{r^2}\frac{\partial}{\partial \mu} \quad , \quad D_\mu = \frac{1}{r}\frac{\partial}{\partial \mu} \qquad D_{\mu\mu} = D_\mu D_\mu$$

In order to relate correlations with the scalar functions Q_1 and Q_2 let us consider the systems of coordinates shown in Fig. 6.1-1. If we use a tilde to represent components of vectors and tensors in the axisymmetric system of coordinates, we have relations between correlations in the two systems of the form

$$R_{11}(x_1,x_2,x_3) = \tilde{R}_{11}(\xi_1,\xi_2,\xi_3)\cos^2\phi - 2\tilde{R}_{12}(\xi_1,\xi_2,\xi_3)\sin\phi\cos\phi + \tilde{R}_{22}(\xi_1,\xi_2,\xi_3)\sin^2\phi \tag{6.1-4}$$

where $\tilde{R}_{11}$, $\tilde{R}_{12}$ and $\tilde{R}_{22}$ are given by the following differential equations (Goldstein and Rosenbaum (1973))

$$\tilde{R}_{11} = -\frac{1}{\sigma}\frac{\partial}{\partial\sigma}\left[\sigma^2\,\frac{Q_1(\xi_1,\sigma)}{\overline{u_1^2}}\right] \tag{6.1-5}$$

$$\tilde{R}_{22} = -\frac{\partial}{\partial\xi_3}\left[\xi_3\,\frac{Q_2(\xi_1,\sigma)}{\overline{u_2^2}}\right] + \left(\xi_3^2\frac{\partial^2}{\partial\xi_1^2} - 2\frac{\partial^2}{\partial\xi_1\partial\xi_2} + \xi_1^2\frac{\partial^2}{\partial\xi_3^2}\right)\frac{Q_1(\xi_1,\sigma)}{\overline{u_2^2}} \tag{6.1-6}$$

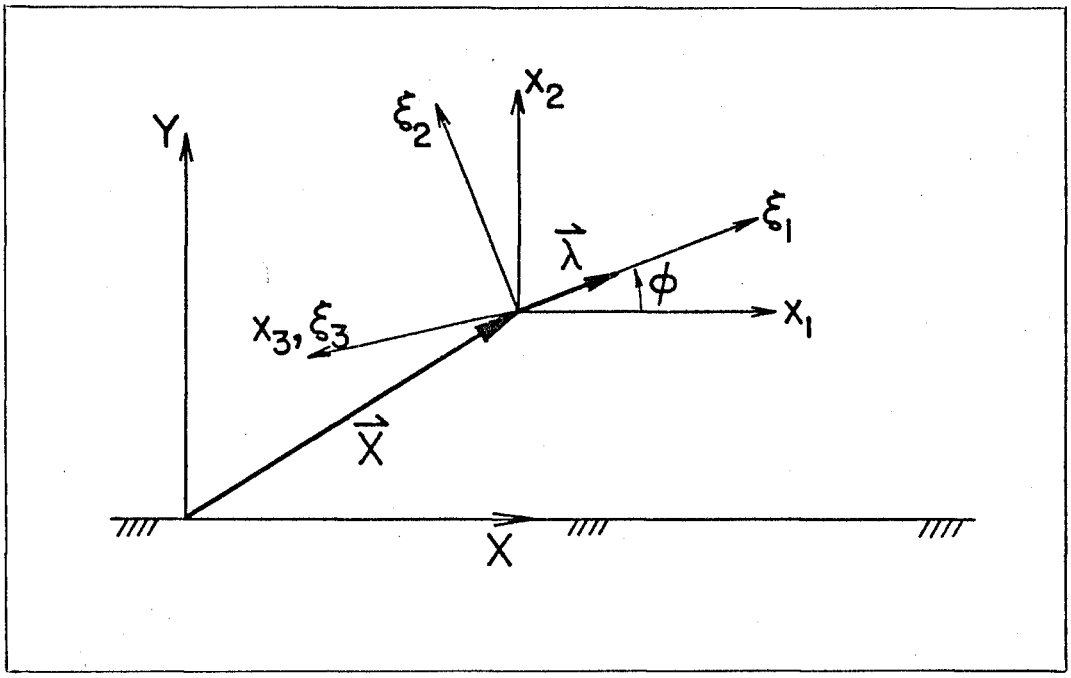

Figure 6.1-1: System of Position Coordinates (X,Y,Z)
Systems of Separation Coordinates:
(x_1, x_2, x_3) - Measurement System

(ξ_1, ξ_2, ξ_3) - Axisymmetric System

$$\tilde{R}_{12} = \frac{\partial}{\partial \xi_1}\left[\frac{Q_1(\xi_1,\sigma)}{\overline{u_1^2}}\right] \tag{6.1-7}$$

with $\sigma^2 = \xi_2^2 + \xi_3^2$ (6.1-8)

The remaining problem to obtain a representation of the two-point correlation functions is the specification of the scalar functions Q_1 and Q_2. Two approaches were analysed: the two parameter model from Goldstein and Rosenbaum (1973) and the four parameter model from Weber (1974).

6.1.2 Two and Four Parameter Models

Goldstein and Rosenbaum (1973) have proposed the following relations for the defining scalars Q_1 and Q_2

$$Q_1(\xi_1,\sigma) = -\frac{\overline{u_1^2}}{2}\exp\left[-\sqrt{\left(\frac{\xi_1}{\ell_1}\right)^2+\left(\frac{\sigma}{\ell_2}\right)^2}\right] \tag{6.1-9}$$

$$Q_2(\xi_1,\sigma) = -\left(\overline{u_2^2}-\overline{u_1^2}\right)\exp\left[-\sqrt{\left(\frac{\xi_1}{\ell_1}\right)^2+\left(\frac{\sigma}{\ell_2}\right)^2}\right] \tag{6.1-10}$$

By using (6.1-9) and (6.1-10) we can solve (6.1-5) through (6.1-7) and then use relations like (6.1-4) to obtain expressions for the correlations in the flow system coordinates. Finally, by integration, we can use measured experimental length scales to evaluate the parameters ℓ_1 and ℓ_2, e.g., through

$$L_{11}^{(2)} = \int_0^{x_{2_0}} R_{11}(0,x_2,0)\,dx_2 \tag{6.1-11}$$

with x_{2_0} = first zero crossing of $R_{11}(o,x_2,o)$. From this we obtain

$$\left(\frac{\ell_1}{\ell_2}\right)^2 = \frac{2\sin^2\phi\left\{\left(\frac{\overline{\tilde{u}_2^2}}{\overline{\tilde{u}_1^2}} - 1\right)\left[(\varphi+1)\cos^2\phi - 1\right] + \varphi\right\}}{1 - 2\cos^2\phi\left\{\left(\frac{\overline{\tilde{u}_2^2}}{\overline{\tilde{u}_1^2}} - 1\right)\left[(\varphi+1)\cos^2\phi - 1\right] + \varphi\right\}} \qquad (6.1\text{-}12)$$

and

$$\ell_1 = \frac{\overline{u_1^2}\, L_{22}^{(2)}\left(\sin^2\phi + \rho_1^2\cos^2\phi\right)^{1/2}}{\overline{\tilde{u}_1^2}\sin^2\phi + \overline{\tilde{u}_2^2}\cos^2\phi} \qquad (6.1\text{-}13)$$

with

$$\varphi = \frac{\overline{u_1^2}\, L_{11}^{(2)}}{\overline{u_2^2}\, L_{22}^{(2)}} \quad , \quad \rho_1 = \frac{\ell_1}{\ell_2} \qquad (6.1\text{-}14)$$

The first difficulty in using this two parameter model is that for a given set of length scales the allowed angles of axisymmetry may not yield realistic correlation functions. For example, from the present pipe flow measurements at Y/R = 0.50, the solutions of (6.1-12) (presented in Fig. 6.1-2) show clearly that only values for the angle of axisymmetry close to 90° are allowed. If we use some ϕ angle in this range the resultant isocorrelation contours (shown in Fig. 6.1-3) are unacceptable for pipe flow (Sabot-Comte Bellot (1972)).

A similar analysis can be applied by using other measured values of length scales, e.g., $L_{11}^{(1)}$ and $L_{11}^{(2)}$. The corresponding equations for these cases are presented in Appendix B. In any case, the range of ϕ angles for which solution is possible will be different, but the end result still will be that we cannot, for pipe flow, represent well and simultaneously the two correlation functions $R_{11}(x_1,x_2)$ and $R_{22}(x_1,x_2)$ with only two free parameters, ℓ_1 and ℓ_2.

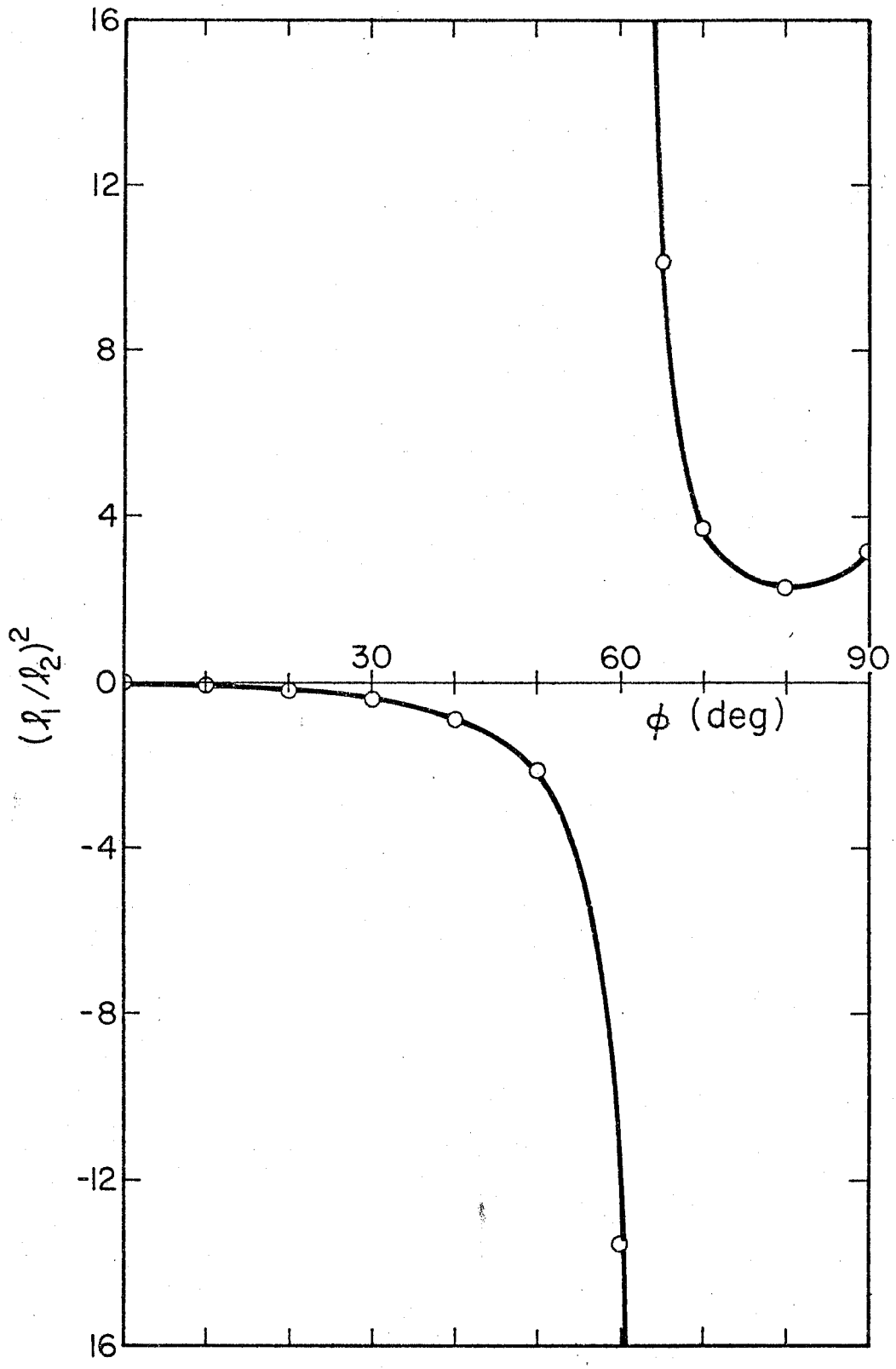

Figure 6.1-2: Angular Dependence of Free Parameter Ratio in Goldstein (1973) Model With $L_{11}^{(2)}/L_{22}^{(2)} = 1.276$

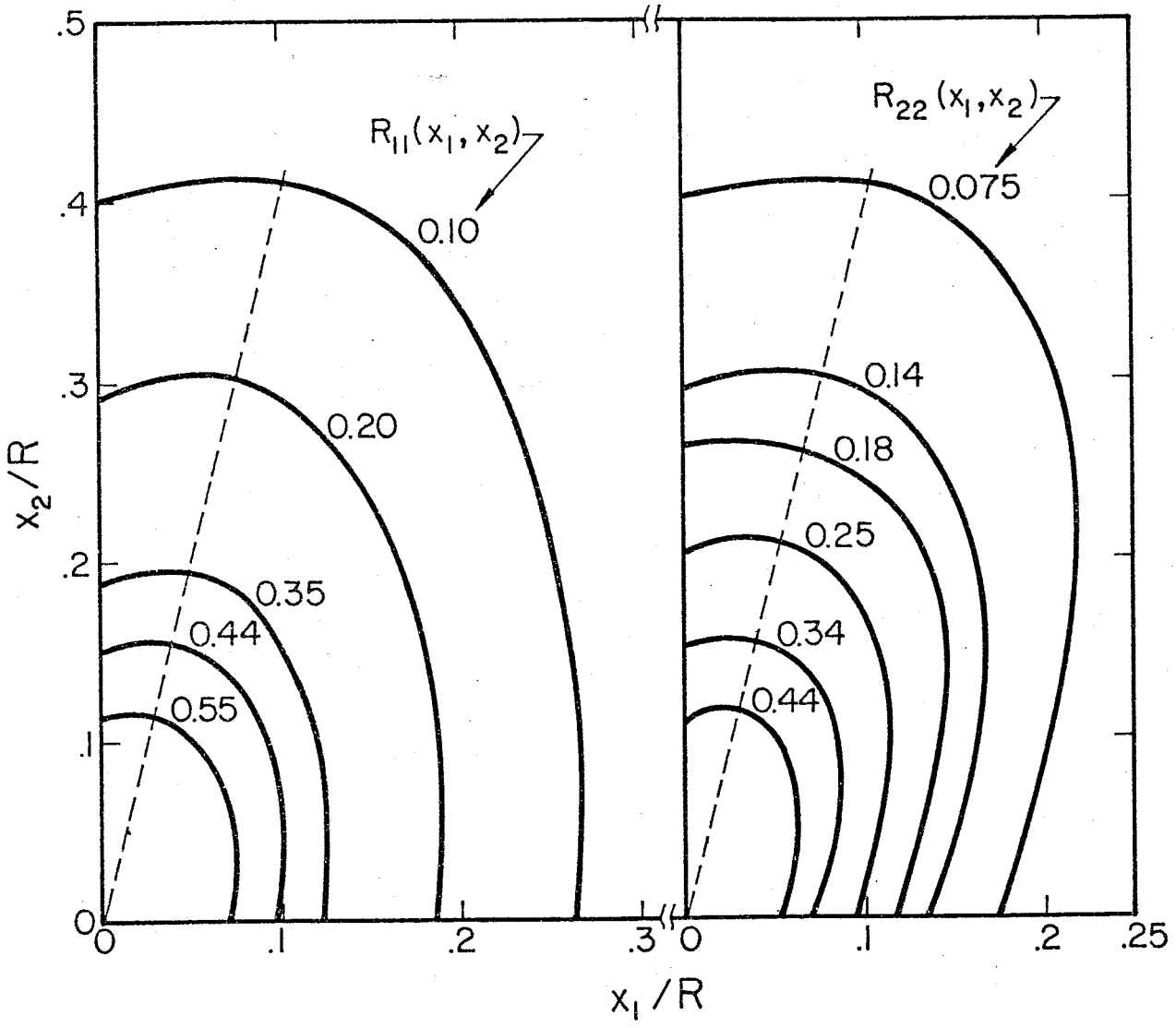

Figure 6.1-3: Isocorrelation Contours-Goldstein (1973) Two Parameter Model

This fact led Weber (1974) to derive a four parameter axisymmetric model. However, instead of postulating functional relations for the scalar functions Q_1 and Q_2 depending on four parameters he examined the behavior of the correlation functions themselves (in a mixing layer of a round jet) and proposed the following expressions to represent them (letting $\xi_3 = 0$, for simplicity, then $\sigma = \xi_2$).

$$\tilde{R}_{11}(\xi_1, \xi_2) = \left[1 - \frac{1}{2}\frac{\xi_2^2}{\ell_2^2\sqrt{\left(\frac{\xi_1}{\ell_1}\right)^2 + \left(\frac{\xi_2}{\ell_2}\right)^2}}\right] \exp\left[-\sqrt{\left(\frac{\xi_1}{\ell_1}\right)^2 + \left(\frac{\xi_2}{\ell_2}\right)^2}\right] \quad (6.1\text{-}15)$$

$$\tilde{R}_{22}(\xi_1, \xi_2) = \left[1 - \frac{1}{2}\sqrt{\left(\frac{\xi_1}{\eta_1}\right)^2 + \left(\frac{\xi_2}{\eta_2}\right)^2}\left(\frac{\xi_1^2}{\xi_1^2 + \xi_2^2}\right)\right] \exp\left[-\sqrt{\left(\frac{\xi_1}{\eta_1}\right)^2 + \left(\frac{\xi_2}{\eta_2}\right)^2}\right] \quad (6.1\text{-}16)$$

The equation for $\tilde{R}_{11}$ is the same as the one in the previous model and so is Q_1 but Q_2 was then calculated from the postulated expression for $\tilde{R}_{22}$.

Following the same procedure as before to relate free parameters to experimentally measured length scales we obtain relations

$$\begin{cases} \frac{1}{\alpha}\overline{\tilde{u}_1^2}A_1 + + \frac{1}{\pi}\overline{\tilde{u}_2^2}C_1 = \overline{u_1^2}L_{11}^{(1)} & (6.1\text{-}17a) \\ \frac{1}{\gamma}\overline{\tilde{u}_1^2}B_1 + + \frac{1}{\Delta}\overline{\tilde{u}_2^2}D_1 = \overline{u_1^2}L_{11}^{(2)} & (6.1\text{-}17b) \\ \frac{1}{\alpha}\overline{\tilde{u}_1^2}A_1 + + \frac{1}{\pi}\overline{\tilde{u}_2^2}C_2 = \overline{u_2^2}L_{22}^{(1)} & (6.1\text{-}17c) \\ \frac{1}{\gamma}\overline{\tilde{u}_1^2}B_2 + + \frac{1}{\Delta}\overline{\tilde{u}_2^2}D_2 = \overline{u_2^2}L_{22}^{(2)} & (6.1\text{-}17d) \end{cases}$$

with $$\alpha = \left(\frac{\cos^2\phi}{\ell_1^2} + \frac{\sin^2\phi}{\ell_2^2}\right)^{1/2} \tag{6.1-18}$$

$$\gamma = \left(\frac{\sin^2\phi}{\ell_1^2} + \frac{\cos^2\phi}{\ell_2^2}\right)^{1/2} \tag{6.1-19}$$

$$\Pi = \left(\frac{\cos^2\phi}{n_1^2} + \frac{\sin^2\phi}{n_2^2}\right)^{1/2} \tag{6.1-20}$$

$$\Delta = \left(\frac{\sin^2\phi}{n_1^2} + \frac{\cos^2\phi}{n_2^2}\right)^{1/2} \tag{6.1-21}$$

The coefficients C_1, C_2, D_1 and D_2 are functions of the angle of axisymmetry (ϕ) alone while A_1, A_2, B_1 and B_2 are functions of ϕ and the ratio (ℓ_1/ℓ_2). The equations for these coefficients are omitted here for convenience, but are given in Appendix B. The solutions of (6.1-17) were obtained by an interactive iterative convergence scheme and the results, for different angles of axisymmetry are presented on Table 6.1-1. Unlike the two parameter Goldstein model the four parameter model allows solutions only for small angles of axisymmetry which means that the axis of axisymmetry is more or less aligned with the mean flow, as would be expected for fully developed pipe flow.

Up to this point nothing has been said about the physical specifications of the ϕ angle. Weber (1974) used the shear angle as ϕ and showed good agreement with experimental results for the mixing layer in a round yet. In the present work a different approach was taken, namely, that of considering the space-time correlation curves available from transverse separation measurements (Fig. 4.2-1). By assuming that the isocorrelation contours can be represented by ellipses and by taking [after Sabot-Comte-Bellot (1972b)].

$$R_{11}(x_1^*, x_2; 0) = R_{11}(0, x_2; \tau_m^*) = \max. R_{11}(0, x_2; \tau) \tag{6.1-22}$$

with $$x_1^* = \tau_m^* U_{AVG} = \tau_m^* \frac{1}{x_2} \int_{-x_2/2}^{+x_2/2} \bar{U}_1(y+\eta)\, d\eta \tag{6.1-23}$$

and $$\left.\frac{\partial R_{11}(x_1, x_2)}{\partial x_1}\right|_{x_1 = x_1^*} = 0 \tag{6.1-24}$$

ϕ (DEG.)	$(\ell_1/\ell_2)^2$	$(n_1/n_2)^2$	Remarks
60	NO SOL	NO SOL	$.1 < \ell_1/\ell_2 < 10$
50	NO SOL	NO SOL	
40	6.20	< 0	
30	0.119 1.195	< 0	
20	0.112	< 0	
10	5.407	0.491	

Table 6.1-1 Angular Dependence of Free Parameter Ratios for 4 Parameter Model (Y/R=0.50)

we can calculate the isocorrelation curves presented in Fig. 6.1-4. In order to check the validity of this procedure, predicted correlations along the x_1 - axis were compared with experimentally measured values (dark symbols in Fig. 6.1-4). Due to this reasonable agreement, we feel, that it is acceptable to equate the ϕ angle to the angle between the major axis of the ellipse and the flow direction. It is clear now in Fig. 6.1-4 that the shear angle (24.1° at the location studied) can be used only for small separations in pipe flow. If one wants to represent mainly the large scale structure of the correlation functions, a much smaller angle would be appropriate, e.g.,

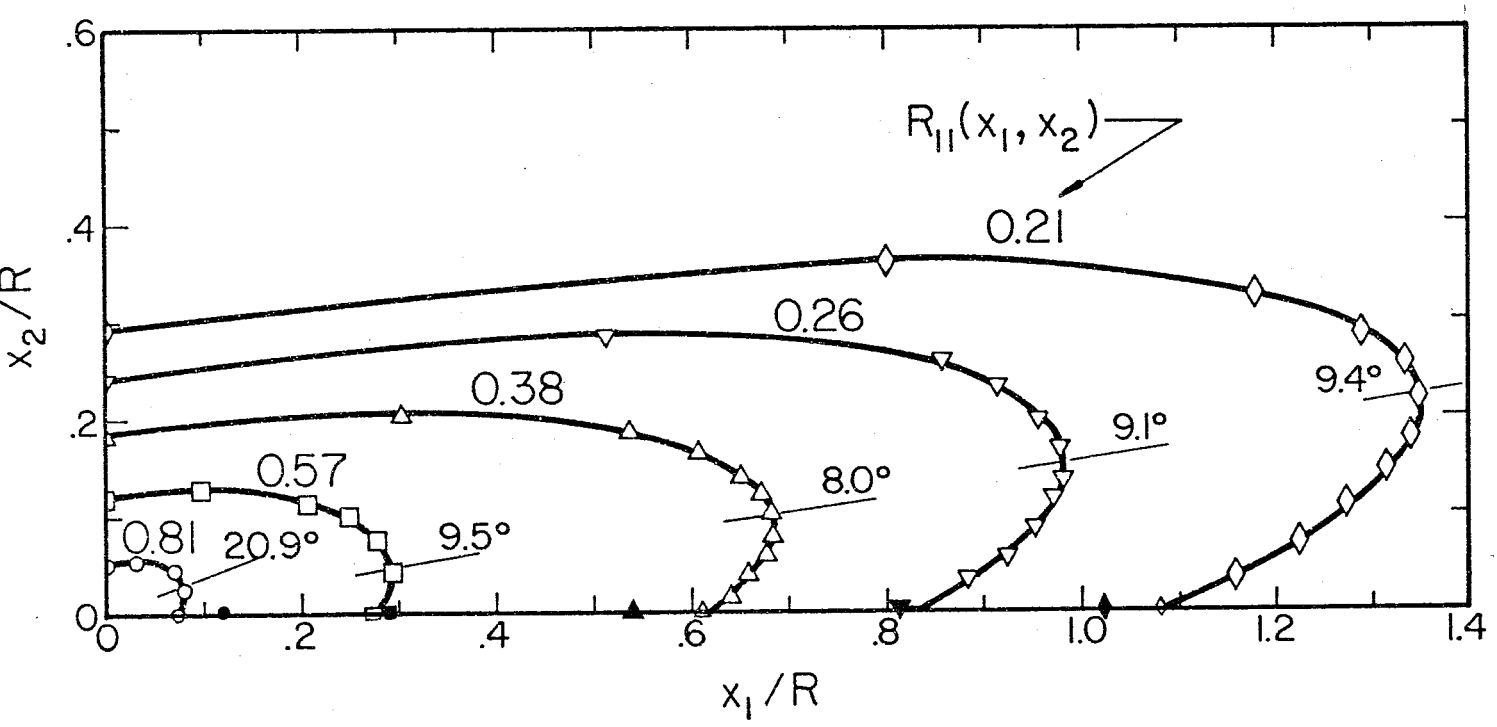

Figure 6.1-4 Ellipse Representation of Isocorrelation Contours-Axial Velocity Component

10°, which is consistent with the previous calculations made for the four parameter model and presented on Table 6.1-1. Isocorrelation maps calculated with this angle and the values for the four free parameters ℓ_1, ℓ_2, n_1 and n_2, as 1.701 in.,0.732 in.,0.149 in. and 0.213 in.,respectively,are shown in Fig.6.1-5.

6.2 Modeling Two-Point Temperature Correlations

Due to the nonexistence of any established theory for modeling two-point correlation functions for a scalar quantity, we have decided to follow a formalism, similar to the one employed in the previous section, to describe the fluctuating temperature field.

Three possible parametric representations were analysed, namely, (letting $\xi_3 = 0$, for simplicity)

Model A
$$R_{tt}(\xi_1,\xi_2) = \exp\left[-\sqrt{\left(\frac{\xi_1}{m_1}\right)^2+\left(\frac{\xi_2}{m_2}\right)^2}\right] \qquad (6.2\text{-}1)$$

Model B
$$R_{tt}(\xi_1,\xi_2) = \left[1-\frac{1}{2}\sqrt{\left(\frac{\xi_1}{m_1}\right)^2+\left(\frac{\xi_2}{m_2}\right)^2}\left(\frac{\xi_1^2}{\xi_1^2+\xi_2^2}\right)\right]\cdot \exp\left[-\sqrt{\left(\frac{\xi_1}{m_1}\right)^2+\left(\frac{\xi_2}{m_2}\right)^2}\right] \qquad (6.2\text{-}2)$$

Model C
$$R_{tt}(\xi_1,\xi_2) = \left[1-\frac{1}{2}\sqrt{\left(\frac{\xi_1}{m_1}\right)^2+\left(\frac{\xi_2}{m_2}\right)^2}\left(\frac{\xi_2^2}{\xi_1^2+\xi_2^2}\right)\right]\cdot \exp\left[-\sqrt{\left(\frac{\xi_1}{m_1}\right)^2+\left(\frac{\xi_2}{m_2}\right)^2}\right] \qquad (6.2\text{-}3)$$

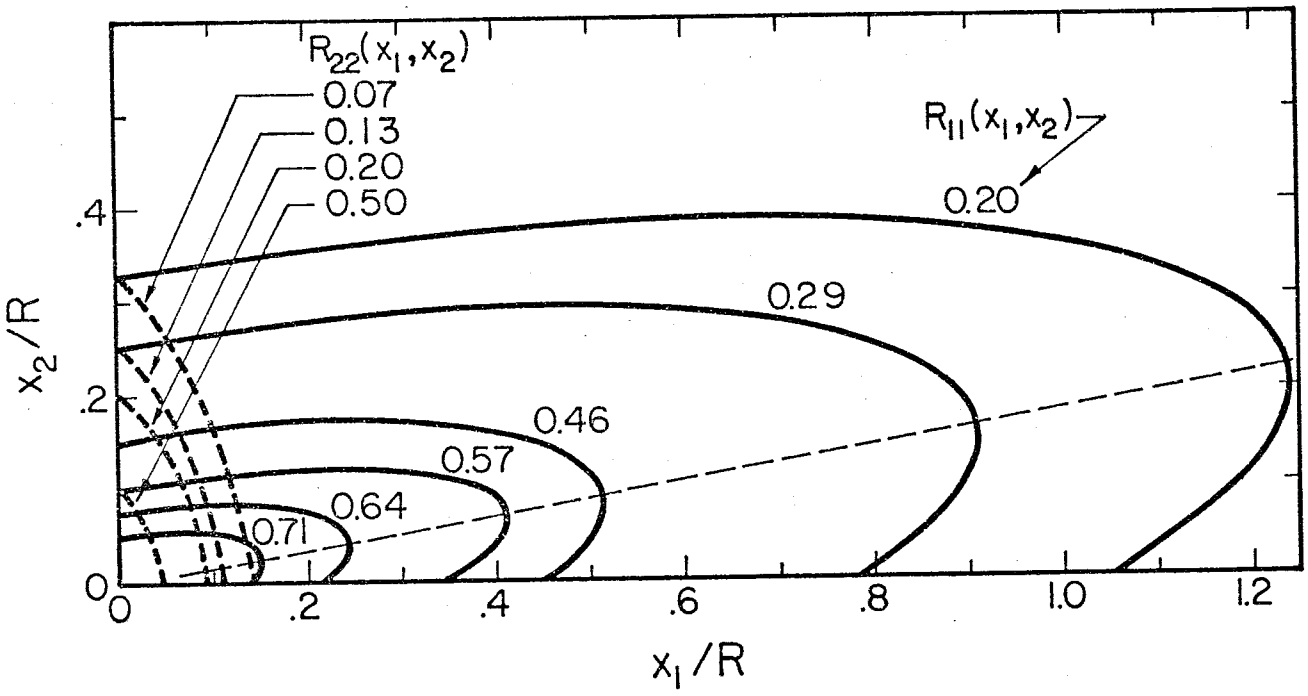

Figure 6.1-5: Isocorrelation Contours-Weber (1974) Four-Parameter Model

where m_1 and m_2 are free parameters and (ξ_1, ξ_2, ξ_3) are again separation coordinates in the axisymmetric system pictured in Fig. 6.1-1 and related to the separation coordinates in the measurement system through the angle of axisymmetry ϕ.

Model A is a straight exponential form and, therefore, assumes the correlation function to be always positive, no matter how large the separation is between the two points whose temperature fluctuating signals are being cross correlated. Models B and C allows the correlation function to become negative depending upon the direction and magnitude of the separation vector. If the turbulent temperature eddies are somewhat aligned with the mean flow, like the velocity ones, this would mean that negative correlations would occur in a direction parallel to the mean flow in model B and normal to it in model C. In this experimental research no such negative values for the two point temperature correlations were obtained, for both axial and transverse separation measurements. However, Subbotin et.al. (1964) have reported a few, small but negative, correlation values for two-point radial separation measurements, in a circular pipe. Similar results were obtained by Ibragimov et.al. (1968a, 1968b) in flows in square channels.

Let us now examine the possibilities of models A, B and C, in light of the present experimental results. In order to use measured experimental length scales to evaluate the free parameters m_1 and m_2, (6.2-1) was integrated along the two orthogonal axis in the flow system of coordinates to yield

$$\left(\frac{m_1}{m_2}\right)^2 = \frac{\left[1 + \left(\frac{L_{tt}^{(1)}}{L_{tt}^{(2)}}\right)^2\right]\cos^2\phi - 1}{1 - \left[1 + \left(\frac{L_{tt}^{(1)}}{L_{tt}^{(2)}}\right)^2\right]\sin^2\phi} \qquad (6.2\text{-}4)$$

It is clear from (6.2-4) that for a given set of measured length scales only certain values for the angle of axisymmetry are allowed. To illustrate this point Fig. 6.2-1 shows the RHS of (6.2-4) for different ϕ and the ratio $(L_{tt}^{(1)}/L_{tt}^{(2)})$. In the present study values for $(L_{tt}^{(1)}/L_{tt}^{(2)})$ ranging from 3.13 at Y/R = 0.10 to 1.47 near the centerline (Y/R=0.75) were obtained. The applicability or non-applicability of (6.2-1), at each radial location, will then depend on the value assigned to the angle of axisymmetry ϕ.

Due to time limitations in all considerations that follow only one radial location will be examined, namely, Y/R = 0.50, for which the experimentally measured value of the ratio $(L_{tt}^{(1)}/L_{tt}^{(2)})$ was 1.61. This location was chosen as being the same used in the previous section, for velocity field modeling.

Following the usual procedure to relate the free parameters to length scales, we obtain for model B, after integration

$$\left(\frac{m_1}{m_2}\right)^2 = \frac{\left(\frac{L_{tt}^{(1)}}{L_{tt}^{(2)}}\right)^2 \cos^2\phi - \left(\frac{A_\phi}{B_\phi}\right)^2 \sin^2\phi}{\left(\frac{A_\phi}{B_\phi}\right)^2 \cos^2\phi - \left(\frac{L_{tt}^{(1)}}{L_{tt}^{(2)}}\right)^2 \sin^2\phi} \qquad (6.2\text{-}5)$$

where

$$A_\phi = 1 - \frac{\cos^2\phi}{2}\left(1 - e^{-\frac{2}{\cos^2\phi}}\right) \qquad (6.2\text{-}6a)$$

$$B_\phi = 1 - \frac{\sin^2\phi}{2}\left(1 - e^{-\frac{2}{\sin^2\phi}}\right) \qquad (6.2\text{-}6b)$$

Similarly, by integration, (6.2-3) yields

$$\left(\frac{m_1}{m_2}\right)^2 = \frac{\left(\frac{L_{tt}^{(1)}}{L_{tt}^{(2)}}\right)^2 \left(\frac{A_\phi}{B_\phi}\right)^2 \cos^2\phi - \sin^2\phi}{\cos^2\phi - \left(\frac{L_{tt}^{(1)}}{L_{tt}^{(2)}}\right)\left(\frac{A_\phi}{B_\phi}\right)^2 \sin^2\phi} \qquad (6.2\text{-}7)$$

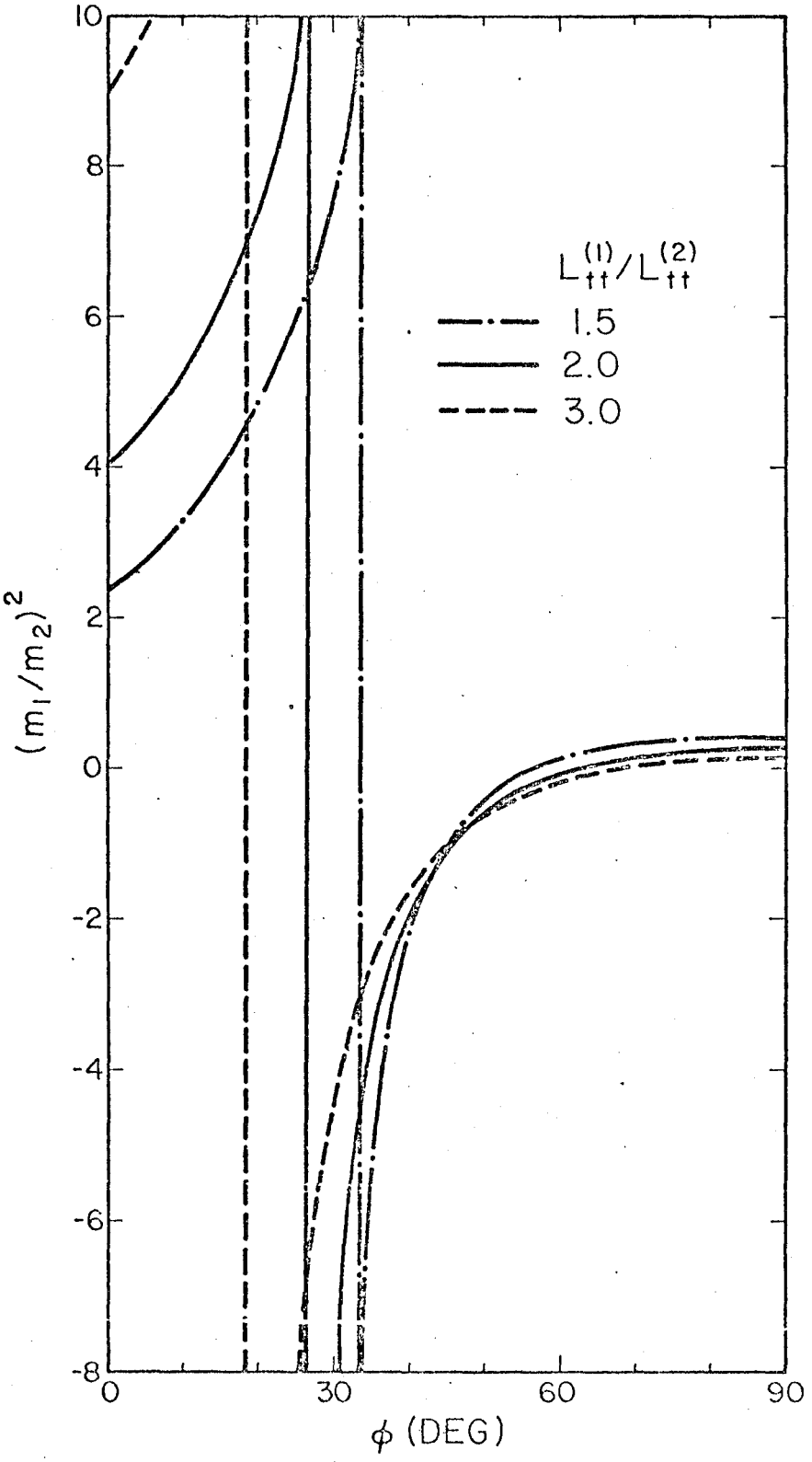

Figure 6.2-1: Dependence of Free Parameter Ratio in Straight Exponential Model on Angle ϕ and $L_{tt}^{(1)}/L_{tt}^{(2)}$

where the coefficients A_ϕ and B_ϕ are also given by (6.2-6).

For $L_{tt}^{(1)}/L_{tt}^{(2)}$ equal to 1.61 (Y/R = 0.50) the angular dependence of (6.2-5) and (6.2-7) is shown in Fig. 6.2-2. Once more it is clear that not all values for the angle of axisymmetry are allowed. In order to gain some feeling about the physical specification of the angle ϕ for two-point temperature correlation modeling, let us follow the same procedure used for the velocity field modeling. Therefore by assuming that the tempreature isocorrelation curves can be represented by ellipses and by taking

$$R_{tt}(x_1^*, x_2; 0) = R_{tt}(0, x_2; \tau_m^*) = \max R_{tt}(0, x_2; \tau) \tag{6.2-8}$$

with

$$x_1^* = \tau_m^* U_{AVG} = \tau_m^* \frac{1}{x_2} \int_{-x_2/2}^{+x_2/2} \bar{U}_1(Y+\eta)\, d\eta \tag{6.2-9}$$

and

$$\left.\frac{\partial R_{tt}(x_1, x_2)}{\partial x_1}\right|_{x_1 = x_1^*} = 0 \tag{6.2-10}$$

we can calculate (with the information provided by the space-time correlation curves from two-point transverse separation measurements shown in Fig. 5.2-1) the isocorrelation plots presented in Fig. 6.2-3. In this figure the dark symbols represent experimentally measured values of the correlations along the x_1-axis, which were used to test the validity of this procedure. Figure 6.2-3 shows that if we want to represent the two-dimensional two-point temperature correlation function at Y/R = 0.50 an angle ϕ of approximately 25° would be appropriate. This value automatically rules out the use of model B as we can see in Fig. 6.2-2. Although the straight expotential form of model A could be used to represent the two-point correlation function at Y/R = 0.50 we shall

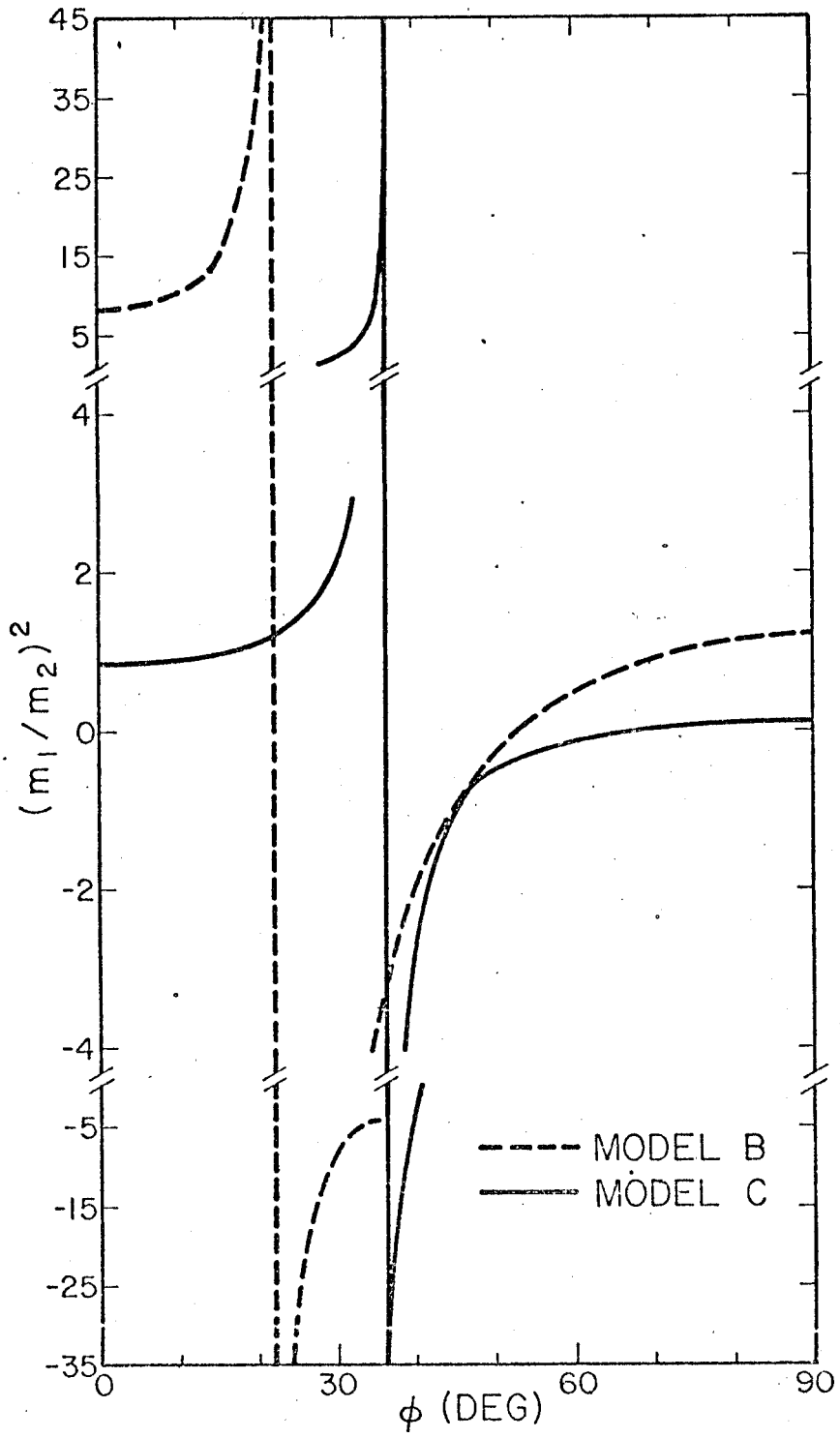

Figure 6.2-2: Angular Dependence of Free Parameter Ratio in Models B and C with $L_{tt}^{(1)}/L_{tt}^{(2)} = 1.61$

now proceed with this analysis with model C since, besides being compatible with the present experimental results, it is also consistent with the experimental findings cited previously (Subbottin et.al. (1964) and Ibragimov et.al. (1968a, 1968b)).

With $\phi = 25°$ we obtain from (6.2-7) for the ratio m_1/m_2, the value 1.17. By integration along the x_1 - axis, (6.2-3) yields

$$m_1 = \frac{L_{tt}^{(1)}}{B_\phi}\left[\cos^2\phi + \left(\frac{m_1}{m_2}\right)^2 \sin^2\phi\right]^{1/2} \qquad (6.2\text{-}11)$$

and we have for $L_{tt}^{(1)} = 0.564$ in. (Y/R = 0.50)

$m_1 = 0.641$ in

$m_2 = 0.548$ in

With these values isocorrelation maps were calculated and are presented in Fig. 6.2-4 along with the isocorrelation contours for the velocity field (including both axial and normal components) from Weber's four parameter model obtained in section 6.1. This figure shows clearly that the turbulent temperature field is dependent upon both components of the velocity field, but at the location examined (Y/R = 0.50) it follows more closely the axial rather than the radial component.

To this point we have obtained in this analysis a reasonable, although approximate, description of the large scale structure of temperature and velocity fields for a pipe flow, in terms of correlation mapping. The results of this and the previous section will now be applied, in the following one, to eddy diffusivity modeling.

6.3 Eddy Diffusivities for Heat and Momentum

One of the purposes of the correlation modeling studied in sections 6.1 and 6.2, was to provide some elements for a visualization of three dimensional

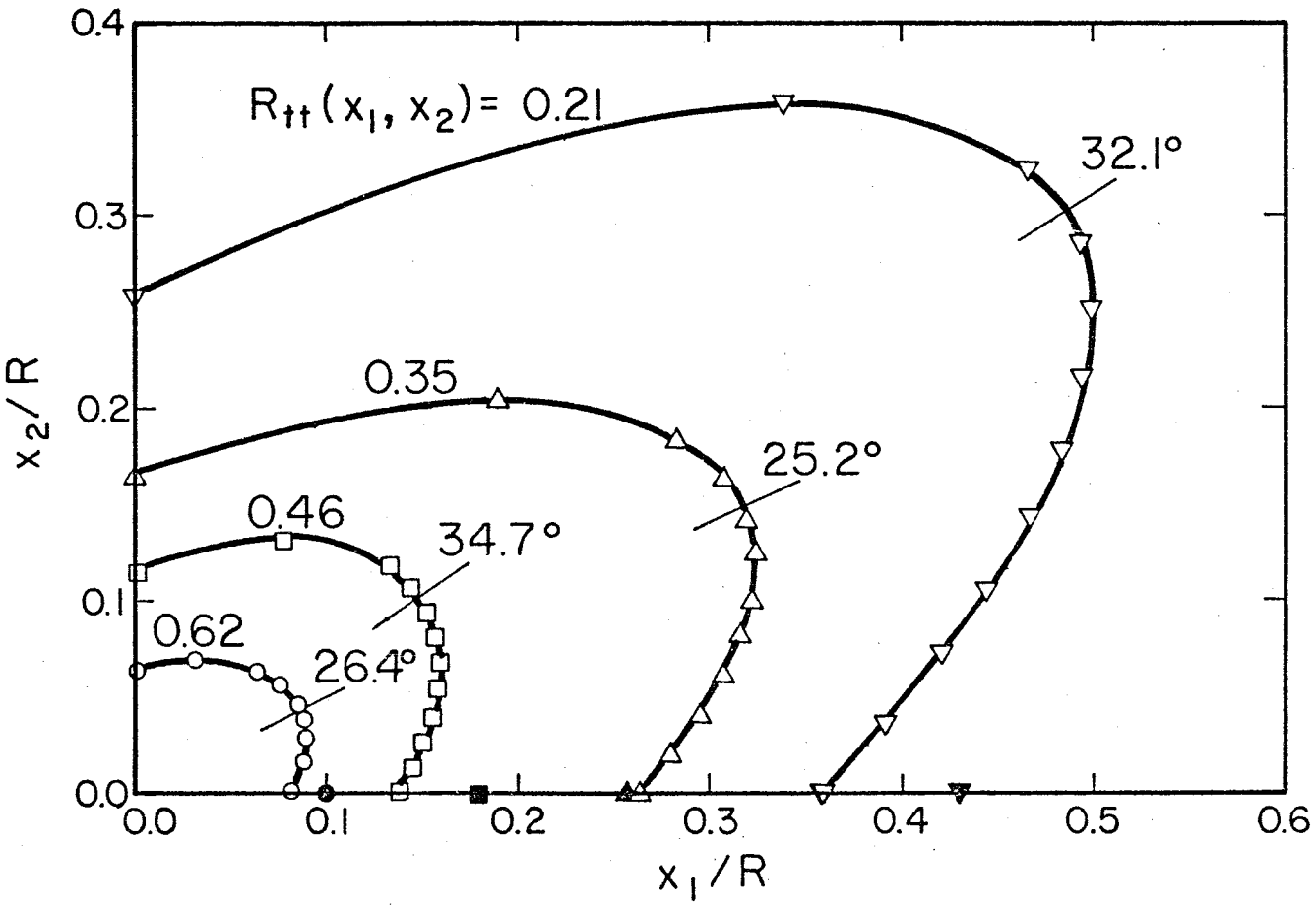

Figure 6.2-3: Ellipse Representation of Temperature Isocorrelation Countours

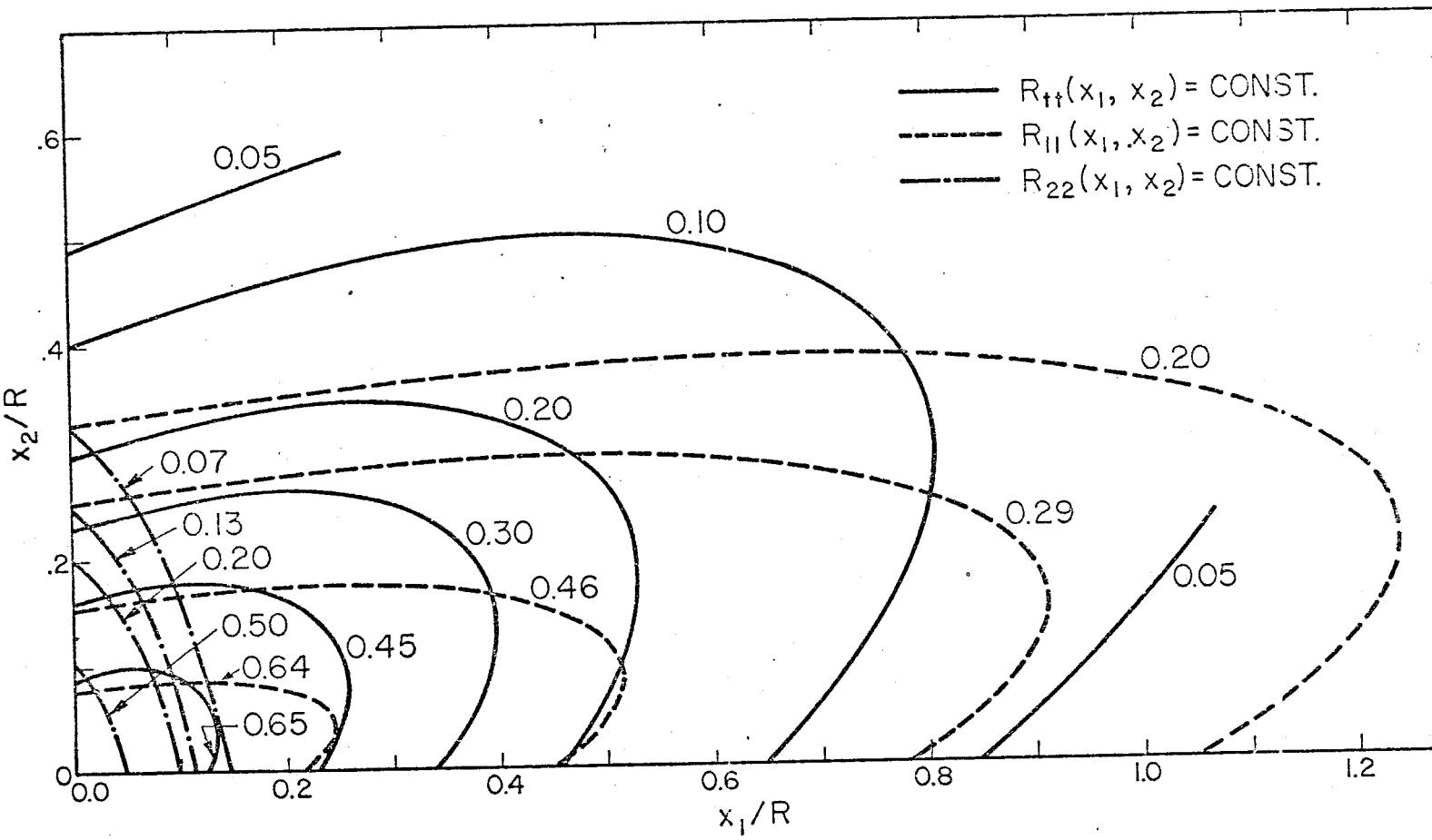

Figure 6.2-4: Modeled Isocorrelation Contours-Temperature and Velocity Fields

correlation structure of eddies. However, before going to the Tyldesley and Silver (1968) "eddy" model which requires at least a two-parameter representation of an eddy, we will examine first the "spherical" model suggested by Kudva et.al. (1968). As described in sub-section 2.2.2 this model needs as inputs:

- Size of the eddy (λ_t or λ_f)
- Lagrangian length scale (ℓ_L)
- Characteristic Lagrangian average velocity of the eddy (V_L)

In the original derivation of (2.2-7) by Kudva et.al. (1968) they used λ_f(longitudinal axial velocity microscale) in the eddy diffusivity for momentum and λ_t (longitudinal temperature microscale) in the eddy diffusivity for heat transfer. However, Hochreiter (1971) after comparing the predictions of this model with his direct experimental measurements of turbulent Prandtl number (i.e., by measuring the Reynolds shear stress $\rho\overline{u_1 u_2}$ and the turbulent heat flux $\rho c_p \overline{u_2 \Theta}$) found that better agreement was obtained whenever macroscales replaced the microscales. Hochreiter's measurements were taken in a turbulent flow of mercury in a pipe. In order to examine this point we have used the transverse integral length scales obtained in this investigation to calculate eddy diffusivities using the Kudva et.al. model. In this calculation ℓ_L was assumed to be equal to the integral length scale (i.e. $L_{11}^{(2)}$ for the eddy diffusivity for momentum and $L_{tt}^{(2)}$ for the thermal eddy diffusivity) and V_L was assumed to be given by the local RMS value of the normal velocity component (i.e. u_2'). The results for the four radial locations for which experimental scales were available are presented in Table 6.3-1. For completeness and some comparison, the results from a similar calculation using the Jenkins' model were also included in this table. The additional set of results for the

Y/R	Jenkins Model			Kudva Et.Al. Model					Remarks
	ε_H/α	ε_M/ν	$\varepsilon_H/\varepsilon_M$	ε_H/α	ε_M/ν	$\varepsilon_H/\varepsilon_M$	$\varepsilon_H/\alpha R^+$	$\varepsilon_M/\nu R^+$	
0.10	1057	184.7	0.982	908	149.6	1.042	0.109	0.105	Integral Scales
0.25	1362	206.3	1.132	1104	167.9	1.128	0.133	0.118	
0.25	-	-	-	745	122.5	1.044	0.090	0.086	Microscales
0.50	1264	200.8	1.080	1128	164.6	1.176	0.136	0.116	Integral Scales
0.75	1044	152.1	1.177	864	120.3	1.232	0.104	0.084	

Table 6.3-1

Eddy Diffusivities for Momentum and Heat Transfer-Spherical Models

Kudva et.al. model at Y/R = 0.25 was obtained by using microscales (instead of integral length scales) reported by Burchill (1970). In general all the values for the eddy diffusivities in Table 6.3-1 appear to be too high although the ones for the ratio $\varepsilon H/\varepsilon M$ are acceptable (as shown in Fig. 6.3-1). This occurs with many eddy models; one can have a model predicting correctly $\varepsilon H/\varepsilon M$ without providing the appropriate magnitudes for the eddy diffusivities (εH and εM) themselves.

Regarding Hochreiter's conclusion that microscales are not appropriate to represent the size of the eddies Figure 6.3-2 shows that in the present case exactly the opposite occurs. In this figure the eddy diffusivities for momentum from Kudva et.al. model are plotted together with the experimental results from Quarmby and Anand (1969) and Hochreiter (1971). The former were obtained in an air flow and the latter in a mercury flow. The dark circle represents the result of the use of Burchill's microscales in place of the integral length scales, for the size of the eddies. By looking at Fig. 6.3-2 it appears that, in the present case, indeed microscales should yield better results (or at least lower values) than integral length scales, when using the Kudva et.al. model. However it is not well established that the use of the dimensionless radius given by

$$R^+ = \frac{R U_\tau}{\nu} \qquad (6.3\text{-}1)$$

should collapse eddy diffusivity data for fluids with different Prandtl numbers. Furthermore, the present results (with integral length scales) show some agreement with the ones from Quarmby and Anand (1969) near the centerline.

Let us now examine the eddy diffusivity model proposed initially and in a simplified form by Tyldesley and Silver (1968) and Silver (1968), and with more details by Tyldesley (1969). This model was also given a more rigorous analysis in the wave number space by Tyldesley (1970).

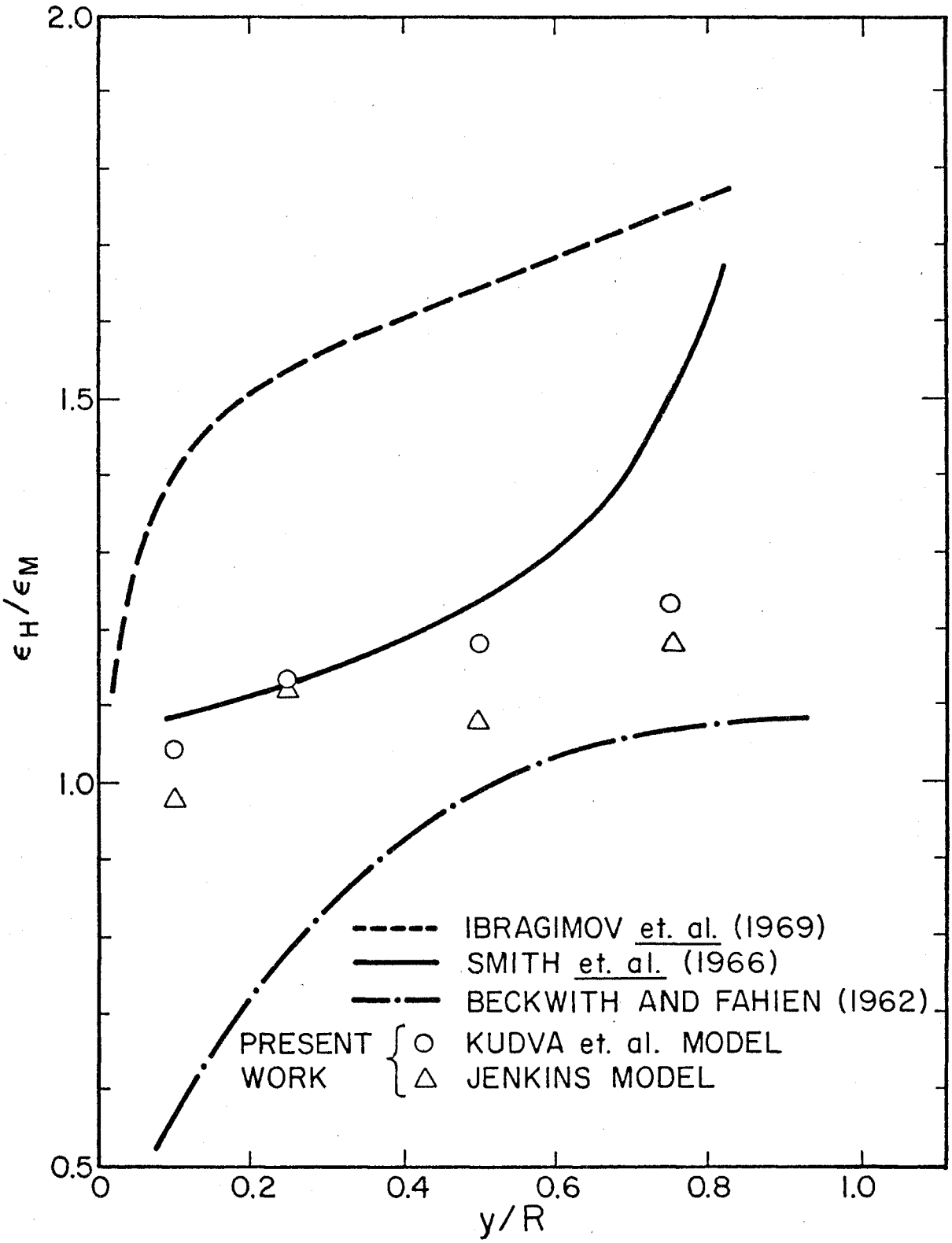

Figure 6.3-1: Eddy Diffusivity Ratio
--- Air, Re = 32,000
—— Water, Re = 11,000 -43,000
-·-·-Water, Re = 18,770

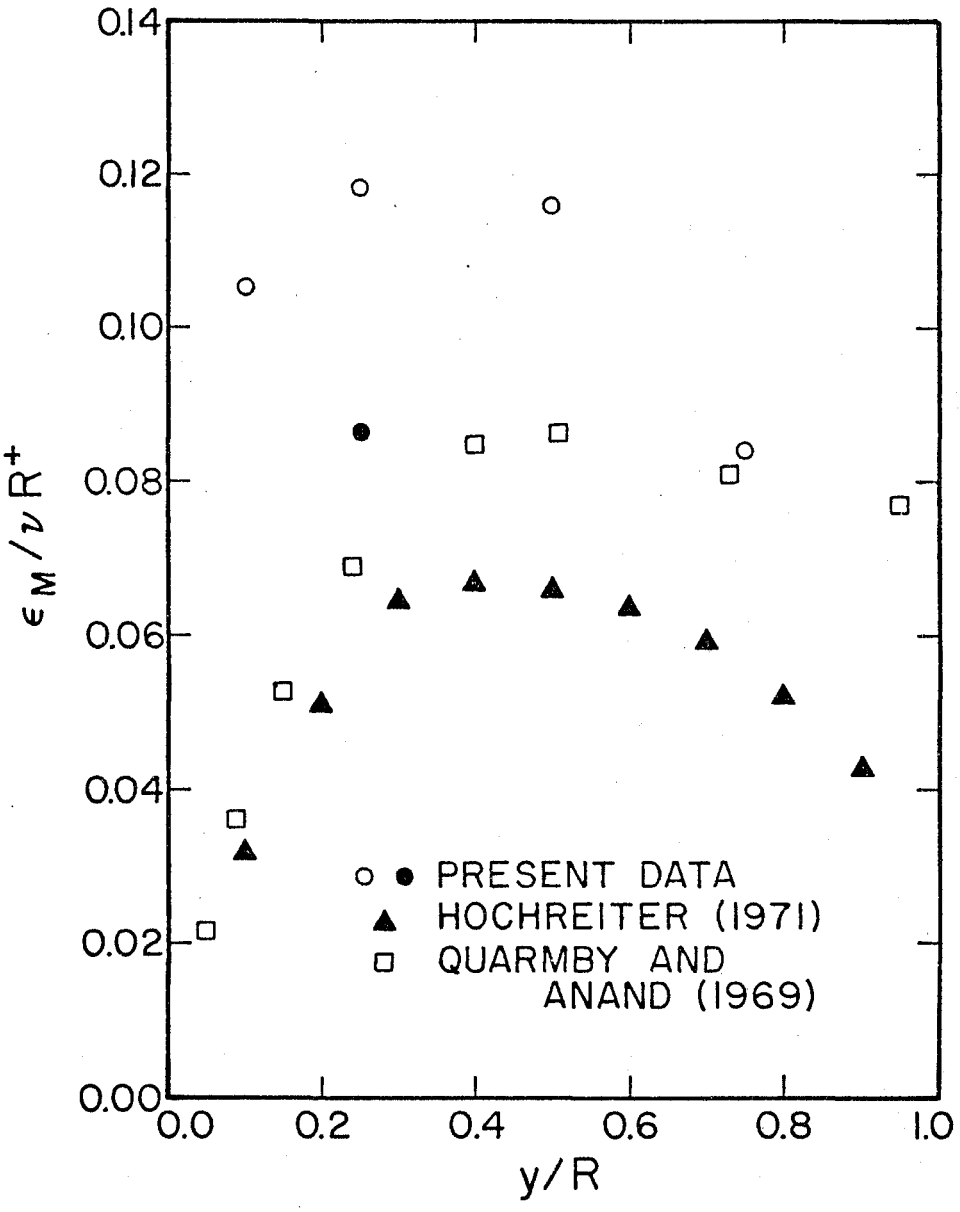

Figure 6.3-2: Eddy Diffusivities for Momentum Transfer
Present Work Results Calculated With
Kudva et.al. Model (1968)
○ Using transverse integral length scales
● Using microscales

Following the notation used by Tyldesley (1969) we have, for the large "entity" system, coefficients for momentum and thermal diffusion given by

$$\varepsilon_\mu^+ = \frac{2(\varepsilon_\mu+\mu)}{27}\left(\frac{\langle \psi_y^+ N_R^{+2}\rangle}{4-\langle \psi_y^+/\psi_x^+\rangle}\right) \tag{2.2-13}$$

and

$$\varepsilon_h^+ = \frac{(\varepsilon_\mu+\mu)}{9}\left(\frac{\langle \psi^{1+} N_R^{+2}\rangle Pr_T}{1+3Pr_T\langle \psi^{1+}/\psi_y^+\rangle}\right) \tag{2.2-14}$$

where ε_μ and ε_h are the corresponding eddy quantities for the "small" entity system and given by

$$\varepsilon_\mu = \frac{2\mu}{27}\langle N_R^2\psi_y\rangle\left(\frac{1}{4-\langle \psi_y/\psi_x\rangle}\right) \tag{2.2-11}$$

and

$$\varepsilon_h = \frac{\mu}{9}\langle \psi^1 N_R^2\rangle\left(\frac{1}{1+3Pr\langle \psi^1/\psi_y\rangle}\right) \tag{2.2-12}$$

Pr_T is the total Prandtl number given by

$$Pr_T = \frac{\varepsilon_\mu+\mu}{\varepsilon_h+\frac{k_t}{c_p}} = \frac{\varepsilon_\mu+\mu}{\varepsilon_h+\frac{\mu}{Pr}} = \frac{\epsilon_M+\nu}{\epsilon_H+\alpha} \tag{6.3-2}$$

By substituting (6.3-2), (2.2-11) and (2.2-12) into (2.2-14) and by assuming for the small scale system that $\psi_y = \psi_x = \psi^1 = \psi$, one can arrive at the following relation for the eddy diffusivity for heat transfer.

$$\frac{\epsilon_H}{\alpha} = \frac{2\psi N_R^2+81}{2187}\left[\frac{Pr\,\psi^{1+}N_R^{+2}}{\frac{3Pr^2N_R^2+27(1+3Pr)}{Pr(1+3Pr)(2\psi N_R^2+81)}+\frac{\psi^{1+}}{\psi_y^+}}\right] \tag{6.3-3}$$

where the averaging brackets were omitted for simplicity.

In order to see the effect of the distortion factors in the behavior of the eddy diffusivity across the pipe radius we can normalize (6.3-3) with the value at some radial location, e.g. half-way between the wall and the centerline.

$$\frac{\epsilon_H}{\epsilon_{H(.5)}} = \frac{\psi^{1+}}{\psi^{1+}_{(.5)}} \quad \frac{A_{(.5)} + \left(\psi^{1+}_{(.5)} / \psi^{+}_{y(.5)}\right)}{A + \left(\psi^{1+} / \psi^{+}_{y}\right)} \tag{6.3-4}$$

where

$$A = \frac{3 Pr^2 N_R^2 + 27(1+3Pr)}{Pr\,(1+3Pr)(2\psi N_R^2 + 81)} \tag{6.3-5}$$

Since for Pr > 1 Tyldesley (1969) has shown that the average initial value of $\langle \psi N_R^2 \rangle$ (in the range 810 to ∞) has almost no effect on the diffusivities, we can assume A to be constant across the radius.

In order to calculate the distortion factors ψ^{1+}, ψ^{+}_{y} and ψ^{+}_{x} using the results from the two-dimensional representation of the isocorrelation curves presented in sections 6.1 and 6.2, the large scale "entities" (eddies) were assumed as being prolate spheroids.

If a and b are the major and minor diameters of the eddy, respectively, the distortion factors ψ^{+}_{x} and ψ^{+}_{y} can be calculated with

$$\psi = \frac{a/b}{K_s^3} = \frac{\phi_e}{K_s^3} \tag{6.3-6}$$

where K_s for flow parallel to the major axis (i.e. for ψ^{+}_{x}) is given by

$$K_s = \frac{8}{3\left[\frac{2\phi_e^2 - 1}{(\phi_e^2 - 1)^{3/2}} \ln\left[\frac{\phi_e + \sqrt{\phi_e^2 - 1}}{\phi_e - \sqrt{\phi_e^2 - 1}}\right] - \frac{2\phi_e}{\phi_e^2 - 1}\right]} \tag{6.3-7}$$

and for flow normal to the major axis (i.e. for ψ^{+}_{y}) is given by

$$K_s = \frac{8}{3\left[\frac{\phi_e}{\phi_e^2-1} + \frac{2\phi_e^2-3}{(\phi_e^2-1)^{3/2}} \ln\left[\phi_e+\sqrt{\phi_e^2-1}\right]\right]} \quad (6.3\text{-}8)$$

Similarly, from a heat transfer balance in a prolate spheroid we have

$$\psi^{1+} = 2.83 \frac{a/b}{\left[\left(\frac{a}{b}+1\right)K\right]^{3/2}} \quad (6.3\text{-}9)$$

where

$$K = 1 + \frac{1}{4}m^2 + \frac{1}{64}m^4 + \frac{1}{256}m^6 + \ldots \quad (6.3\text{-}10)$$

$$m = \frac{a-b}{a+b} \quad (6.3\text{-}11)$$

The estimates for a/b for different radial locations from the procedure given in section 6.2 were then used to calculate the thermal eddy diffusivity ratios presented on Table 6.3-2 and Fig. 6.3-3

Y/R	a/b	ψ^{1+}	ψ^{1+}/ψ_Y^+	$\varepsilon_H^+/\varepsilon_{H.5}^+$
0.75	2.13	1.038	1.432	1.045
0.50	2.3	1.025	1.492	1.0
0.25	2.86	0.980	1.684	0.871
0.22	3.65	0.915	1.926	0.730

Table 6.3-2: Distortion Factors and Thermal Eddy Diffusivities Evaluated From Tyldesley's (1969) Model

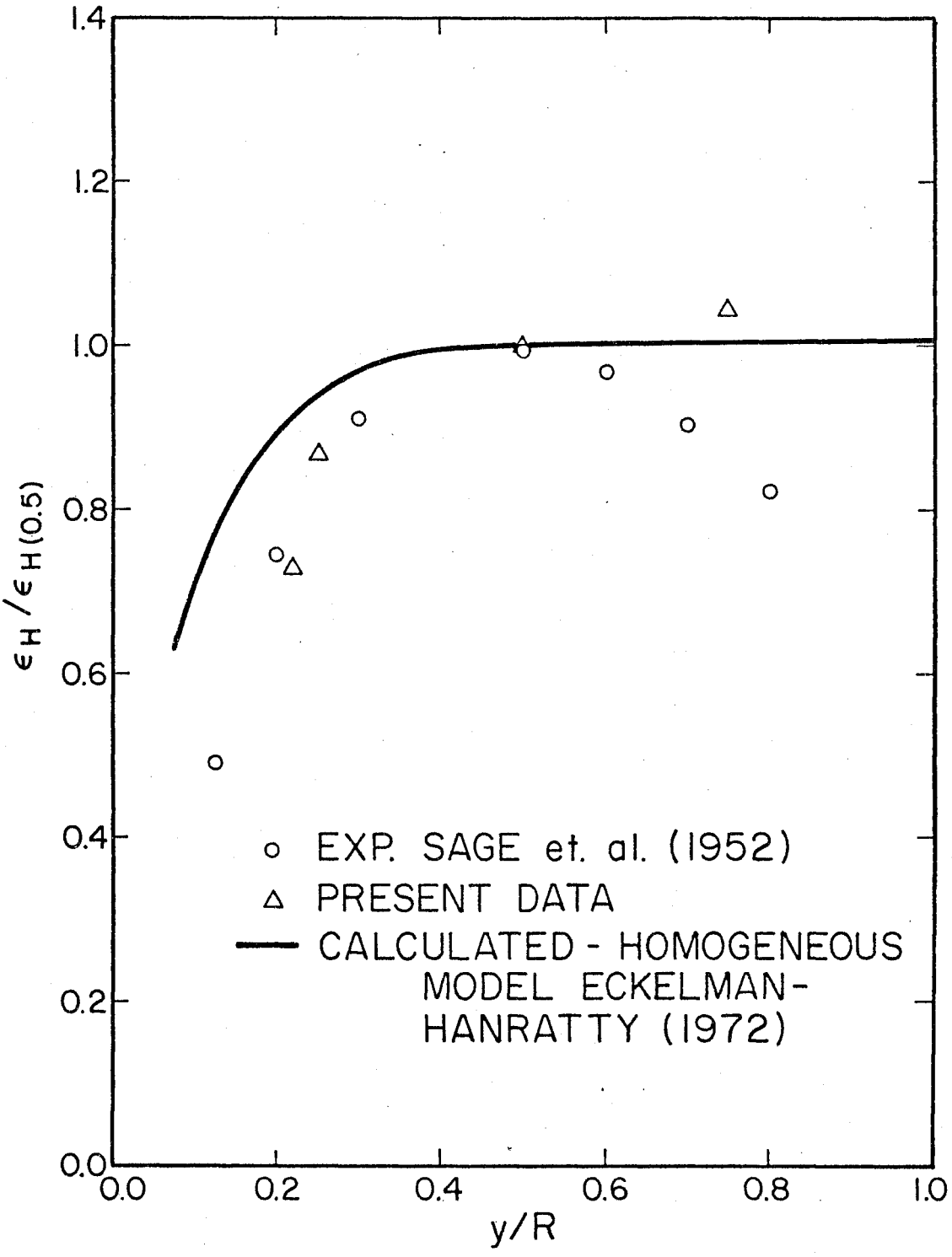

Figure 6.3-3: Radial Dependence of Thermal Eddy Diffusivities Present Work Data Calculated With Tyldesley and Silver Model (1968)

In Fig. 6.3-3 a comparison is made between the present calculations and the experimental measurements from Sage et.al. (1952) and the analytical predictions from the homogeneous model of Eckelman-Hanratty (1972). The reasonable agreement shows that distortion factors can be used to estimate eddy diffusivities, provided that the eddies can be approximately represented by ellipsoids of revolution. This can usually be done except very close to solid walls. The simplicity of the method relies on the fact that only algebraic equations are involved. Furthermore, we don't need a complete mapping of two-point correlations to get the shape of the large eddies since this can be inferred, for example, by considering the space-time correlations with transverse separations, as shown in sections 6.1 and 6.2.

In testing both the axisymmetric correlation and the eddy diffusivity models we have assumed that the dependence of the correlation between two-point signals (for both velocity and temperature fluctuations), on the x_3-separation coordinate was always the same as the dependence on the x_2-separation coordinate. As a result $L_{11}^{(2)} = L_{11}^{(3)}$ and $L_{tt}^{(2)} = L_{tt}^{(3)}$ was implied in all models although there is no experimental evidence that this holds for pipe flows. In order to investigate this point we shall now proceed to examine the implications of the theory developed by Phillips (1967,1969) to explain the mechanism by which the Reynolds shear stress is maintained in a turbulent shear flow. He has arrived at a relationship between the gradient of the Reynolds stress and the curvature of the mean velocity profile. Following the equations used by Phillips (1969) we have

$$\rho \frac{d\overline{u_1 u_2}}{dy} = \mu_e(y) \frac{d^2 \overline{U}_1}{dy^2} \qquad (6.3\text{-}12)$$

where the eddy viscosity $\mu_e(Y)$ is given by

$$\mu_e(Y) = \pi \beta \rho \overline{u_2^2} \, \mathcal{J}_{22}^{(1)} \tag{6.3-13}$$

The factor of anisotropy β depends on the shape of the energy containing eddies in the plane (x_2, x_3) and therefore is not necessarily a constant at different locations in the flow field.

By integrating (6.3-12) we have

$$\rho \overline{u_1 u_2} = \mu_e(Y) \frac{d\overline{U}_1}{dY} + \int_{Y_o}^{Y} \frac{d\mu_e(Y)}{dY} \frac{d\overline{U}_1}{dY} \, dY \tag{6.3-14}$$

which shows that, only when μ_e is independent of Y , (6.3-14) reduces to the conventional relationship between shear stress and mean velocity gradient.

The eddy viscosity defined by (6.3-13) depends on the time history of the turbulence through the integral time scale in the convected frame for the normal velocity component. Large values of the convected integral time scale, which correspond to a slow "decay rate" of the velocity fluctuations, will give large values of the eddy viscosity and vice-versa. At this point it seems reasonable to use the same formalism for the transfer of heat by relating the gradient of the turbulent heat flux to the curvature of the mean temperature profile through a variable thermal eddy diffusivity, which in this case is a function of the "decay rate" of the temperature fluctuations. Therefore, we postulate

$$\frac{d\overline{u_2\theta}}{dY} = \pi \beta_t \overline{u_2^2} \, \mathcal{J}_{tt}^{(1)} \frac{d^2\overline{T}}{dY^2} \tag{6.3-15}$$

By using the measured values for $\mathcal{J}_{tt}^{(1)}$ and the estimated values for $\mathcal{J}_{22}^{(1)}$, presented in section 4.2, the values for the β coefficients in Table 6.3-3

were obtained. Since the flow configuration required cylindrical coordinates, the following relations were used in this calculation instead of (6.3-12) and (6.3-15)

$$\rho \frac{d}{dr}\left[r\,\overline{u_1 u_2}\right] = \pi \beta \overline{u_2^2} J_{22}^{(1)} \frac{d}{dr}\left[r \frac{d\overline{U}_1}{dr}\right] \qquad (6.3\text{-}16)$$

$$\frac{d}{dr}\left[r\,\overline{u_2\theta}\right] = \pi \beta_t \overline{u_2^2} J_{tt}^{(1)} \frac{d}{dr}\left[r \frac{d\overline{T}}{dr}\right] \qquad (6.3\text{-}17)$$

The derivatives $\frac{d\overline{U}_1}{dr}$, $\frac{d\overline{T}}{dr}$, $\frac{d^2\overline{U}_1}{dr^2}$ and $\frac{d^2\overline{T}}{dr^2}$ were calculated from semi-log fits to measured mean velocity and mean temperature profiles and both $\frac{\overline{u_1 u_2}}{u_\tau^2}$ and $\frac{\overline{u_2\theta}}{u_\tau T^*}$ were assumed to vary linearly with radial location

Y/R	$J_{tt}^{(1)}$	$J_{22}^{(1)}$ EST	u_2'	β	β_t
	(msec)	(msec)	(in/sec)	-	-
0.75	354.3	227.1	0.723	0.516	0.356
0.50	377.9	132.8	0.844	0.574	0.218
0.25	322.0	87.6	0.977	0.244	0.072
0.10	307.8	42.9	1.067	0.081	0.012

Table 6.3-3: Factors of Anisotropy - Phillips' (1969) Theory

Figure 6.3-4 presents values for the β factors measure in a boundary layer over a flat plate by Blackwelder-Kovasnay (1972) and in a pipe flow by Sabot-Comte Bellot (1974) both being air flows. The straight line with slope 0.446 was proposed by Sabot-Comte Bellot (1974) to represent the radial dependence of this factor in a pipe flow. It is interesting to note the good

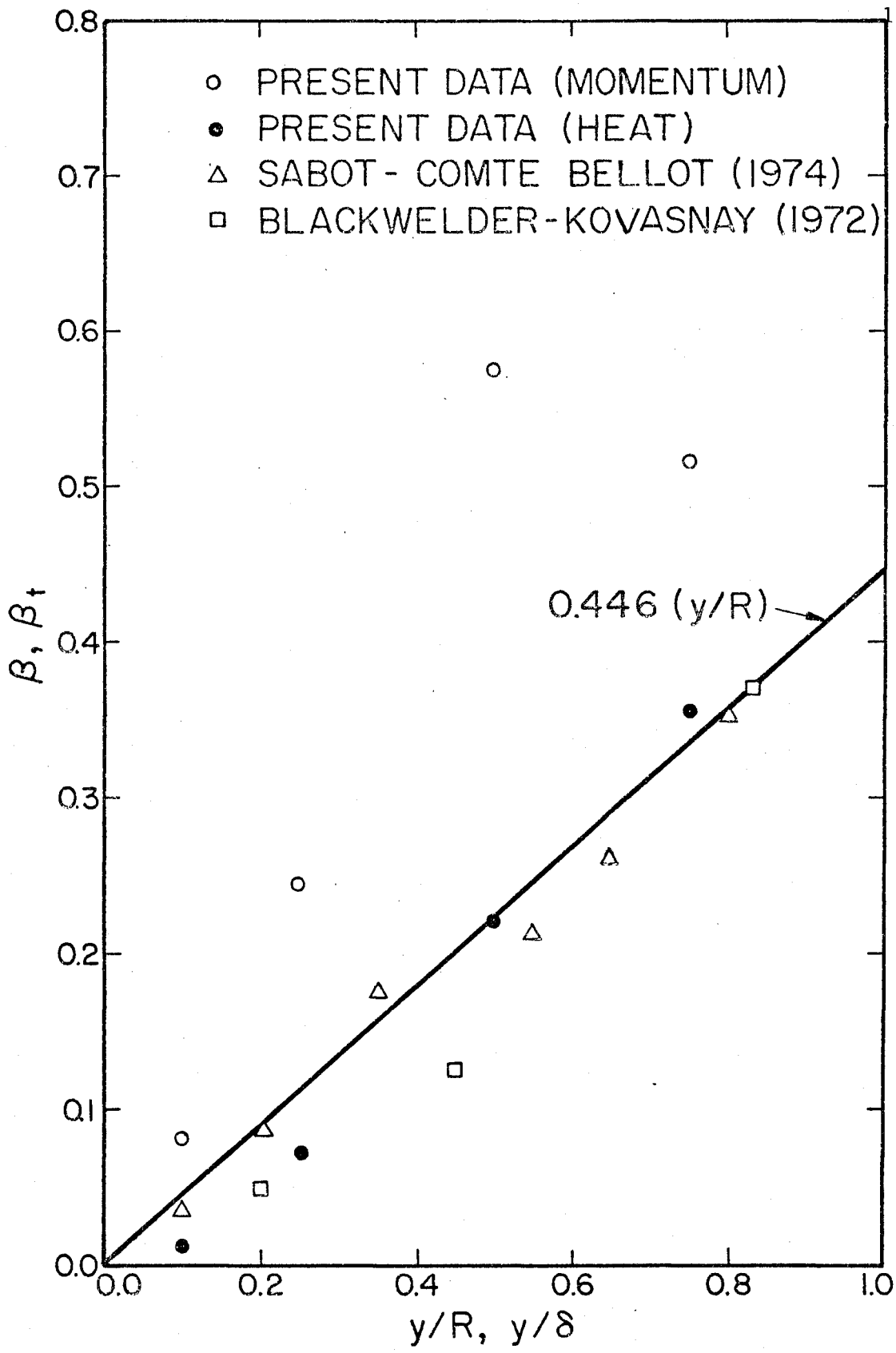

Figure 6.3-4: Coefficients of Anisotropy-Phillips (1969) Theory

agreement between the β for heat transfer (β_t), calculated in the present work, and the ones for momentum transfer from the boundary layer and pipe flow studies.

The β factors for momentum transfer calculated in the present work seem to be too high, probably due to underestimated values for the convected integral time scale for the normal velocity fluctuations. However, measurements of Kovasnay et.al. (1970) in a boundary layer over a flat plate have shown that at $Y/\delta = 0.80$ the isocorrelation contours of the normal velocity component are approximately cicular suggesting that β should be approximately unity. Even closer to the wall ($y/\delta=0.45$ and 0.20) they pointed out that their aspect ratio never exceeded 1.5 and correspondingly β should never decrease below 0.6.

Figure 6.3-4 shows that more experimental evidence is still needed to confirm or deny the applicability of Phillips' theory to confined shear flows as well as the validity of the previous assumptions concerning equality between azimuthal and transverse length scales.

7. CONCLUSIONS, REMARKS AND RECOMMENDATIONS

The research conducted in these investigations involved two parts: an experimental study and a modeling study. In the first part, two point correlation measurements were made in a turbulent flow of water in a pipe. Velocity and temperature fluctuating signals were obtained with hot film anemometers and analyzed digitally to yield both space and space-time correlations. In the isothermal measurements (velocity) a single flow rate was chosen giving a pipe Reynolds number of 56,590. All the non-isothermal measurements (temperature) were made with this same flow rate and a wall heat flux of 3,820 BTU/hr ft^2. In both cases the bulk water temperature was 80°F.

In the second part of this investigation, the experimental results were used in correlation and eddy diffusivity modeling studies. The axisymmetric models proposed by Goldstein and Rosenbaum (1973) and Weber (1974) were examined in connection with the problem of describing two-point velocity correlations in a pipe. Similar forms were used for the fluctuating temperature field. Finally the prediction capabilities of the "spherical eddy" model by Kudva et.al. (1968) and the "arbitrary shape entity model" by Tyldesley and Silver (1968) were examined.

We shall now summarize the principal conclusions and observations from the measurements and modeling studies made in this investigation:

(1) From convection velocities obtained from two-point axial separation correlation measurements, for both velocity and temperature fluctuations and with the separations used and the experimental errors involved, no difference whatsoever could be detected between these convection velocities and the corresponding local mean velocity of the fluid.

(2) Space-time cross correlations with transverse separations can be

used to estimate the shape of isocorrelated regions (for both velocity and temperature) in the turbulent field in pipe flow.

(3) The main orientation of the isocorrelation contours in pipe flow shows a declining angle of inclination with respect to the mean flow direction, for decreasing isocorrelation levels. A similar result is obtained when one uses a three-dimensional Gaussian distribution to predict the average shape of a patch of pollutant released in a homogeneous shear flow, as a function of the diffusion time. [See Monin and Yaglom (1971)]

(4) The two parameter Goldstein and Rosenbaum (1973) model is not adequate for a two-dimensional representation of the correlation functions for the two components of the fluctuating velocity (u_1 and u_2) in pipe shear flow. The four parameter Weber (1974) model can provide a reasonably good description for this type of flow.

(5) The best value for the angle of axisymmetry to represent large scale axial velocity eddies in a pipe flow is much smaller than the shear angle. For the large scale structure of the temperature field the appropriate angle of axisymmetry is somewhat larger than the one for the velocity field, the respective ranges for $\emptyset$ being $\simeq 25°$ for temperature and $\simeq 10°$ for velocity.

(6) The inequality relationship between properties of the temperature and velocity integral scale structure, namely,

$$\left\{\begin{array}{c}\text{normal velocity}\\ \text{component integral}\\ \text{scale}\end{array}\right\} \angle \left\{\begin{array}{c}\text{temperature}\\ \text{integral}\\ \text{scale}\end{array}\right\} < \left\{\begin{array}{c}\text{axial velocity}\\ \text{component integral}\\ \text{scale}\end{array}\right\}$$

was found for all radial locations examined in this work and applies for both length and time integral scales.

(7) The use of integral length scales in the transverse direction has yielded too large values for the magnitudes of the eddy diffusivities, for both momentum and heat transfers. In spite of this the Kudva et.al. (1968)

model has been shown to provide an improvement over the Jenkins (1951) model since it predicts correctly the trends in the radial dependence. Unlike Hochreiter's (1971) findings using macroscales from mercury flow, in the present case with water flow more realistic eddy diffusivity values were obtained with the Kudva et.al. (1968) model in which microscales are used to represent the size of the eddies.

(8) In the Tyldesley and Silver (1968) model, it is observed the distortion factors can account for practically all variation of the eddy diffusivities accross the pipe radius. It appears that the deviation of the experimentally measured values from the calculated ones could be significantly reduced by considering, besides the shape of the eddy, the variation of its velocity with radial location.

(9) A good agreement between factors of anisotropy for both temperature and velocity fluctuating fields was obtained, provided that the Phillips (1968, 1969) theory, concerning the maintenance of the Reynolds stress, can be extended to pipe flow and also to the turbulent heat flux.

The following limitations must be added to the previous conclusions and observations:

(a) The testing of the axisymmetric models in this study was done at only one radial location. The extension of the results and conclusions to all other points in the flow field may not be completely valid.

(b) No experimental two-point measurements are available, in planes x_1 = const., for a pipe flow. Therefore, no definite conclusion can be drawn, as yet, regarding the applicability of Phillips' theory and the validity of the assumption that scales in the azimuthal and transverse directions are equal.

This last limiting remark can lead us to the first recommendation for a

possible extension of the present work, i.e., two point temperature and velocity measurements with both axial (x_1) and azimuthal (x_3) separations. By cross correlating the two-point fluctuating signals, space-time correlations could be generated and used for similar analysis of the large scale structure to the one employed by Kovasnay et.al. (1970) in a boundary layer flow over a flat plate.

Another study could be the use of the two-point axial separation turbulent signals (both temperature and velocity) recorded in this study, plus additional measurements (with larger separations) if needed, for either a cross spectral or a narrow frequency band pass correlation analysis. By doing so, one could investigate the dependence of the convection velocities upon frequency and/or size of the eddies, at different radial locations in the pipe. The results could be extremely useful, for example, in testing Cliff and Sandborn (1973) theory concerning convection velocities in a wall bounded shear flow.

The existence of a low frequency secondary peak in the spectral function of temperature fluctuations, reported by Verollet and Fulachier (1970) and Trinite and Valentin (1972), for boundary layer flows, and by Bremhorst and Bullock (1970), for pipe flow, also could be investigated. In the present study two-point transverse separation temperature fluctuating signals were recorded in the thermal entrance region. Therefore, a somewhat more complex analysis, than a straight spectral analysis with a single point signal, could be done. For example, some sort of conditional spectral analysis could be applied to the signal from the wall sensor, by generating the triggering function with the signal from the center sensor, which would be placed in a region where the temperature fluctuating field is intermittent. The dependence of the turbulent temperature fluctuations in the "internal" region upon the "external" non-turbulent temperature field could then be examined.

For pipe flows the dependence of the scales (both length and time) on Reynolds number has been more or less neglected in turbulence studies; particularly for ones in which two-point measurements were involved. However, as shown by Bobkov et.al. (1966), this dependence is negligible only if one considers Reynolds numbers above 100,000, and many cases of interest lie below this value. Therefore, since the experimental facility used in this investigation can generate different Reynolds number flows (up to 100,000), an investigation of the Reynolds number dependence of two-point length and time scales, for both temperature and velocity fields, could be undertaken.

Finally, the heat transfer loop, traversing mechanism, multi-probe holders and electronic instrumentation used in this work could be adapted to make, besides velocity and temperature, pressure fluctuation measurements. We feel that this would be a very promising, novel and worthy investigation. The reason is clearly seen by looking at the governing equations for turbulent velocity and temperature fields. Whenever one wants to compute Reynolds stresses or turbulent heat fluxes from these equations one is confronted with the difficult problem of estimating pressure diffusion terms which cannot be neglected. Due to the difficulty of measuring directly pressure fluctuations in many momentum and energy balance studies, e.g. for kinetic energy or $\overline{\theta^2}$, these terms have been left as "final entries". However, it appears that the technique for measuring pressure fluctuations, proposed by Spencer and Jones (1971) and successfully modified and applied to free jets by, among others, Planchon (1974) and Hammersley (1974), could be well adapted to perform similar measurements in a pipe flow. If this is achieved, measurements of pressure-velocity, pressure-temperature and two-point pressure correlations could provide a great deal of improvement in our understanding of the mechanisms for turbulent transfer of momentum and heat.

APPENDIX A: ERROR ANALYSIS IN CORRELATION AND LENGTH SCALE MEASUREMENTS

A.1. Uncertainties in Sensitivities and Gains

Let us consider the probe arrangement shown in Fig. A.1-1, and call the outputs of the four sensors e_{A_1}, e_{B_1}, e_{A_2} and e_{B_2}. By using the techniques described in Chapter 3 we have, at the output of the 1015C Sum and Difference Correlators, signals given by

$$G_{A_1} e_{A_1} \pm G_{B_1} e_{B_1} = \left(G_{A_1} S_{A_1} \pm G_{B_1} S_{B_1}\right) u_1 + \left(G_{A_1} S_{A_1} \mp G_{B_1} S_{B_1}\right) v_1 \tag{A.1-1}$$

$$G_{A_2} e_{A_2} \pm G_{B_2} e_{B_2} = \left(G_{A_2} S_{A_2} \pm G_{B_2} S_{B_2}\right) u_2 + \left(G_{A_2} S_{A_2} \mp G_{B_2} S_{B_2}\right) v_2 \tag{A.1-2}$$

where the thesis nomenclature was simplified for convenience as follows:

u_1 - axial velocity component in point 1

v_1 - normal velocity component in point 1

u_2 - axial velocity component in point 2

v_2 - normal velocity component in point 2

e_i - linearized voltage of i^{th} channel

G_i - gain of i^{th} channel

S_i - sensitivity of i^{th} channel

Other thesis nomenclature has been retained.

If we set G_{A_1}, G_{B_1}, G_{A_2} and G_{B_2} such that

$$G_{A_1} S_{A_1} = G_{B_1} S_{B_1} = G_1 S_1' \tag{A.1-3a}$$

and

$$G_{A_2} S_{A_2} = G_{B_2} S_{B_2} = G_2 S_2' \tag{A.1-3b}$$

we have

$$G_{A_1} e_{A_1} + G_{B_1} e_{B_1} = 2 G_1 S_1' u_1 \tag{A.1-4a}$$

$$G_{A_1} e_{A_1} - G_{B_1} e_{B_1} = 2 G_1 S_1' v_1 \tag{A.1-4b}$$

$$G_{A_2} e_{A_2} + G_{B_2} e_{B_2} = 2\, G_2 S_2 u_2 \qquad \text{(A.1-4c)}$$

$$G_{A_2} e_{A_2} - G_{B_2} e_{B_2} = 2\, G_2 S_2 v_2 \qquad \text{(A.1-4d)}$$

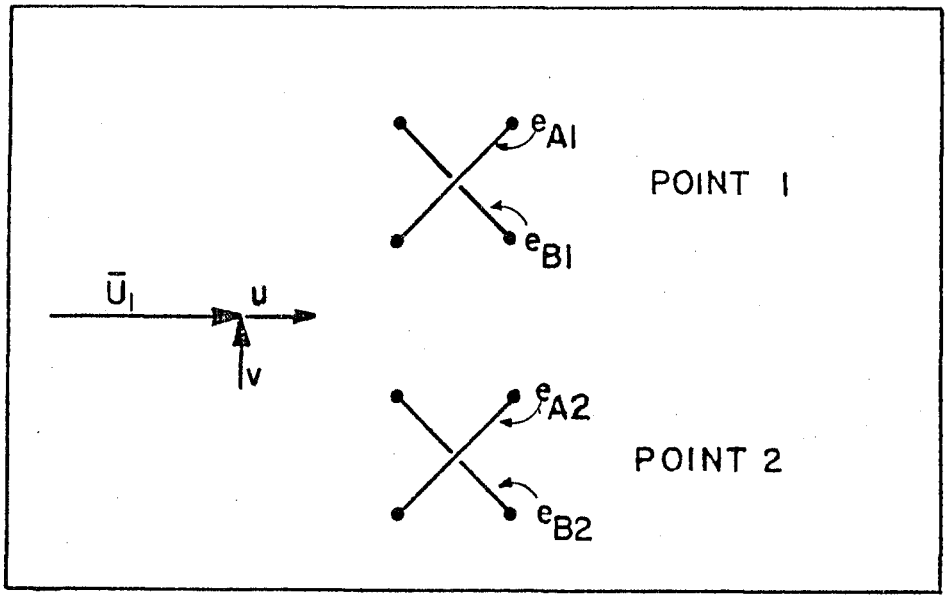

Figure A.1-1

'X' Sensor Probes Configuration For Two-Point Measurements

In order to estimate the effects of some uncertainties in the calculation of sensitivities and in setting the compensating gains, we take

$$G_{A_1} S_{A_1} = (1+\Pi_1)\, G_{B_1} S_{B_1} \qquad \text{(A.1-5a)}$$

$$G_{A_2} S_{A_2} = (1+\Pi_2)\, G_{B_2} S_{B_2} \qquad \text{(A.1-5b)}$$

Hence we have

$$G_{A_1} S_{A_1} + G_{B_1} S_{B_1} = (2+\Pi_1)\, G_{B_1} S_{B_1} = (2+\Pi_1) S_1 \qquad \text{(A.1-6a)}$$

$$G_{A_1} S_{A_1} - G_{B_1} S_{B_1} = \Pi_1 G_{B_1} S_{B_1} = \Pi_1 S_1 \qquad \text{(A.1-6b)}$$

The normalized correlation between axial components of the velocity at points 1 and 2, R_{11}, is given by

$$R_{11} = \frac{\overline{(G_{A_1}e_{A_1} + G_{B_1}e_{B_1})(G_{A_2}e_{A_2} + G_{B_2}e_{B_2})}}{\left[\overline{(G_{A_1}e_{A_1} + G_{B_1}e_{B_1})^2} \cdot \overline{(G_{A_2}e_{A_2} + G_{B_2}e_{A_2})^2}\right]^{1/2}}$$

$$= \frac{\overline{\left[(2+n_1)S_1u_1 + n_1S_1v_1\right]\left[(2+n_2)S_2u_2 + n_2S_2v_2\right]}}{\left\{\overline{\left[(2+n_1)S_1u_1 + n_1S_1v_1\right]^2} \cdot \overline{\left[(2+n_2)S_2u_2 + n_2S_2v_2\right]^2}\right\}^{1/2}} \qquad \text{(A.1-7)}$$

By assuming $n_1 = n_2 = n$ and by neglecting second order terms (n is small) we obtain an estimate of the uncertainty in R_{11} of

$$\text{Error}_{R_{11}}(\%) = \left\{\frac{1 + n\left[1 + \frac{1}{2R_{11}}\left[R_{12}\left(\frac{v'}{u'}\right)_2 + R_{21}\left(\frac{v'}{u'}\right)_1\right]\right]}{1 + n\left[1 + \frac{1}{2}\left[K_{uv_2}\left(\frac{v'}{u'}\right)_2 + K_{uv_1}\left(\frac{v'}{u'}\right)_1\right]\right]} - 1\right\} \times 100 \qquad \text{(A.1-8)}$$

with K_{uv_1} and K_{uv_2} being the shear coefficients evaluated, respectively, at points 1 and 2.

Similarly we have, for the uncertainty in R_{22},

$$\text{Error}_{R_{22}}(\%) = \left\{\frac{1 + n\left[1 + \frac{1}{2R_{22}}\left[R_{21}\left(\frac{u'}{v'}\right)_2 + R_{12}\left(\frac{u'}{v'}\right)_1\right]\right]}{1 + n\left[1 + \frac{1}{2}\left[K_{uv_2}\left(\frac{u'}{v'}\right)_2 + K_{uv_1}\left(\frac{u'}{v'}\right)_1\right]\right]} - 1\right\} \times 100 \qquad \text{(A.1-9)}$$

The same analysis procedure can be applied to estimate the error, corresponding to uncertainties in sensitivities and gains, involved in the calculation of the single-point shear coefficient defined by

$$K_{uv} = \frac{\overline{uv}}{u'v'} \qquad \text{(A.1-10)}$$

The final result is

$$\text{Error}_{K_{uv}}(\%) = \left\{ \frac{1+n\left[1+\frac{1}{2K_{uv}}\left(\frac{u'^2+v'^2}{u'v'}\right)\right]}{1+n\left[1+\frac{K_{uv}}{2}\left(\frac{u'^2+v'^2}{u'v'}\right)\right]} - 1 \right\} \times 100 \qquad \text{(A.1-11)}$$

Typical estimates of those errors from experimental results for y/R = 0.50 are presented in Table A.1-1

$\Delta r/R$	n	ε_{R11}	ε_{R22}	ε_{Kuv}
	%	%	%	%
0	10	0	0	20.1
	5	0	0	10.7
	1	0	0	2.3
0.2	10	0.32	5.0	-
	5	0.17	2.7	-
	1	0.04	0.57	-
0.45	10	2.7	9.4	-
	5	1.4	5.0	-
	1	0.3	1.1	-

Table A.1-1

Errors (ε) in Correlation and Shear Coefficients Due to Uncertainties in Sensitivities and Gains

Table A.1-1 shows that for a given uncertainty about the setting of gains in the Sum and Difference correlators we have an enhanced error in the single point shear coefficient calculation and reduced errors in two-point correlation coefficient calculations. In all two-point correlations, for small separations, we have $\Delta r \to 0$, R_{11} and $R_{22} \to 1.0$ and the Error $\to 0$.

A.2 Inter-channel Time Base Errors

The four fluctuating velocity signals from the four channels of

anemometry in the two-point 'X' probe measurements were not recorded on the same head. Therefore, an analysis to estimate the resulting inter-channel time base errors was necessarily made.

For simplicity let $\underline{x}$ and $\underline{y}$ given respectively by (A.2-1a) and (A.2-1b) be the signals from channels 1 and 2.

$$x = a \sin \omega t \tag{A.2-1a}$$

$$y = b \sin \omega (t-\Delta) \tag{A.2-1b}$$

For the sum and difference of these signals we have

$$x \pm y = a \sin \omega t \pm b \sin \omega (t-\Delta) \tag{A.2-2}$$

The errors in the RMS values of x-y and x+y are given by

$$\varepsilon_{RMS\,(x \mp y)}\,(\%) = \left[\left(\frac{a^2 \mp 2ab \cos \omega\Delta + b^2}{a^2 \mp 2ab + b^2} \right)^{1/2} - 1 \right] \times 100 \tag{A.2-3}$$

Hence to estimate $\omega\Delta$ we have

$$\omega\Delta = \cos^{-1} \left\{ \frac{1}{ab} \left[RMS^2_{x-y_{meas.}} - RMS^2_{x-y_{calc.}} \right] \right\} \tag{A.2-4}$$

By playing back the reference sine wave recorded before each group of turbulent signals, we can obtain $\omega\Delta$ with (A.2-4) and then estimate the corresponding tolerance (Δ_L), in the distance head-to-head, between the record heads and the playback heads as well as the length change of the magnetic tape between record and playback modes. From the present experimental data we have $\omega\Delta \simeq 6°$ and, hence, $\Delta_L \simeq 0.0006''$. This result is within the accepted range for high precision tape recorder/reproducers (e.g. Sangamo Model 3564).

The time base errors given by (A.2-3) are frequency dependent. Therefore, for the same Δ_L we have different errors for the various velocity components.

In Table A.2-1 estimated time base errors are presented for u and v, obtained with Δ_L = 0.001" and using the characteristic frequencies from spectral results reported by Burchill (1970). It was also assumed that all the energy for each component was concentrated at the corresponding characteristic (n_c) frequency.

Y/R	fc,u (Hz)	fc,v (Hz)	$\varepsilon u'$ $(\%)\times 10^{-3}$	ε_v' %
0.005	4.6	60.5		
0.10	6.9*	57.3*	2.42	3.61
0.25	9.0	50.4	2.40	2.21
0.50	9.8*	38.7*	2.39	1.11
0.75	9.8*	27.0*	2.43	0.89
0.86	9.8	21.8		
* interpolated values				

Table A.2-1

Inter-channel Time Base Errors

Table A.2-1 shows that the effect of recording two-component velocity signals on different heads is only slightly significant for the normal velocity component and can be completely ignored for the axial velocity component.

A.3 Statistical Errors (Finite Sample Time History Record)

Let x and y be two random functions from which we have a finite sample time history record. The variance of the estimate $\hat{R}_{xy}(\tau)$, the cross-correlation between these two signals, will be given by (see Bendat and Piersol (1971)).

$$\text{VAR}\left[\hat{R}_{xy}(\tau)\right] = E\left[\left(\hat{R}_{xy}(\tau) - R_{xy}(\tau)\right)^2\right] \qquad \text{(A.3-1)}$$

$$\mathrm{VAR}\left[\hat{R}_{xy}(\tau)\right] = \frac{1}{T^2}\int_0^T\int_0^T E\left[x(u)y(u+\tau)x(v)y(v+\tau) - \hat{R}^2_{xy}(\tau)\right]du\,dv \qquad \text{(A.3-2)}$$

where T = averaging time

If x_1, x_2, x_3, and x_4 are four random variables with zero mean values, which follow a four dimensional Gaussian distribution, we have

$$E\left[x_1x_2x_3x_4\right] = E\left[x_1x_2\right]E\left[x_3x_4\right] + E\left[x_1x_3\right]E\left[x_2x_4\right] + E\left[x_1x_4\right]E\left[x_2x_3\right] \qquad \text{(A.3-3)}$$

By applying (A.3-3) to (A.3-2) and using the following definitions

$$\left.\begin{aligned} x_1 &= x(u) \\ x_2 &= y(u+\tau) \\ x_3 &= x(v) \\ x_4 &= y(v+\tau) \end{aligned}\right\} \qquad \text{(A.3-4)}$$

we arrive at the following expression, which is valid for large T

$$\mathrm{VAR}\left[\hat{R}_{xy}(\tau)\right] \simeq \frac{1}{T}\left\{\int_{-\infty}^{+\infty} R_{xx}(\xi)R_{yy}(\xi)\,d\xi + \int_{-\infty}^{+\infty} R_{xy}(\xi+\tau)R_{yx}(\xi-\tau)\,d\xi\right\} \qquad \text{(A.3-5)}$$

If we assume

$$\left.\begin{aligned} R_{xx}(\xi) &= R_{11}(\xi) = \overline{u^2}\, e^{-\xi/T_{11}} \\ R_{yy}(\xi) &= R_{22}(\xi) = \overline{v^2}\, e^{-\xi/T_{22}} \\ R_{xy}(\xi) &= R_{12}(\xi) = u'v'\, e^{-\xi/T_{12}} \\ R_{yx}(\xi) &= R_{21}(\xi) = u'v'\, e^{-\xi/T_{21}} \end{aligned}\right\} \qquad \text{(A.3-6)}$$

we have, for zero lag cross-correlations,

$$\mathrm{VAR}\left[\hat{R}_{12}\right] = \frac{2}{T}\left[\frac{T_{11}\,T_{22}}{T_{11}+T_{22}} + \frac{T_{12}\,T_{21}}{T_{12}+T_{21}}\right] \qquad \text{(A.3-7)}$$

and, for the auto-correlations,

$$VAR\left[\hat{R}_{11}\right] = 2\,\frac{T_{11}}{T}\,\overline{u^2} \tag{A.3-8}$$

$$VAR\left[\hat{R}_{22}\right] = 2\,\frac{T_{22}}{T}\,\overline{v^2} \tag{A.3-9}$$

The corresponding normalized random errors are given by

$$\varepsilon_{R_{11}} = \frac{\sqrt{VAR\left[\hat{R}_{11}\right]}}{R_{11}} \tag{A.3-10}$$

$$\varepsilon_{R_{22}} = \frac{\sqrt{VAR\left[\hat{R}_{22}\right]}}{R_{22}} \tag{A.3-11}$$

Similarly, for temperature fluctuations, we can arrive at estimates for the variance and its error of

$$VAR\left[\hat{R}_{tt}\right] = 2\,\frac{T_{tt}}{T}\,\overline{\theta^2} \tag{A.3-12}$$

and

$$\varepsilon_{R_{tt}} = \frac{\sqrt{VAR\left[\hat{R}_{tt}\right]}}{R_{tt}} \tag{A.3-13}$$

In the present work no measurements were made of the Eulerian time scales. However, from the values of the length scales presented on sections 4.2 and 5.2, we can estimate these time scales through the Taylor's hypothesis (see Hinze (1959)). Then we have

$$L_{11}^{(1)} \simeq \overline{U}_1\, \mathcal{J}_{11}^{E} \simeq \overline{U}_1\, T_{11} \tag{A.3-14}$$

$$L_{22}^{(1)} \simeq \overline{U}_1\, \mathcal{J}_{22}^{E} \simeq \overline{U}_1\, T_{22} \tag{A.3-15}$$

$$L_{tt}^{(1)} \simeq \overline{U}_1\, \mathcal{J}_{tt}^{E} \simeq \overline{U}_1\, T_{tt} \tag{A.3-16}$$

with $\overline{U}_1$ being the local mean velocity.

The fluctuating signals were recorded for 8 minutes on magnetic tapes. Table A.3-1 shows estimated errors obtained from (A.3-10), (A.3-11) and (A.3-13) by using length scales, Taylor's hypothesis and T = 419.4 sec. (Typically these signals were processed with the Correlation and Probability Analyser set at 2 x 128 x 1024 summations and using 100 μs time steps at a playback tape speed of 16 times the original data recording tape speed, giving T = 419.4 sec.).

Y/R	E_{11} (msec)	E_{22} (msec)	E_{tt} (msec)	$\varepsilon[\hat{R}_{11}]$ (%)	$\varepsilon[\hat{R}_{22}]$ (%)	$\varepsilon[\hat{R}_H]$ (%)
0.78	61.7	7.4	21.1	1.72	0.59	1.00
0.53			26.9			1.13
0.50	62.6	5.4		1.73	0.51	
0.29			33.4			1.26
0.25	68.7	4.6		1.81	0.47	
0.125	69.2	2.8	42.8	1.82	0.36	1.43

Table A.3-1

Statistical Errors Due to Finite Time History Records

A.4 Estimated Errors in Calculating Integral Length Scales

In the previous sections of this appendix we have presented estimates for the principal errors involved in correlation measurements. By using these values we can now estimate the resulting error on the calculation of integral length scales. In Fig. A.4-1 a typical correlation curve for y/R = 0.50 is presented. The dotted lines correspond to estimated upper and lower bounds for this curve.

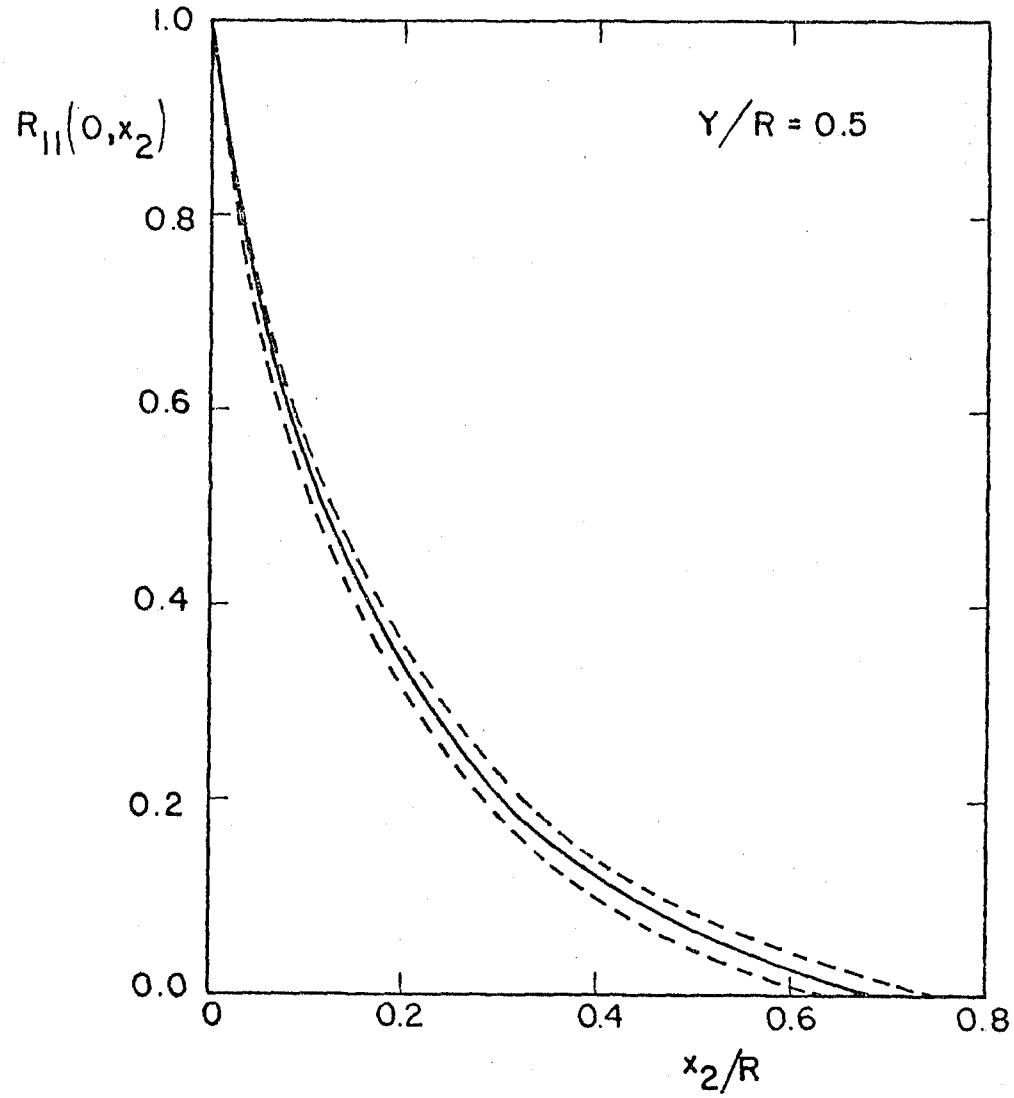

Figure A.4-1: Typical Space Correlation Curve Showing Estimated Effects of Experimental Errors

By calculating the areas underneath the dotted and full lines we can arrive at an estimated error of approximately $\pm$ 6.6%, for the integral length scale L_{11}. Similarly we have, for the normal velocity component and temperature scales, estimated errors of approximately $\pm$ 9.2% and $\pm$ 4%, respectively. In all of these calculations it was assumed a quantization error of 0.4%.

APPENDIX B: EQUATIONS FOR AXISYMMETRIC CORRELATION MODELING

In Chapter 6 we have indicated that if axisymmetry is assumed the two-point velocity correlation tensor Q_{ij} can be completely determined in terms of two scalar functions Q_1 and Q_2. By specifying these functions we can arrive at expressions for the correlation functions $\tilde{R}_{11}(\xi_1,\xi_2,\xi_3)$, $\tilde{R}_{22}(\xi_1,\xi_2,\xi_3)$ and $\tilde{R}_{12}(\xi_1,\xi_2,\xi_3)$ in the axisymmetric system of coordinates (see Fig. 6.1-1). To transform these correlation functions to the measurement system of coordinates we have the following relations

$$R_{11}(x_1,x_2,x_3) = \tilde{R}_{11}(\xi_1,\xi_2,\xi_3)\cos^2\phi - 2\tilde{R}_{12}(\xi_1,\xi_2,\xi_3)\sin\phi\cos\phi + \tilde{R}_{22}(\xi_1,\xi_2,\xi_3)\sin^2\phi \tag{B-1}$$

$$R_{22}(x_1,x_2,x_3) = \tilde{R}_{11}(\xi_1,\xi_2,\xi_3)\sin^2\phi + 2\tilde{R}_{12}(\xi_1,\xi_2,\xi_3)\sin\phi\cos\phi + \tilde{R}_{22}(\xi_1,\xi_2,\xi_3)\cos^2\phi \tag{B-2}$$

with

$$x_1 = \xi_1\cos\phi - \xi_2\sin\phi \tag{B-3a}$$

$$x_2 = \xi_1\sin\phi + \xi_2\cos\phi \tag{B-3b}$$

$$x_3 = \xi_3 \tag{B-3c}$$

We have examined two models; namely, the two parameter (ℓ_1,ℓ_2) Goldstein and Rosenbaum (1973) and the four parameter (ℓ_1,ℓ_2,n_1,n_2) Weber (1974) models. In these models the correlation functions are given by:

Goldstein and Rosenbaum (1973) Model

$$\tilde{R}_{11}(\xi_1,\sigma) = \left[1 - \frac{\sigma^2}{2\ell_2^2 A}\right]\exp(-A) \tag{B-4}$$

$$\tilde{R}_{22}(\xi_1,\sigma) = \left\{ \frac{(\overline{u_2^2}-\overline{u_1^2})}{\overline{u_2^2}} \left[1 - \frac{\xi_3^2}{A l_2^2} \right] + \frac{\overline{u_1^2}}{2\,\overline{u_2^2}} \left[2 + \frac{1}{A} \left(\frac{\xi_1}{l_1} \right)^2 \left[\left(\frac{l_1}{l_2} \right)^2 - 2 \right] \right. \right.$$

$$\left. \left. + \frac{1}{A} \left(\frac{\xi_3}{l_2} \right)^2 \left[\left(\frac{l_2}{l_1} \right)^2 - 2 \right] - \frac{\xi_1^2 \xi_3^2}{l_1^2 l_2^2} \left(\frac{1}{A^2} + \frac{1}{A^3} \right) \left(\frac{l_2}{l_1} - \frac{l_1}{l_2} \right)^2 \right] \right\}$$

$$\cdot \exp(-A) \qquad \text{(B-5)}$$

$$\tilde{R}_{12}(\xi_1,\sigma) = \left(\frac{\overline{\tilde{u}_1^2}}{\overline{\tilde{u}_2^2}} \right)^{1/2} \frac{\xi_1 \xi_2}{2 l_1^2 A} \exp(-A) \qquad \text{(B-6)}$$

with $$\sigma^2 = \xi_2^2 + \xi_3^2 \quad , \quad A = \sqrt{\left(\frac{\xi_1}{l_1} \right)^2 + \left(\frac{\sigma}{l_2} \right)^2} \qquad \text{(B-7)}$$

Weber (1974) Model

$$\tilde{R}_{11}(\xi_1,\xi_2) = \left[1 - \frac{1}{2} \frac{\xi_2^2}{l_2^2 A} \right] \exp(-A') \qquad \text{(B-8)}$$

$$\tilde{R}_{22}(\xi_1,\xi_2) = \left[1 - \frac{B}{2} \left(\frac{\xi_1^2}{\xi_1^2+\xi_2^2} \right) \right] \exp(-B) \qquad \text{(B-9)}$$

$$\tilde{R}_{12}(\xi_1,\xi_2) = \left(\frac{\overline{\tilde{u}_1^2}}{\overline{\tilde{u}_2^2}} \right)^{1/2} \frac{\xi_1 \xi_2}{2 l_1^2 A'} \exp(-A') \qquad \text{(B-10)}$$

with

$$A' = \sqrt{\left(\frac{\xi_1}{\ell_1}\right)^2 + \left(\frac{\xi_2}{\ell_2}\right)^2} \quad , \quad B = \sqrt{\left(\frac{\xi_1}{r_1}\right)^2 + \left(\frac{\xi_2}{r_2}\right)^2} \tag{B-11}$$

For the Goldstein and Rosenbaum (1973) model, after integration of the correlation functions, we have arrived at a relationship between the parameters ℓ_1 and ℓ_2 and the experimentally measured transverse integral length scales. This relationship is given by

$$\left(\frac{\ell_1}{\ell_2}\right)^2 = \frac{2\sin^2\phi\left\{\left(\frac{\overline{u_2^2}}{\overline{u_1^2}} - 1\right)\left[(\gamma+1)\cos^2\phi - 1\right] + \gamma\right\}}{1 - 2\cos^2\phi\left\{\left(\frac{\overline{u_2^2}}{\overline{u_1^2}} - 1\right)\left[(\gamma+1)\cos^2\phi - 1\right] + \gamma\right\}} \tag{B-12}$$

and

$$\ell_1 = \frac{\overline{u_2^2}\, L_{22}^{(2)}\left(\sin^2\phi + \rho_1^2\cos^2\phi\right)^{1/2}}{\overline{u_1^2}\sin^2\phi + \overline{u_2^2}\cos^2\phi} \tag{B-13}$$

with

$$\gamma = \frac{\overline{u_1^2}\, L_{11}^{(2)}}{\overline{u_2^2}\, L_{22}^{(2)}} \quad , \quad \rho_1 = \frac{\ell_1}{\ell_2} \tag{B-14}$$

Following a similar procedure we can relate the parameters ℓ_1 and ℓ_2 to other pairs of integral length scales. For example, to relate ℓ_1 and ℓ_2 with the axial velocity component scales we have

$$\ell_1 = \frac{\overline{u^2}\, L_{11}^{(2)}\left(\sin^2\phi + \rho_1^2\cos^2\phi\right)^{1/2}}{\left\{\left(\overline{u_1^2}\cos^2\phi + \overline{u_2^2}\sin^2\phi\right) + 2\,\frac{\sin^2\phi\left(\rho_1^2 - 1\right) - \rho_1^2}{2\left(\sin^2\phi + \rho_1^2\cos^2\phi\right)}\right\}} \tag{B-15}$$

and

$$\left(\frac{\ell_1}{\ell_2}\right)^2 = \rho_1^2 = \frac{\left[\overline{\tilde{u}_1^2}\cos^2\phi + \overline{\tilde{u}_2^2}\sin^2\phi\right]^2 \ell_1^2 - \cos^2\phi\left[\overline{u_1^2}\,L_{11}^{(1)}\right]^2}{\left[\overline{u_1^2}\,L_{11}^{(1)}\right]^2 \sin^2\phi} \quad \text{(B-16)}$$

The parameters ℓ_1 and ℓ_2 can also be obtained in terms of the longitudinal integral length scales of the normal and axial velocity components. The resulting equations are

$$\left(\frac{\ell_1}{\ell_2}\right)^2 = \frac{2\cos^2\phi\left\{\left(\frac{\overline{\tilde{u}_2^2}}{\overline{\tilde{u}_1^2}} - 1\right)\left[(\eta+1)\sin^2\phi - 1\right] + \eta\right\}}{1 - 2\sin^2\phi\left\{\left(\frac{\overline{\tilde{u}_2^2}}{\overline{\tilde{u}_1^2}} - 1\right)\left[(\eta+1)\sin^2\phi - 1\right] + \eta\right\}} \quad \text{(B-17)}$$

and

$$\ell_1 = \frac{\overline{u_1^2}\,L_{11}^{(1)}\left(\cos^2\phi + \rho_1^2\sin^2\phi\right)^{1/2}}{\overline{\tilde{u}_1^2}\cos^2\phi + \overline{\tilde{u}_2^2}\sin^2\phi} \quad \text{(B-18)}$$

with

$$\eta = \frac{\overline{u_2^2}\,L_{22}^{(1)}}{\overline{u_1^2}\,L_{11}^{(1)}} \quad , \quad \rho_1 = \frac{\ell_1}{\ell_2} \quad \text{(B-19)}$$

To calculate the four parameters $(\ell_1, \ell_2, n_1, n_2)$ in the Weber (1974) model we have integrated the modeled correlation functions along two directions (parallel and normal to the mean flow) and have arrived at

$$\begin{cases} \frac{1}{\alpha}\overline{\tilde{u}_1^2}\,A_1 + \frac{1}{\pi}\overline{\tilde{u}_2^2}\,C_1 = \overline{u_1^2}\,L_{11}^{(1)} & \text{(B-20a)} \\ \frac{1}{\gamma}\overline{\tilde{u}_1^2}\,B_1 + \frac{1}{\Delta}\overline{\tilde{u}_2^2}\,D_1 = \overline{u_1^2}\,L_{11}^{(2)} & \text{(B-20b)} \\ \frac{1}{\alpha}\overline{\tilde{u}_1^2}\,A_2 + \frac{1}{\pi}\overline{\tilde{u}_2^2}\,C_2 = \overline{u_2^2}\,L_{22}^{(1)} & \text{(B-20c)} \end{cases}$$

$$\frac{1}{\gamma}\overline{\tilde{u}_1^2}\,B_2 + \qquad \frac{1}{\Delta}\overline{\tilde{u}_2^2}\,D_2 = \overline{u_2^2}\,L_{22}^{(2)} \tag{B-20d}$$

with

$$\alpha = \left(\frac{\cos^2\phi}{\ell_1^2} + \frac{\sin^2\phi}{\ell_2^2}\right)^{1/2} \tag{B-21}$$

$$\gamma = \left(\frac{\sin^2\phi}{\ell_1^2} + \frac{\cos^2\phi}{\ell_2^2}\right)^{1/2} \tag{B-22}$$

$$\Pi = \left(\frac{\cos^2\phi}{n_1^2} + \frac{\sin^2\phi}{n_2^2}\right)^{1/2} \tag{B-23}$$

$$\Delta = \left(\frac{\sin^2\phi}{n_1^2} + \frac{\cos^2\phi}{n_2^2}\right)^{1/2} \tag{B-24}$$

The coefficients A_1, B_1, A_2 and B_2 are functions of the ratio (ℓ_1/ℓ_2) and the angle of axisymmetry (ϕ) and are given by

$$A_1 = \cos^2\phi + \frac{\sin^2\phi\cos^2\phi\,(2 - E_{11}\rho_1^2)}{2\,(\cos^2\phi + \rho_1^2\sin^2\phi)} \tag{B-25}$$

$$B_1 = \cos^2\phi - \frac{\cos^2\phi\,(E_{12}\cos^2\phi\,\rho_1^2 + 2\sin^2\phi)}{2\,(\sin^2\phi + \rho_1^2\cos^2\phi)} \tag{B-26}$$

$$A_2 = \sin^2\phi - \frac{\sin^2\phi\,(E_{11}\sin^2\phi\,\rho_1^2 + 2\cos^2\phi)}{2\,(\cos^2\phi + \rho_1^2\sin^2\phi)} \tag{B-27}$$

$$B_2 = \sin^2\phi + \frac{\sin^2\phi\cos^2\phi\,(2 - E_{12}\rho_1^2)}{2\,(\sin^2\phi + \rho_1^2\cos^2\phi)} \tag{B-28}$$

with

$$E_{11} = 1 - \exp\left[-\frac{2\,(\cos^2\phi + \rho_1^2\sin^2\phi)}{\rho_1^2\sin^2\phi}\right] \tag{B-29}$$

$$E_{12} = 1 - \exp\left[-\frac{2(\sin^2\phi + \rho_1^2\cos^2\phi)}{\rho_1^2\cos^2\phi}\right] \qquad \text{(B-30)}$$

The coefficients C_1, D_1, C_2 and D_2 depend only upon ϕ and are given by

$$C_1 = \frac{1}{2}\left(2 - E_{21}\cos^2\phi\right)\sin^2\phi \qquad \text{(B-31)}$$

$$D_1 = \frac{1}{2}\left(2 - E_{22}\sin^2\phi\right)\sin^2\phi \qquad \text{(B-32)}$$

$$C_2 = \frac{1}{2}\left(2 - E_{21}\cos^2\phi\right)\cos^2\phi \qquad \text{(B-33)}$$

$$D_2 = \frac{1}{2}\left(2 - E_{22}\sin^2\phi\right)\cos^2\phi \qquad \text{(B-34)}$$

with

$$E_{21} = 1 - \exp\left[-2/\cos^2\phi\right] \qquad \text{(B-35)}$$

$$E_{22} = 1 - \exp\left[-2/\sin^2\phi\right] \qquad \text{(B-36)}$$

LIST OF REFERENCES

Abbrecht,P.H.,and Churchill,S.W.,1960,"The thermal entrance region in fully developed turbulent flow",A.I.Ch.E. Journal,V.6,2,268-273

Azer,N.Z., and Chao,B.T.,1960,"A mechanism of turbulent heat transfer in liquid metals",Int.J.Heat Mass Transfer,1,121-138

Batchelor,G.K.,1946,"The theory of axisymmetric turbulence",Proc.Roy. Soc.-A,186,480-502

Beckwith,W.F.,and Fahien,R.,1962,"Determination of turbulent thermal diffusivities for flow of liquids in pipes",U.S. AEC Report,I.S. 734

Bendat,J.S.,and Piersol,A.G.,1971,"Random data: analysis and measurement procedures",John Wiley & Sons Inc. - New York

Blackwelder,R.F.,and Kovasnay,L.S.,1972,"Time scales and correlations in a turbulent boundary layer",Phys.Fluids,V.15,9,1545-1554

Blom,J.,1970,"Experimental determination of the turbulent Prandtl number in a developing temperature boundary layer",Paper FC.2.2 presented at the Fourth International Heat Transfer Conference - Paris

Bobkov,V.P. et.al.,1966,"The three-dimensional correlation coefficients and the transverse scales of the temperature perturbation in turbulent flow of mercury in a round tube",High Temperature,V.4,3, 367-374

Bobkov,V.P. et al.,1968,"Time characteristics and temperature pulsation spectrum for the turbulent flow of liquid in a pipe",High Temperature,V.6,1,93-99

Bose,B.,1971,"Some measurement in pipe flow",AIAA Journal,V.9,7, 1405-1407

Bourke,P.J.,and Pulling,D.J.,1970,"A turbulent heat flux meter and some measurements of turbulence in air flow through a heated pipe", Int.J.Heat Mass Transfer,13,1331-1338

Boussinesq,J.,1877,"Essai sur la theorie des eaux courants",Mem.pres. par div. savants a l'Acad.Sci.,Paris,23,No. 1,1-680

Boussinesq,J.,1897,"Theorie de l'ecoulement tourbillonant et tumultueux des liquides dans les lits rectilignes a grande section" Gauthier-Villars,Paris

Bremhorst,K.,and Bullock,K.J.,1970,"Spectral measurements of temperature and longitudinal velocity fluctuations in fully developed pipe flow", Int.J.Heat Mass Transfer,13,1313-1329

Bremhorst,K.,and Bullock,K.J.,1973,"Spectral measurements of turbulent heat and momentum transfer in fully developed pipe flow",Int.J.Heat

Mass Transfer,16,2141-2154

Brodkey,R.S.,1967,"The phenomena of Fluid Motions",Addison-Wesley, Reading, Mass.

Brown,C.K.,and Gauvin,W.H.,1966,"Temperature profiles and fluctuations in combined free and forced convection flows",Chem.Eng.Sci.,21, 961-970

Buleev,N.I.,1964,"Theoretical model of turbulent transfer in three-dimensional fluid flows",Proc.of the Third Int.Conf.on the Peaceful uses of Atomic Energy,V.8,305-314; see also LA-TR-68-52,(October 1968)

Burchill,W.E.,1970,"Statistical properties of velocity and temperature fields in isothermal and non-isothermal turbulent pipe flow",Ph.D. Thesis,Nuclear Engineering Program, University of Illinois

Chandrasekhar,F.R.S.,1950,"The theory of axisymmetric turbulence", Philosophical Transactions of the Royal Society - A,242,557-577

Chou,P.Y.,1945,"On velocity correlations and the solution of the equations of turbulent fluctuation",Quart.Appl.Math.,3,31

Cliff,W.C.,and Sandborn,V.A.,1973,"Measurements and a model for convective velocities in the turbulent boundary layer",NASA TN D-7416

Corrsin,S.,and Comte Bellot,G.,1971,"Simple Eulerian time correlation of full and narrow-band velocity signals in grid generated 'isotropic' turbulence",J.Fluid Mech.,48,273-337

Daly,B.J.,and Harlow,F.H.,1970,"Transport equations in turbulence", Phys.Fluids,V.13,11,2634-2649

Davydov,B.I.,1959a,"On the statistical dynamics of an incompressible turbulent fluid",Soviet Physics-Doklady,V.4,4,769-772

Davydov,B.I.,1959b,"On the statistical theory of turbulence",Soviet Physics-Doklady,V.4,4,779-781

Deissler,R.G.,1951,"Investigation of turbulent flow and heat transfer in smooth pipes, including the effects of variable fluid properties", Trans.ASME,73,101-105

Deissler,R.G.,1958,"On the decay of homogeneous turbulence",Phys. Fluids,1,111-121

Deissler,R.G.,1960,"A theory of decaying homogeneous turbulence",Phys. Fluids,3,176-187

Deissler,R.G.,1961,"Effects of inhomogeneity and of shear flow in weak turbulent fields",Phys.Fluids,V.4,10,1187-1198

Deissler,R.G.,1963,"Turbulent heat transfer and temperature fluctuations in a field with uniform velocity and temperature gradients",Int.J. Heat Mass Transfer,6,257-270

Deissler,R.G.,1965,"Problem of steady state shear turbulence",Phys. Fluids,V.8,3,391-398

Donaldson,C.duP.,1972a,"Calculation of turbulent shear flows for atmospheric and vortex motions",AIAA Journal,V.10,1,4-12

Donaldson,C.duP.,1972b,"The relationship between eddy transport and second order closure models for stratified media and vortices",NASA SP-321,233-258

Eckelman,L.D.,and Hanratty,T.J.,1972,"Interpretation of measured variations of the eddy conductivity",Int.J.Heat Mass Transfer,15, 2231-2239

Fulachier,L. et al.,1974,"Structure des pertubations dans une couche limite turbulente: zone interne",C.R.Acad.Sci.Paris,278,Series B, 683-687

Goldstein,M.,and Rosenbaum,B.,1973,"Effect of anisotropic turbulence on aerodynamic noise",J.Acous.Soc.,V.54,3,630-645

Gowen,R.A.,and Smith,J.W.,1967,"The effect of the Prandtl number on temperature profiles for heat transfer in turbulent pipe flow",Chem. Eng.Sci.,22,1701-1711

Hammersley,R.J.,1974,"An experimental investigation of the turbulent characteristics of co-anular jets and their role in aerodynamic noise generation",Ph.D. Thesis, Nuclear Engineering Program, University of Illinois

Hanjalic,K.,and Launder,B.E.,1972,"A Reynolds stress model of turbulence and its application to thin shear flows",J.Fluid Mech., V.52,4,609-638

Happel,J.,and Brenner,H.,1965,"Low Reynolds Number Hydrodynamics", Prentice Hall Inc.,Englewood Cliffs, N.J.

Hinze,J.O.,1959,"Turbulence",McGraw Hill,New York,N.Y.

Hishida,M.,1967,"Turbulent heat transfer and temperature distribution in the thermal entrance region of a circular pipe",Bulletin of JSME, V.10,37,113-123

Hochreiter,L.E.,1971,"Turbulent structure of isothermal and non-isothermal liquid metal pipe flow",Ph.D. Thesis,Dept. Nuclear Eng., Purdue University

Hochreiter,L.E.,and Sesonske,A.,1969,"Thermal turbulence characteristics in sodium-potassium",Int.J.Heat Mass Transfer,12,114-118

Hochreiter,L.E.,and Sesonske,A.,1974,"Turbulent structure of isothermal and non-isothermal liquid metal pipe flow",Int.J.Heat Mass Transfer,17,113-123

Howard,N.M.,1974,"Experimental measurements of particle motion in a turbulent pipe flow",Ph.D. Thesis, Nuclear Engineering Program, University of Illinois

Hughmark,G.A.,1971,"Heat and mass transfer for turbulent pipe flow", A.I.Ch.E. Journal,V.17,4,902

Ibragimov,M.K. et al.,1968a,"Spatial structure of temperature perturbations in the non-isothermal turbulent flow of a liquid in a square channel",High Temperature,V.6,3,441-446

Ibragimov,M.K. et al.,1968b,"Space-time characteristics of temperature pulsations during turbulent liquid flow in a square channel",High Temperature,V.6,6,1020-1024

Ibragimov, et al.,1969,"Determination of the correlation between pulsations of velocity and temperature in turbulent air flow in a tube",Soviet Physics-Doklady,V.13,12,1208-1210

Jenkins,R.,1951,"Variations of the eddy conductivity with Prandtl modulus and its use in the prediction of heat transfer coefficients", Heat Transfer and Fluid Mechanics Institute Preprints, Stanford University Press,147-158

Johnk,R.E.,and Hanratty,T.J.,1962a,"Temperature profiles for turbulent flow of air in a pipe - I - The fully developed heat transfer region", Chem.Eng.Sci.,17,867-879

Johnk,R.E.,and Hanratty,T.J.,1962b,"Temperature profiles for turbulent flow of air in a pipe - II - The thermal entrance region",Chem.Eng. Sci.,17,881-892

Johnson,D.S.,1959,"Velocity and temperature fluctuation measurements in a turbulent boundary layer downstream of a stepwise discontinuity in wall temperature",J.Applied Mechanics,Trans ASME,81,Series E, 325-336

Karman,T.von,1930,"Mechanische Ähnlickeit und Turbulenz",Nach.Ges. Wiss.Göttingen,Math.Phys.,K 1,58-76; see also Proc. Third Intern. Congress Appl.Mech.,Stockholm,Pt.I,85,1930

Knudsen,J.G.,and Katz,D.L.,1958,"Fluid dynamics and heat transfer", McGraw Hill Book Co.,New York,N.Y.

Kovasnay,L.S.G. et al.,1970,"Large scale motion in the intermittent region of a turbulent boundary layer",J.Fluid Mech.,V.41,2,283-325

Kudva,A.K.,and Sesonske,A.,1972,"Structure of turbulent velocity and temperature fields in ethylene glycol pipe flow at low Reynolds number",Int.J.Heat Mass Transfer,15,127-145

Kudva,A.K. et al.,1968,"Turbulence scales and eddy diffusivities", Paper presented at the Tenth National Heat Transfer Conference, Philadelphia,Penn.(August 11-14)

Laufer,J.,1954,"The structure of turbulence in fully developed pipe flow",NACA Report 1174

Launder,B.E.,and Spalding,D.B.,1972,"Mathematical models of turbulence",Academic Press,London and New York

Loitsiansky,L.G.,1939,"Some basic laws for isotropic turbulent flow",NACA TM 1079

Lundgren,T.S.,1967,"Distribution functions in the statistical theory of turbulence",Phys.Fluids,10,969-975

Lundgren,T.S.,1969,"Model equation for non-homogeneous turbulence", Phys.Fluids,12,485-497

Meek,C.C.,1972,"Statistical characterization of dilute particulate suspensions in turbulent fluid fields",Ph.D. Thesis,Nuclear Engineering Program,University of Illinois

Monin,A.S.,and Yaglom,A.M.,1971,"Statistical Fluid Mechanics",(V.I), The MIT Press,Cambridge,Mass.

Morton,J.B.,and Clark,W.H.,1971,"Measurements of two-point velocity correlations in a pipe flow using laser anemometers",J.of Physics - E:Scientific Instruments,4,809-814

Nee,V.W.,and Kovasnay,L.S.G.,1969,"Simple phenomenological theory of turbulent shear flows",Phys.Fluids,V.12,3,473-484

Nikuradse,J.,1932,"Gesetzmässigkeiten der turbulenten Strömung in glatten Röhren",VDI-Forschungsheft,356

Pessoni,D.H.,1974,"An experimental investigation into the effects of wall heat flux on the turbulence structure of developing boundary layers at moderately high Reynolds numbers",Ph.D. Thesis,Mechanical Engineering Dept.,University of Illinois

Phillips,O.M.,1967,"The maintenance of Reynolds stress in turbulent shear flow",J.Fluid Mech.,V.27,1,131-144

Phillips,O.M.,1969,"Shear flow turbulence",Annual Reviews of Fluid Mechanics,V.1,245-263

Planchon,H.P.,1974,"The fluctuating static pressure field in a round jet turbulent mixing region",Ph.D. Thesis,Nuclear Engineering Program, University of Illinois

Prandtl,L.,1925,"Bericht über Untersuchungen zur ausgebildeten Turbulenz",Z. angew.Math.u.Mech.,5,2,136-139;see also Proc.Second Int. Congress Appl.Mech.,Zurich(1926)

Prandtl,L.,1945,"Uber ein neues Formelsystem für die ausgebildete Turbulenz",Nachr.Ges.Wiss.Göttingen,Math.Phys. K.1,6-19

Quarmby,A.,and Anand,R.K.,1969,"Axisymmetric turbulent mass transfer in a circular tube",J.Fluid Mech.,V.38,3,433

Quarmby,A.,and Quirk,R.,1972,"Measurements of the radial and tangential eddy diffusivities of heat and mass in turbulent flow in a plain tube", Int.J.Heat Mass Transfer,15,2309-2327

Quarmby,A.,and Quirk,R.,1974,"Axisymmetric and non-axisymmetric turbulent diffusion in a plain circular tube at high Schmidt number", Int.J.Heat Mass Transfer,17,143-147

Reynolds,O.,1894,"On the dynamical theory of incompressible viscous fluids and the determination of the criterion",Phil.Trans.Roy.Soc. London,186,123-161

Rodi,W.,and Spalding,D.B.,1970,"A two-parameter model of turbulence and its application to free jets",Wärme und Stoffübertragung,3,85-95

Sabot,J,and Comte-Bellot,G.,1971,"Correlations spatio-temporelles de vitesses en turbulence de conduites",C.R.Acad.Sc.Paris,273,Series A, 638-641

Sabot,J.,and Comte-Bellot,G.,1972a,"Memoires des fluctuations longitudinales de vitesse en conduite lisse circulaire",C.R.Acad.Sc. Paris,274,Series A,1647-1650

Sabot,J.,and Comte-Bellot,G.,1972b,"Courbes d'iso-correlations spatiales et d'iso-correlations spatio-temporelles relatives aux fluctuations longitudinales de vitesse en conduite lisse circulaire", C.R.Acad.Sc.Paris,275,Series A,667-670

Sabot,J. et al.,1973,"Space-time correlations of the transverse velocity fluctuation in pipe flow",Phys.Fluids,V.16,9,1403-1405

Sabot,J,and Comte-Bellot,G.,1974,"Temps de coherence de la fluctuation radiale de vitesse en conduite lisse circulaire",C.R.Acad.Sc.Paris, 278,Series A,105-107

Sage,B.H. et al.,1952,"Temperature and velocity distributions in uniform flows between parallel plates",Ind.Engng.Chem.,44,419

Schlichting,H.,1968,"Boundary Layer Theory",McGraw Hill Book Co.,New York,N.Y.

Silver,R.S.,1968,"Reynolds flux concept in heat and mass transfer", The Osborne Reynolds Centenary Symposium,University of Manchester, (September 1968)

Smith,J.W. et al.,1966,"Diffusion coefficients and temperature profiles for flow of liquids in pipes",Paper presented at A.I.Ch.E. meeting, Detroit,Mich.

Spencer,B.W.,and Jones,B.G.,1971,"A bleed-type pressure transducer for in-stream measurements of static pressure fluctuations",Rev.Sci. Inst.,V.42,4,450-454

Subbotin,V.I. et al.,1964,"Statistical study of turbulent temperature

pulsations in a liquid stream",High Temperature,V.2,1,59-64

Tanimoto,S.,and Hanratty,T.J.,1963,"Fluid temperature fluctuations accompanying turbulent heat transfer in a pipe",Chem.Eng.Sci.,18, 307-311

Taylor,G.I.,1932,"The transport of vorticity and heat through fluids in turbulent motion",Proc.Roy.Soc.London,135,A

Trinite,M.,and Valentin,P.,1972,"Couche limite turbulente avec discontinuite de temperature et de concentration a la paroi",Int.J. Heat Mass Transfer,15,1337-1354

Tyldesley,J.R.,and Silver,R.S.,1968,"The prediction of the transport properties of a turbulent fluid",Int.J.Heat Mass Transfer,11, 1325-1340

Tyldesley,J.R.,1969,"Transport phenomena in free turbulent flows", Int.J.Heat Mass Transfer,12,489-496

Tyldesley,J.R.,1970,"A theory to predict the transport and relaxation properties of a turbulent fluid",Proc.Roy.Soc.Edinburgh, 68,A,271-297

Verollet,E.,and Fulachier,L.,1969,"Mesures de densites de flux de chaleur et de tensions de Reynolds dans une couche limite turbulente avec aspiration a la paroi",C.R.Acad.Sci.Paris,268,Series A,1577-1580

Weber,D.P.,1974,"Turbulent velocity field structure in a round jet and its relation to fluctuating pressure",Ph.D. Thesis,Nuclear Engineering Program,University of Illinois

Wills,J.A.B.,1964,"On convection velocities in turbulent shear flows", J.Fluid Mech.,V.20,3,417-432

VITA

Joaquim de Sylos Cintra, Jr. was born on June 29, 1944 in Sao Paulo, Brazil. He entered the University of Sao Paulo in March, 1963 and was awarded a Bachelor of Science degree in Mechanical Engineering in January 1968. He received his Master of Science degree in Nuclear Engineering from the University of Sao Paulo in March 1971.

He is a member of the American Nuclear Society and the honorary society of Phi Kappa Phi.

He accepted a position as a research engineer with the Instituto de Energia Atomica (Brazil) in February 1968. He was later given a leave of absence to begin his Doctor of Philosophy degree program at the University of Illinois in February 1972. Following graduation he will be rejoining the research staff at the IEA.